EXPERIMENTAL AND THEORETICAL INVESTIGATION OF NATURAL CONVECTION HEAT TRANSFER IN AN INTEGRAL SOLAR COLLECTOR STORAGE (ISCS)

A THESIS SUBMITTED TO
THE GRADUATE SCHOOL OF NATURAL AND APPLIED SCIENCES
OF
UNIVERSITY OF TURKISH AERONAUTICAL ASSOCIATION

BY

HADI AL-DAYYENI

IN PARTIAL FULFILLMENT OF THE REQUIREMENTS
FOR
THE DEGREE OF DOCTOR OF PHILOSOPHY
IN
MECHANICAL AND AERONAUTICAL ENGINEERING

DECEMBER 2020

Approval of the thesis:

EXPERIMENTAL AND THEORETICAL INVESTIGATION OF NATURAL CONVECTION HEAT TRANSFER IN AN INTEGRAL SOLAR COLLECTOR STORAGE (ISCS)

submitted by **HADI AL-DAYYENI** in partial fulfillment of the requirements for the degree of **Doctor of Philosophy in Mechanical and Aeronautical Engineering, University of Turkish Aeronautical Association** by,

Assoc. Prof. Dr. Suat Dengiz
Dean, Graduate School of **Natural and Applied Sciences**

Prof. Dr. İbrahim Halil Güzelbey
Head of the Department, **Mechanical and Aeronautical Eng**

Prof. Dr. Cihan Karataş
Supervisor, **Mechatronics Eng, UTAA**

Assist. Prof. Dr. Wisam J. Khudhayer
Co-Supervisor, **Energy Eng, University of Babylon**

Examining Committee Members:

Prof. Dr. Ferhat Kadıoğlu
Aerospace Eng, Ankara Yıldırım Beyazıt University

Prof. Dr. Cihan Karataş
Mechatronics Eng, UTAA

Assoc. Prof. Dr. Munir Elfarra
Aerospace Eng, Ankara Yıldırım Beyazıt University

Assist. Prof. Dr. Reza Aghazadeh
Mechatronics Eng, UTAA

Assist. Prof. Dr. Durmuş Sinan Körpe
Aeronautical Eng, UTAA

Date: 25.12.2020

I hereby declare that all information in this document has been obtained and presented in accordance with academic rules and ethical conduct. I also declare that, as required by these rules and conduct, I have fully cited and referenced all material and results that are not original to this work.

Hadi Al-dayyeni

Signature:

ABSTRACT

EXPERIMENTAL AND THEORETICAL INVESTIGATION OF NATURAL CONVECTION HEAT TRANSFER IN AN INTEGRAL SOLAR COLLECTOR STORAGE (ISCS)

Al-dayyeni, Hadi
Doctor of Philosophy, Mechanical and Aeronautical Engineering
Supervisor: Prof. Dr. Cihan Karataş
Co-Supervisor: Assist. Prof. Dr. Wisam J. Khudhayer

December 2020, 117 pages

The current research includes a practical study of the thermal performance of solar collector integral storage system (ISCS) in which different types of heat exchangers are immersed in its enclosure for comparison. The first type is a straight tube heat exchanger (ST) and the other is a heat exchanger in the form of a coiled tube (CT). The effect of single and double glass layers and fluid flow rates inside the heat exchanger on the natural convection heat transfer of the ISCS system is experimentally evaluated by determining the temperature difference of inlet and outlet water through the heat exchanger immersed into the ISCS enclosure, the temperature distribution inside the enclosure, the ISCS efficiency, and the amount of thermal storage during evening times. Three sets of experiments are performed for a different water flow rates (1.0, 1.5, 2.0, and 2.5 LPM) inside the heat exchanger that is immersed in the thermally insulated enclosure and different glassing layers. The first set represents the presence of a heat exchanger in the form of a straight tube with a single glass was layer on the top face of the enclosure that is called (STSG). The second set uses a coiled tube heat exchanger with a single glass on the upper side of the enclosure and it's named (CTSG). The last set of experiments is

represented by a heat exchanger in the form of a coiled tube with a double glass on the upper face of the enclosure and it's abbreviated as (CTDG). At a water flow rate of 1.0 LPM, the CTDG exhibited higher temperature difference (28 C and 19.9 C than (19.4 and 11.4 C) for CTSG and (12 and 7.3 C) for STSG during the day and night times, respectively. The results reveal that the thermal efficiency (77.8%) of the (CTDG) case at a water flow rate of 2.5 Lpm was higher than the efficiency (56.6%) of (CTSG) case and that (39.7%) of (STSG) case. . It was also observed that the internal energy exceeds the amount of solar radiation during the day and provides thermal storage at night due to the complete isolation of the collector. The temperature measurements near the tube allow the calculation of the Rayleigh number during the heat transfer process, and empirical relationships haves been deduced for each set of experiments between the Nusselt number and the Rayleigh number.

Keywords: Heat Exchanger, Solar Water Heating System, Integral Collector Storage, Natural Convection, Single & Double Glazing.

ÖZ

ENTEGRAL GÜNEŞ KOLLEKTÖRÜ DEPOLAMASINDA (ISCS) DOĞAL KONVEKSİYON ISI TRANSFERİNİN DENEYSEL VE TEORİK YATIRIMI

Al-dayyeni, Hadi
Doktora, Makine ve Uçak Mühendisliği Anabilim Dalı
Tez Yöneticisi: Prof. Dr. Cihan Karataş
Ortak Tez Yöneticisi: Yrd.Doç.Dr.Wisam J. Khudhayer

Aralık 2020, 117 sayfa

Mevcut araştırma, farklı tipte ısı eşanjörlerinin karşılaştırma için mahfazasına daldırıldığı güneş kolektörü entegre depolama sisteminin (ISCS) termal performansının pratik bir çalışmasını içermektedir. İlk tip, düz borulu bir ısı değiştiricidir (ST) ve diğeri, sargılı bir boru (CT) formunda bir ısı değiştiricidir. ISCS mahfazasına daldırılan ısı eşanjöründen giriş ve çıkış suyunun sıcaklık farkı belirlenerek ısı eşanjörü içindeki tek ve çift cam tabakaların ve sıvı akış hızlarının etkisi deneysel olarak değerlendirilmiştir. muhafaza içindeki dağıtım, ISCS verimliliği ve akşam saatlerinde termal depolama miktarı. Isı yalıtımlı muhafaza ve farklı cam katmanlarına daldırılmış ısı eşanjörünün içinde farklı bir su akış hızları (1.0, 1.5, 2.0 ve 2.5 LPM) için üç set deney gerçekleştirilmiştir. İlk set, muhafazanın üst yüzünde (STSG) olarak adlandırılan tek bir cam tabakaya sahip düz bir tüp şeklinde bir ısı eşanjörünün varlığını temsil eder. İkinci set, muhafazanın üst tarafında tek bir cam bulunan ve (CTSG) olarak adlandırılan sarmal borulu bir ısı eşanjörü kullanır. Son deney grubu, muhafazanın üst yüzünde çift cam bulunan sarmal tüp şeklinde bir ısı eşanjörü ile temsil edilir ve (CTDG) olarak kısaltılır. 1.0 LPM'lik su akış hızında, CTDG, gündüz ve gece saatlerinde sırasıyla CTSG için

(19.4 ve 11.4 C) ve STSG için (12 ve 7.3 C) daha yüksek sıcaklık farkı (28 C ve 19.9 C) sergilemiştir. Sonuçlar, 2.5 Lpm su akış hızındaki (CTDG) durumunun ısıl veriminin (% 77.8) (CTSG) durumunun (% 56.6) ve STSG'nin (% 39.7) veriminden daha yüksek olduğunu ortaya koymaktadır. . Kollektörün tam izolasyonu sayesinde iç enerjinin gündüz güneş radyasyonu miktarını aştığı ve geceleri de termal depolama sağladığı görülmüştür. Tüpün yakınındaki sıcaklık ölçümleri, ısı transfer işlemi sırasında Rayleigh sayısının hesaplanmasına izin verir ve Nusselt sayısı ile Rayleigh sayısı arasındaki her deney seti için deneysel ilişkiler çıkarılmıştır.

Anahtar Kelimeler: Eşanjör, Güneş Enerjili Su Isıtma Sistemi, Entegre Kollektörlü Depolama, Doğal Konveksiyon, Tek ve Çift Cam.

Dedicated This Thesis to my country IRAQ, to the Ministry of Electricity, to My Parents and my family.

ACKNOWLEDGMENTS

Praise be to God, Lord of the Worlds, and May blessings and peace be upon the most honorable creation of Muhammad and his family. Firstly, I would like to thank God Almighty regarding grant me this great blessing and guiding me to complete my doctoral thesis successfully. I would like to express my special gratitude and sincere thanks to my supervisor Prof. Dr. Cihan Karataş and his assistant's Assist. Prof. Dr. Wisam J. Khudhayer and Assist. Prof. Dr. Mustafa W. JABER. Dr. Jaber gave me an excellent chance to work on the current study and supported me during their scientific advice and guidance through any stage of this study on the research project. Thank you to the supervising committee for their constant eagerness and interest in providing advice and guidance to me regarding my Ph.D. thesis. Thanks to Dr. Suat Dengiz and Dr. Masoud LATIFI-NAVID from Turk Hava Kurumu University. I also thank Dr. Ikhlas Al-FAYYAD for her great help in overcoming the difficulties of the practical side in a great way. I would like to express my sincere thanks to my dear father, Rasheed AL-DAYYENI. I always felt that he stood beside me at every step and cheering me up all the time. My sincere thanks to my mother, Safiya ABOOB, for not forgetting me in her prayers and her supplications. I also don't deny the role of my amazing wife Heba ABOOB in accomplishing the current study, who has always added a difference to my life and made it more beautiful, besides that she was always by my side when I needed her. Many thanks and gratitude to all my brothers and friends, and to everyone who supplemented this research, even with a word, and in particular to the late friend Saleh Abu Mahdi, may God have mercy on him, and he brought him into paradise. I would also like to extend my sincere thanks and appreciation to the Republic of Turkey and the Turkish people for their generous hospitality and fine morals throughout my stay with them. I express my sincere gratitude to the Ministry of Electricity and The General Company of Electrical Power Systems Rehabilitation. Finally, thanks to the University of Turkish Aeronautical Association.

TABLE OF CONTENTS

LIST OF TABLES

TABLES

LIST OF FIGURES

FIGURES

LIST OF ABBREVIATIONS

ABBREVIATIONS

ICS	:	Integral Collector Storage
ISCS	:	Integral Solar Collector Storage
ST	:	Straight Tube
CT	:	Coiled Tube
STSG	:	Straight Tube Single Glass
CTSG	:	Coiled Tube Single Glass
CTDG	:	Coiled Tube Double Glass
Lpm	:	Liters per minute
ave	:	Average
En	:	Enclosure
Ng	:	Number of glass
V	:	Average wind speed (m/s)
w	:	Wall

LIST OF SYMBOLS

SYMBOLS

f	:	Correction of heat transfer coefficient by wind
c	:	Correction coefficient of tilt angle
L	:	Long of the collector (m)
to.	:	Top of flat plate solar collector
bot.	:	Bottom of flat plate solar collector
ed.	:	Edge of flat plate solar collector
ba.	:	Back of flat plate solar collector
Q_u	:	Rate of useful energy gained (W)
Q_i	:	Internal energy inside the enclosure (W)
Q_{loss}	:	Total losses energy (W)
$Q_{to.}$	:	Top losses energy of flat plate solar collector (W)
$Q_{bo.}$	:	Bottom losses energy of flat plate solar collector (W)
$Q_{ed.}$	:	Edge losses energy of flat plate solar collector (W)
$t_{ba.}$	:	Thickness of back insulation (m)
$t_{ed.}$	:	Thickness of edge insulation (m)
$k_{ba.}$	:	Conductivity of back insulation ($W/m.K$)
$h_{C,b-a}$	:	Convection heat loss coefficient from back to ambient ($W/m^2.K$)
$h_{c,ed-a}$	:	Convection heat loss coefficient from edge to ambient ($W/m^2.K$)
ṁ	:	Mass flow rate of fluid flow(kg/sec)
C_p	:	Specific heat at constant pressure ($J/Kg.K$)
T_i	:	Inlet fluid temperature of the solar collector (°C)
T_o	:	Outlet fluid temperature of the solar collector (°C)
U_{in}	:	Input velocity of fluid (m/sec)
q	:	Heat transfer rate (w)
A_c	:	Surface area of the solar collector (m^2)
A_s	:	Cross-section area of pipe (m^2)
D_i	:	Tube inside diameter (m)
D_o	:	Tube outside diameter (m)

R_e	:	Reynolds number
R_a	:	Rayleigh number
g	:	Gravity acceleration (m/s^2)
β	:	Volume Expansion Coefficient $(1/K)$
ΔT_{sw}	:	Different surrounding wall temperature (°C)
Θ	:	Tilt collector angle (°)
υ	:	Kinematic viscosity (m^2/s)
α	:	Thermal diffusion (m^2/s)
N_u	:	Nusselt number
h	:	Local heat transfer coefficient $(W/m^2.K)$
K	:	Thermal conductivity $(W/m.K)$
U_L	:	Overall heat loss coefficient based on collector area $(W/m^2.K)$
T_p	:	Plate temperature (°C)
T_a	:	Ambient temperature (°C)
T_{ave}	:	Average temperature (°C)
h_w	:	Wind heat transfer coefficient $(W/m^2.K)$
$T_{p.ave}$	:	Average plate temperature (°C)
$T_{a.ave}$	:	Average ambient temperature (°C)
h_{fi}	:	Heat transfer coefficient inside absorber tube $(W/m^2.K)$
ρ	:	Density (kg/m^3)
μ	:	Viscosity $(N.s/m^2)$
υ	:	Kinematic viscosity (m^2/s)
ε_p	:	Absorber plate emissivity
ε_g	:	Glass emissivity
σ	:	Boltz man constant =5.67 * 10^{-8}
β	:	Tilt collector angle (°)
η	:	Collector efficiency
τ	:	Transmittance
α	:	Absorptance
δ	:	Thickness of plate (m)

CHAPTER 1

INTRODUCTION

1.1 Overview

The sun produces enormous quantities of energy called (Solar Radiation) every second. Sunlight (47 percent), infrared radiation or heat (46 percent), and ultraviolet rays (7 percent) are radiated into space as energy. Just the Earth, one part in a billion, intercepts a small portion of the energy but this amount is still enormous. To fulfill the needs of the fire-heated water for bathing, washing, and cooking, in the past the water must be heated by fuel, but today, some utility companies integrate the wind and sun renewable energy systems into their production of energy.

One of the applications of the solar energy is the solar water heating systems, some of them used the collector as the storage tank without providing a pump to circulating the water inside the collectors, where it depends on the natural convection process. In the immersed heat exchanger & collector, mechanisms of the heat transfer are conceived as the interaction of negatively formed buoyant plumes in a heat exchanger boundary layer and a large-scale buoyant flow inside the collector storage center. However, the thermal stratification inside ICS, the geometric parameters (the enclosure inclination, the aspect ratio, and the relative size and location of heat exchangers) and the incoming solar radiation magnitude will assess types of mixing in the collector storage fluid [1].

1.2 Natural Convection

Natural convections are processes or methods of the transport of heat in which no external source (such as a fan, pump, suction system, etc.) induces fluid movement, but just density variations in the fluid that occur due to temperature gradients. In the

natural convections, the fluids surrounding the heat sources receive heat and become less dense and rises due to thermal expansion, then move for replacing the colder fluid above. The colder fluids are gradually heated and the process proceeds to form the convection current, which moves heat energy from bottoms to tops of the convection cells. For natural convection, driving forces are buoyancy, the product of fluid density differences, and so the existence of suitable acceleration, like equivalent force, or gravity resistance (centrifugal force, acceleration, and/or Coriolis impact), is necessary for natural convection. Natural convection, ex., fundamentally doesn't work in inertial (free-fall) conditions, like those of the orbiting International Space Station, where other methods of the transfer of heat are necessary to avoid overheating of the electronic components.

Because of its role in both engineering and nature applications, natural convections have gained a huge deal of interest from scientists. In nature, a big aspect of all systems of weather is convection cells produced from air growing over sunlight-warmed water or soil. In the rising plume of the hot air from tectonics of plate, fire, sea-wind formation, and ocean currents (thermohaline circulation) (where upward convection too is adjusted by the forces of Coriolis), convection is also seen. In the engineering usages, the convection is typically visualized in the micro-structures creation through fluid flows around shrouded solar ponds, fins, and heat-dissipation and the cooling of the molten metal. Free air cooling without any of the help of the fan is too general manufacturing use of natural convection: this may happen on small-scales (chips of the computer) of large-scale processing equipment [2-13].

1.3 Solar Water Heating Systems

Systems of solar water heating use the sun for heating either the heat-transfer fluids or water in collectors. An unshaded, south-facing location (typically a roof) is the best site for the collectors. In the tank close to the electric or traditional gas water heaters, then the heated water is collected.

The work of solar water heaters depends on the water temperature entering the system and on the availability of solar energy at the site. The colder the fluid, the more effectually the system operates. Approximately any climate, a conventional backup system is necessary.

Water conservation measures are a good way to reduce the overall hot water demand in a residence. Some examples include installing low-flow shower-heads, placing flow restrictors and aerators on the faucet, and managing water levels in household appliances. Lowering the thermostat on a water heater is another way to reduce the energy required for water heating [14-16].

1.4 Types of Collectors in Solar Water Heating Systems

There are 3 main types of collectors: concentrating and evacuated-tube, flat-plate, collectors. The flat plate collector is the insulated, weatherproof box involving the deep absorber plates under 1 or more translucent or transparent covers as shown in Figure 1.1. The small tube runs during the box and carries the fluid to be heated. The tube is connected to deep absorber plates. As heat builds up in collectors, it raises the temperatures of the fluids passing during tubes. This is the most common type of collector.

Evacuated-tube collectors were made up of rows of parallel and transparent glass tubes stored in the rigid boxes. All tubes consist of the glass inner and outer tubes, or absorber, covered with the selective coating that absorbs solar energy. The air is evacuated from the space between tubes for forming the vacuum, which eliminates conductive and convective heat loss. The fluid in these tubes may reach extremely high temperatures, which makes them suitable for industrial or commercial uses.

Concentrating collectors are usually parabolic troughs that use mirrored surfaces to concentrate the sun's energy on a tube containing the heat-transfer fluid [17-28].

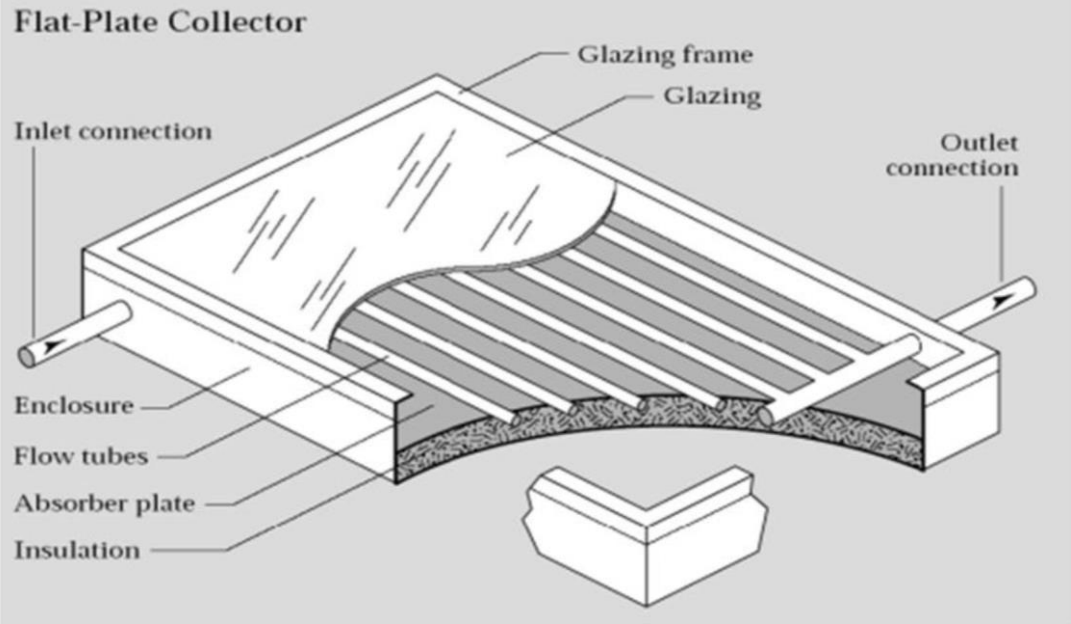

Figure 1.1: Flat-plate collector [20].

1.5 Classification of Solar Water Heaters and Primary Characteristics

The solar water heater needs a well-insulated storage tank. Different systems place the solar storage tanks in series with traditional water heaters. However, in the current design, the solar water heaters preheat water before they enter a traditional water heater.

Table 1.1. & 1.2. Summarizes the Primary Characteristics of different types of systems of solar water heaters [29-30].

Table 1.1: Classification of Systems of the Solar Water Heater (Active) [29-30]

	DIRECT Water heats in collectors flow directly to taps of hot water.	**INDIRECT** Heat transfer fluids, which include the heat exchangers, are separate from a home water source.
ACTIVE The electric pump was employed to circulate fluids that absorb heat.	**The Drain down System** Water was pumped between the storage tanks for hot water and the collector panels. The freeze protection is offered by a temperature sensor electric drain down valve draining water from the collectors and exposed plumbing until the freezing temperature is reached. Water fills up into the drain of a building. When temperatures rise above zero, the machine refills automatically with the water. The offer defenses for freeze (see Figure 1.3) [29]. **The Direct (Open Loop) System** Between storage tanks and collector panels, the pump circulates heated water. The device has very little protection from frost. It can be set up to provide minimum security against freezing or employed for 3 seasons & shutdown in the winter. Not acceptable with the hard water [30].	**The Pressurized Glycol (closed-loop) Anti-freeze System** Via solar collector panels, anti-freeze fluid is pumped and moved during the heat exchangers to the water storage tanks. Offers defense for freeze (see Figure 1.2) [29]. **The Drainback System** Between the storage tank and the collector panel, anti-freeze or distilled water (DW) circulates and was drained from the device during the freeze. The fluid in the collector panels was different from the supply of home water and when drained, was stored in the holding tank. The gravity mechanism drains without the employe of the electric drain valves. The heat exchanger is required to move heat to the storage tanks (see Figure 1.4) [30].

Table 1.2: Classification of Solar Water Heating Systems (Passive) [29-30]

	DIRECT Heated water in the collector flows directly to a tap of hot water.	**INDIRECT** Heat transfer fluid, which includes the heat exchanger, is separate from a home water source.
PASSIVE The movement of hot water or heat transfer fluids relies on natural convection. No electric pump whatsoever.	**The ICS (Integral Collector Storage) System** There are a storage tank and a hybrid solar collector. Such systems are less costly and quick, but require a greater loss of heat at night and do not provide sufficient protection against freezing. it is the most popular type of home-made solar water heaters (see Figure 1.5) [30]. **The Thermosiphon (Direct) System** Usages of the storage tank and the solar collector panel. Through natural convection, the hot water circulates from the collectors to the tanks. The tanks must be at least (18 in) elevated above the collectors. Not appropriate for locations that are cold or have hard water. (Can be changed with the pump, making it the direct open) device to protect freezes in locations where freezes are very limited) (See Figure 1.6) [30].	**The Thermosiphon System** Usages of the storage tank and the panel for solar collectors. In the collector panel, anti-freeze fluid is spread and heat is transferred through the heat exchangers to the water storage tank. The tank must be at least (18 in) elevated above collectors. Reasonable for places that freeze. Nevertheless, the performance is poor. [29].

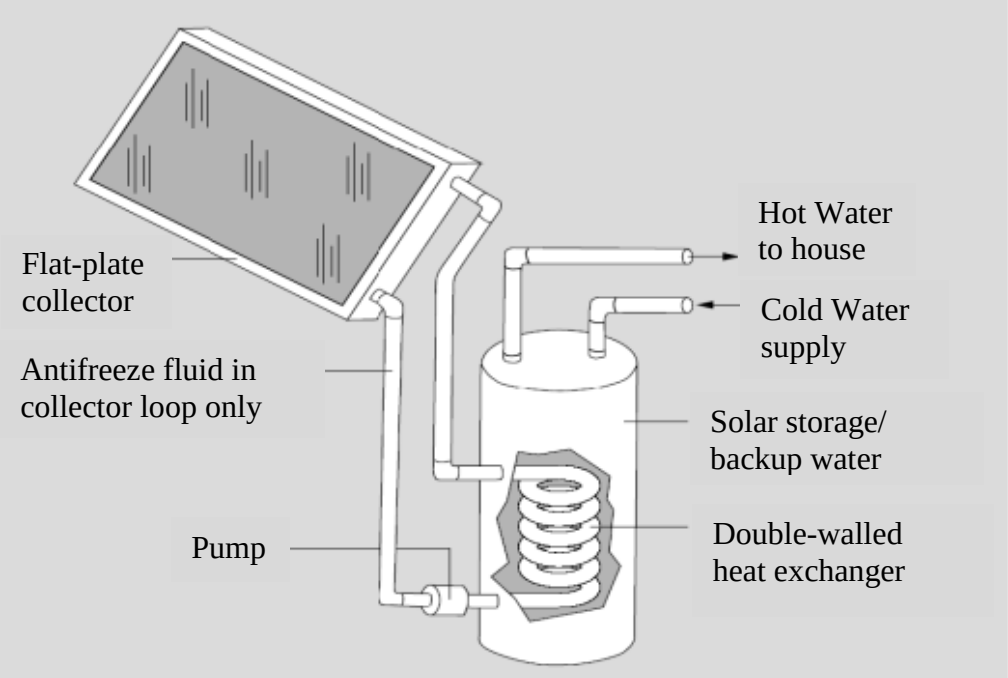

Figure 1.2: Active, closed-loop solar water heating system [30].

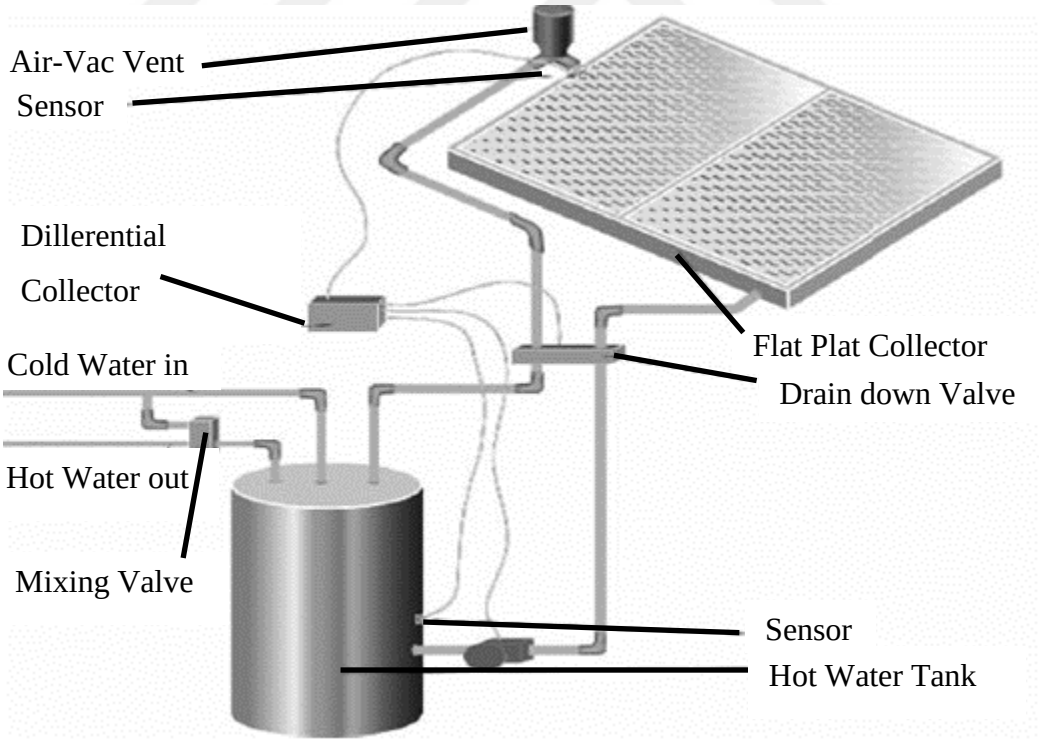

Figure 1.3: Drain down system is a direct active solar water heating system [30].

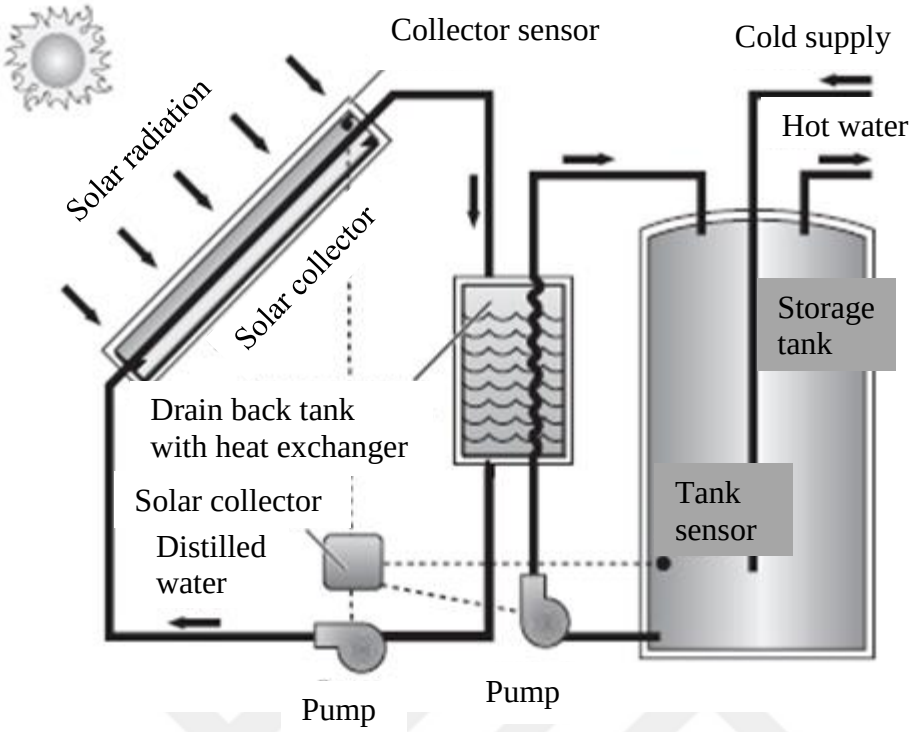

Figure 1.4: Drain back solar water heating system [30].

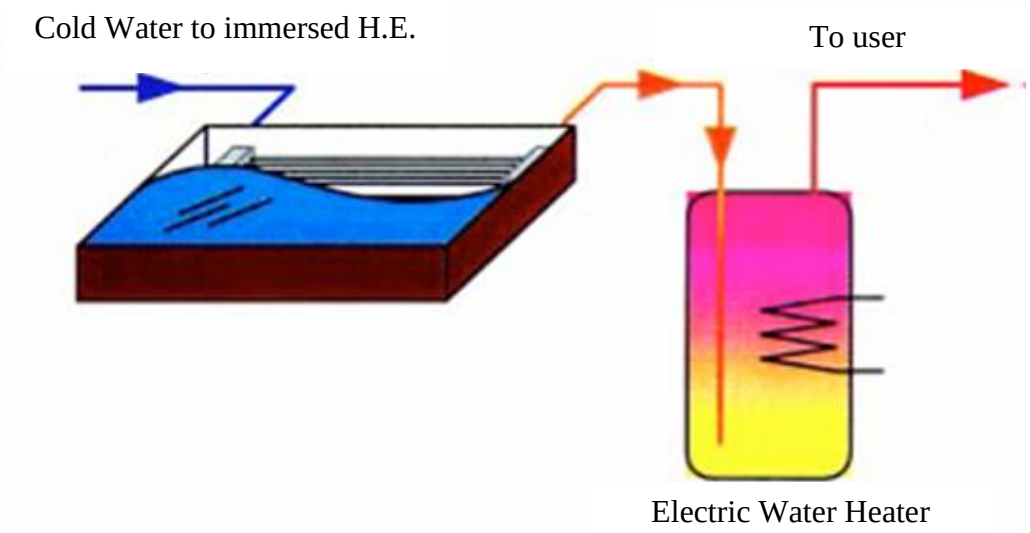

Figure 1.5: Conceptual sketch of a suggested integral collector storage solar water heater with the immersed heat exchanger [30].

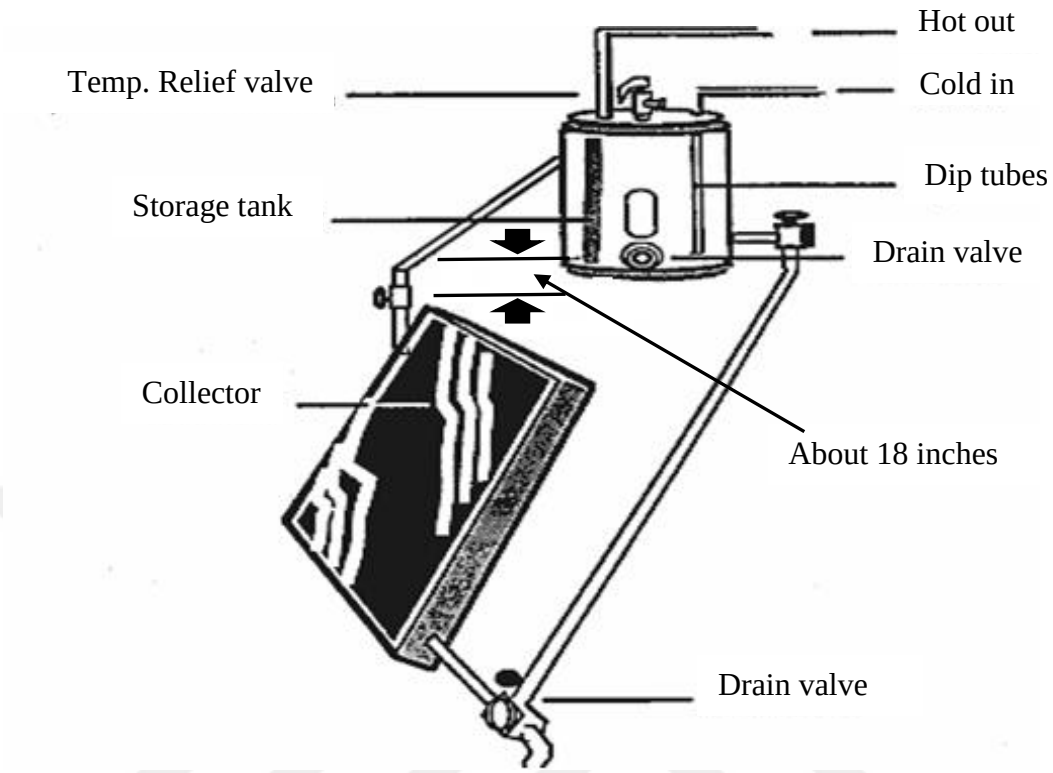

Figure 1.6: Thermo siphon Solar Water Heating System [30].

1.6 Integral Collector Storage (ICS) Systems

The ICS is a batch type system in which the household water is directly heated by the sun and storage tanks serve as solar collectors. Batch water heaters were passive devices wherein the hot water was supplied to a point of usage by using the pressure of water in houses or storage tanks from the solar heated tank.

Of all the different solar water heaters, the most widely designed and used by homeowners are batch systems. They are less costly, particularly when they are residence, are often made of recycled material, and have several components. Usually, the batch system composed of 1 or more tanks covered with black & sealed in the insulated enclosure, with the glazed side cover facing the sun, shown in Figure 1.7 [31].

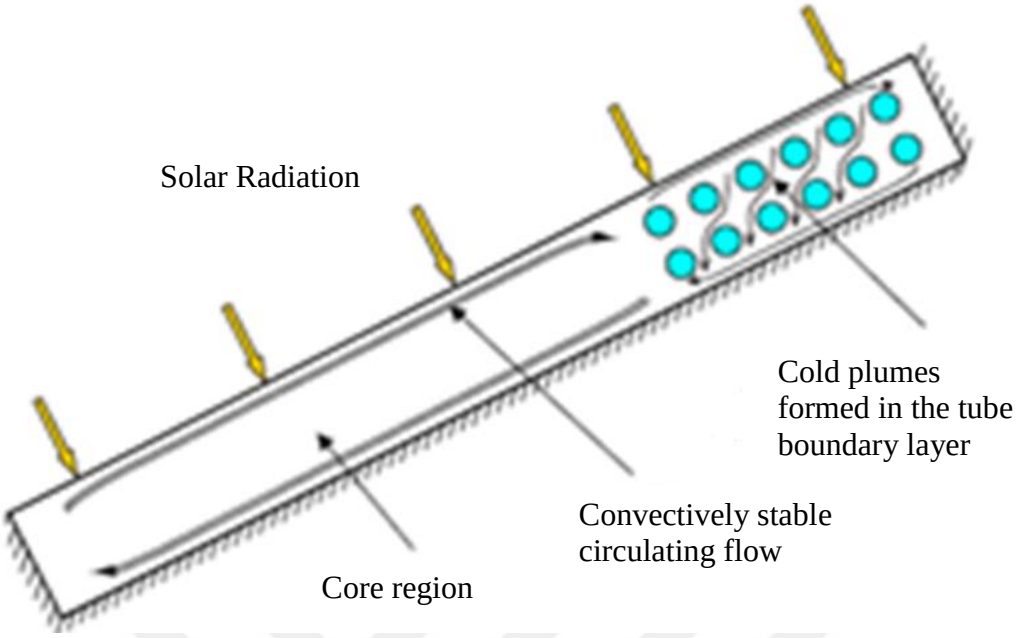

Figure 1.7: The collector flow is intended to communicate with small-scale negative buoyant plume generated in boundary layers of heat exchangers and the large-scale circulating flow in the storage fluids center. [31].

1.7 Heat Exchanger

A system used for thermal transfer among fluids is a heat exchanger. There are two types of heat exchanger. The first is a direct contact of liquids and the second one is to prevent mixing. They are commonly used in air conditioning, refrigeration, natural-gas processing, space heating, and refineries of petroleum, petro-chemical plants, treatments of sewage, chemical plants, and power stations. In internal combustion engines, the classic example of the heat exchanger is seen in which the circulating fluid known as motor air flows past the coils and coolant passes through radiator coils, which heats the incoming air and cools the coolant [32].

1.8 Objectives

The main objectives (experimental work) of this research can be divided into several points as follows:

1) Manufacture of two types of heat exchangers (immersed in the enclosure), the first is a straight tube and the second is a coiled tube.
2) The use of two cases when doing experiments for each model of heat exchangers, the first using single glass and the second using double glass.
3) Study effects of changing the rate of flow.
4) Study the efficiency of experimental work when using every case and model of heat exchangers at every flow rate.
5) Establishing non-dimensional relationships for each case.
6) Study the amount of thermal storage for this project and compare the change of all the above parameters.
7) Study the real effectiveness of solar energy and its effect on increasing the internal energy of the (ISCS).
8) A study of improving heat transfer by natural convection due to the effect of all of the above.

CHAPTER 2

LITERATURE SURVEY

2.1 Preface

One of cleaner sources of the renewable energies is solar energy. The enhancement of heat transfers in the solar devices is one of the main issues in the compact designs & energy conservation. Previous researchs will be classified into several groups depending on the factors studied in the current research.

2.2 The Effect of Heat Exchanger Types in Systems of Solar Water Heating

Wei Liu et. al., 2002 [31] studied the rates of heat transfers of the single horizontal tubes immersed in the water-filleds enclosure tilted at 30°. For the solar water heating devices with the heat exchangers submerged in the integral collector storages, the results serve as a base case. Experiments have been performed for both uniform and adiabatic heat flux boundary conditions for stratified and isothermal enclosures. From calculated distributions of water temperature, the natural convection flow in enclosures was described. The formation of a suitable difference in temperature that drives natural convection was calculated. Correlations in the numbers of Rayleigh and Nusselt for the overall heat transfer coefficients are shortened to the following shape NuD= 0.675 $Ra_D^{0.25}$ for $10^6 \leq$ RaD$\leq 10^8$.

The rates of heat transfers of the single horizontal tubes submerged in the water-filled enclosures tilted at 30° were investigated experimentally [33]. The results also serve as the base case for the solar water heating device with the heat exchangers submerged in the integral collector storages. The tests were carried out under the uniform and adiabatic heat flux boundary conditions for isothermal and stratified

enclosures. From calculated distributions of water temperature, the natural convection flow in enclosures is described. The formation of suitable differences in temperature that drives the natural convection was calculated. Correlations in the numbers of Rayleigh and Nusselt for the overall heat transfer coefficients are limited to the state shape NuD=0.675$RaD^{0.25}$ for 9X10^5<RaD<4X10^7.

W. Liu et. al., 2004 [34] evaluated the coefficients of the natural convection heat transfers for the rectangular array of 8 tubes integrated in the thin enclosures of the ratio 9.3:1.0 and inclined at 30 degree. However, the experiments were carried out the range of modes od the transient operating typical of the load side heat exchangers in un-pressurized integral collector-storage devices as shown in Figure 2.1. Water is a working fluid, and by a continuous heat flux on upper boundary, thermal charging is achieved. The other borders are all well enclosed. For the overall Nusselt number, results for stratified & isothermal enclosures yield the next correlations: NuD=(0.7286±0.002)$RaD^{0.25}$, 4.0X10^5<RaD<1.4X10^7.

From calculated temperature distributions, the flow fields in enclosures are assumed. Also, the temperature differences that drive natural convection are calculated. For the state of the single tubes, the results expand earlier work and provide a restrictive case of the datum of heat transfers for the tube bundle that occupies the collector storage upper portions. The larger numbers of Nusselt in the tube bundle were due to better fluids motion in the bundle and the greater momentum in the approaching flow from the lower location of enclosures and higher rates of overall circulation compared to Nusselt numbers for the single tube.

The heat transfer and transient fluid dynamics in the inclined adiabatic water-filled enclosures with the submerged cylindrical cold sinks have been studied in the dimensionless scale analysis and the 3D model [35]. The integral collector storage device with the submerged heat exchangers reflects the geometry. The model enclosure is inclined at 30degrees and has an aspect ratio of 6:1. The scale analyses of the process of transient heat transfers identify 4 temporal times: quasi-steady, conduction, decay & fluctuating. Moreover, the general forms of the volume-

averaged water temperatures in enclosures and the transient number of Nusselt are given. By isothermal contours and presenting instantaneous flow streamlines during each transient period, insight into the thermal processes and transient fluid is given. Two distinct regions consist of the flow area. The zone is almost static above the cold sink.

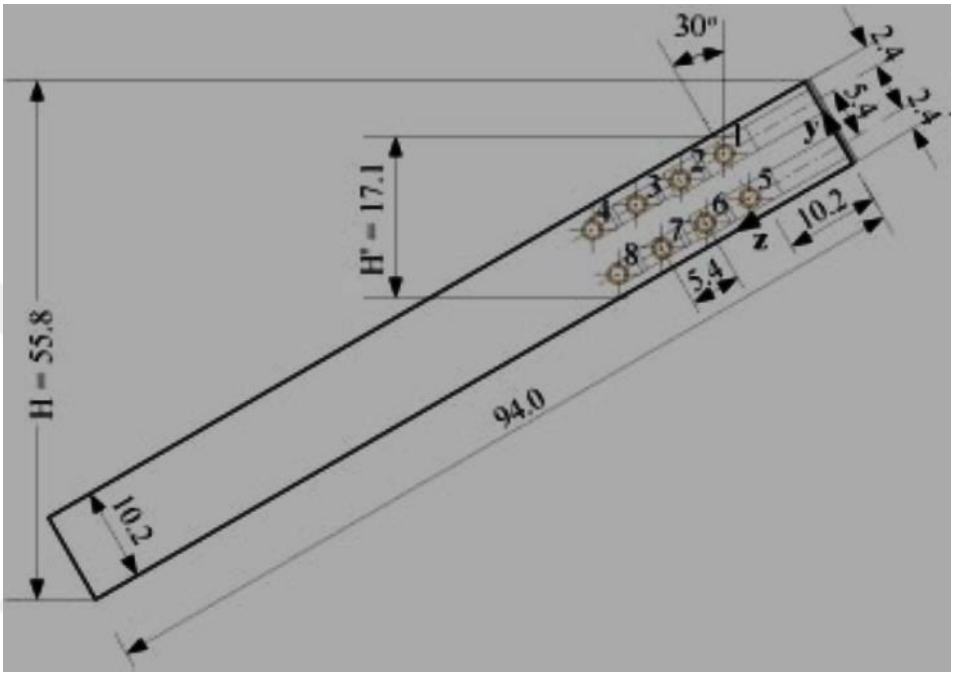

Figure 2.1: Cross-section of the experimental ICS with submerged tube bundle [34].

One of the strong blending and recirculation triggered using cold plumes produced in boundary layers of cylindrical sinks is the larger region below the sink. Correlations between the expected dimensionless volume-averaged tank temperatures & the transient number of Nusselt compare positively to previously measured results. In contrast to that of the cylinder in the unbounded fluid, fluid motion in enclosures increases heat transfers.

Finally, W. Liu et al., 2005, [36] studied the natural convection in enclosures that represent the device of the ICS (integral collector storage) with the submerged tube-

bundle heat exchangers. The heat transfer coefficients of bundles of 240tubes contained in the thin enclosures of the aspect ratio of 9.3:1.0 & inclined at 30 degrees to the horizontal were taken for the range of models of transient operating and ratios of pitch-to-diameter of 3.3, 2.4 & 1.5. The results of the stratified and isothermal enclosures yield the correlations of the overall number of Nusselt NuD=(2.45±0.030)$RaD^{0.188}$, 230<RaD<9800. Moreover, the Rayleigh number's signature temperature differences are that between the temperatures of tube walls and the rated temperature of the water within the bundle. For the eight-tube bundle and the promised single-tube, the Nusselt figures are 3 times greater than those. This rise is due to higher fluid flow inside the package and higher overall rates of large-scale circulation in enclosures. William Logie et al., 2010 [37], current implementation of IHX (Immersed Coil Heat Exchanger) into systems of SDHW (Solar Domestic Hot Water) employ simple guidelines based on the planned solar collector zone to dimension their surface zone - or range thereof. However, the literature from which these guidelines come (1970 s and 1980s) is focused on tests with several models of IHX (copper, flange-retrofitted) to those employed today and is assumed entirely on the efficiency of heat transfer, so it is considered important to re-evaluate the current guidelines. The study posed the attempt to integrate stratification evaluation and the heat transfer efficiency based on measurements from 3 samples of IHX with geometric arrangements of different materials. The correlation between low stratification efficiencies and high convective heat transfer coefficients is indicated by preliminary research.

At heating, the nuclear industry, ventilation, heat recovery process plants, & air conditioning devices, the coil, and shell heat exchangers are widely used. Easy design, the high heat transfer, and the low value of pressure drop support this form of the recuperator. In a helical coil, because the curvature of tubes results in growth, centrifugal force acts on the moving fluid. Owing to the secondary flow occurrence in the planes normal to the major flow within helical structures, the heat transfer in helical tubes has long been established to be much higher than in the straight ones. In the heat transfer augmentation, helical tubes display great efficiency, whereas the

uniform curvatures of the spiral structures in heat exchangers are uncomfortable in the installation of pipe. The authors also introduced their tube & shell heat exchangerS construction with the enhanced heat transfers. The current paper aimed to evaluate the impact of the modification of the surface on the completion of the coefficient and quality. The tests of the steady-state heat transfers have been conducted. For turbulent and laminar flow, both of countercurrent and co-current-flow arrangements, test data points were obtained. The number of transfer units analysis applied to the shell-side authors to find optimum heat transfer intensification [38].

A. Siddique Ahmed Ghias et. al. 2016 [39], the numerical work and the experimental investigation of properties of the coil heat transfers in heat exchangers of the shell. Using FLUENT, the numerical study of the heat exchanger has been done. The impacts of the changes in the tube shape on heat transfers were investigated. For the current issue, the helical coil has been manufactured and designed. The distinction between this and previous studies is that the coil geometry is unique. Previous studies have just used a single helical coil stretch, but there are two helical coil sets linked by a narrow straight tube in this case. The designed heat exchanger is a counter-following arrangement to optimize the amount of heat transferred. During the experiments, the rate of flow of shell side was kept constant with varying the side flow rates for each tube and the readings have been collected for various temperatures. To take values of the convective coefficient of heat transfers, the Wilson plots have been plotted. The findings showed that the values of the number of Nusselt and the friction factor were within reasonable theoretical value limits.

2.3 Effect of Single & Double-Glazing

In the thermal energy form, the solar energy derived from the sun can be converted into usable energy. The solar flat plate collector is 1 of the most powerful methods of heating water. Also, for domestic as well as industrial applications, this heated water can be used. Collector efficiencies depend on different parameters, like the

glass cover number, the collector area, the velocity of winds, and the overall coefficient of top heat loss. However, the traditional solar flat plate collector has been enhanced with double glazing arrangements to decrease top loss heat transfer coefficients and maximize heat transfer. The adapted solar collectors have been installed at a 12-degree latitude angle facing north-south directions. The assays were conducted from 10:00 to 16:00 hrs under the thermosiphon theory. The current results exhibit that the heat transfer coefficient has slightly decreased overall top losses and 68 percent collector efficiency has been obtained. Also, the flow pattern was investigated using the analysis of CFD [40].

J. Manikandan and B. Sivaraman, 2016 [41], evaluated experimentally the efficiency of DGFPSWH (the double glazed flat plate solar water heaters), and SGFPSWH (the single glass flat plate solar water heaters). As flat absorber plates, galvanized Fe sheets (1.420 x 0.70 m2) were used. For SGFPSWH, a glass plate of the same size has been employed as a top cover and for DGFPSWH, 2 glass plates of the same size with a gap reached 2 cm have been employed as glass plates employed to shield the heat loss from absorber plates to the atmosphere. The DGFPSWH and SGFPSWH performance at various rates of mass flow (0.0125, 0.00830, 0.0041 kg/s) have been done and recorded. The thermal efficiencies are found to be lower for the SGFPSWH than the DGFPSWH.

H.Vettrivel and P.Mathiazhagan, 2017 [42], performed an experimental study to decrease the overall top loss heat transfer coefficients and enhance the efficiency of solar collectors. To evaluate the overall top loss heat transfer coefficient (Ut), the double glaze method has been implemented and gaps between absorber plates and the glass covers (1) and the glass covers (2) have been optimized. Solar flat plate collectors with the double and single glazing were produced with the same dimensions & mounted at the 12th-degree latitude angle facing the direction of N-S. The test with the thermosyphon theory was performed between 10.00 AM and 4.00 PM. The results indicate that, relative to single glazing devices of the same solar strength, the efficiency of double glazing is greater. The higher efficiency is due in

double glazing devices to the reduction in the average top loss heat transfer coefficients.

Moreover, based on the above literature, it can be candidly seen that there were few studies fixated on evaluating the performance of the integral solar collector storage devices ISCS, and a more in-depth investigation is required. Thus, it is useful for evaluating the thermal efficiency of ISCS devices using different configurations of heat exchangers that are immersed into its slanted, thermally insulated enclosure. On the other hand, an experimental study is also required to demonstrate the effect of single and double glazing layers of the ISCS enclosure on the heat storage capacity as well as the transfer of heat by natural convection of the device of solar water heating from the enclosure to the heat exchanger at the discharge.

CHAPTER 3

EXPERIMENTAL APPARATUS AND PROCEDURE

3.1 Introduction

The investigation of the tests has been done to evaluate the effects of the heat exchangers types (straight tube and coiled tube) immersed in a storage enclosure as well as the single and double glazing factor of the enclosure on natural convection heat transfers within systems of solar water heating. To meet these experimental objectives, accustom-made apparatus is designed and installed and a detailed experimental procedure is presented as characterized in the next sections.

3.2 Experimental Apparatus

Figures 3.1 & 3.2 shows the Experimental Apparatus consist of seven parts explained as follows:

Figure 3.1: Front view of the ISCS experimental apparatus.

Figure 3.2: Side view of the ISCS experimental apparatus.

3.2.1 The Storage Enclosure

The enclosure is a rectangular Galvanized sheet iron (corrosion resistible) with a thickness of 1.5 mm. The inside dimensions of the enclosure are 122cm (width) × 94cm (length) × 11cm (depth). The top side (front plate) of enclosures was the removable door through which the instrumentation and heat exchanger was mounted. However, the ports enclosure (0.5 mm diameter) for the thermocouples insertion are located along the bottom face. An additional Port with a diameter of 25 mm is used to drain the enclosure. The big upper face is used as a base of the glass facing solar rays. The internal surfaces of enclosures are painted with a black paint that absorbs waves of solar radiation and reflects the long waves. Figures 3.3 & 3.4 show the storage enclosure.

Figure 3.3: Demonstrates the storage enclosure.

Figure 3.4: Close view of the position of the glass in the enclosure.

3.2.2 Removable Door

The removable door is made from the same metal as the enclosure. It is used to insert the heat exchanger inside the storage enclosure and there is a valve that controls the flow of water into the enclosure and contains a slot for air ventilation from the enclosure during fill-up as shown in Figure 3.5.

Figure 3.5: The removable door.

3.2.3 The Enclosure Inclination Base

The inclined base is manufactured to give the desired degree of inclination of the enclosure which is about 45˚ depending on the Baghdad latitude. The base consists of an angular steel plate with dimensions of 6 mm (thickness) and 6 cm (width) and its height from the Earth's surface is approximately 1 meter as shown in Figure 3.6.

Figure 3.6: Inclination Base.

3.2.4 The Insulation

The heating element and enclosure are insulated from the bottom and all peripheral sides for minimizing the heat loss from enclosures. The insulation has a low conductivity and consists of two layers with different thicknesses; the first layer is polyolefin foam (Thermo break) 5 cm thick and the thermal conductivities reach 0.032 W /m.K. While the second layer is Aluminum-foil with emissivity reaches (0.02). The plywood box with the thermal conductivities of 0.19 W / m.K fixes the enclosure reduces the heat loss from the bottom and peripheral sides of the enclosure as shown in Figure 3.7.

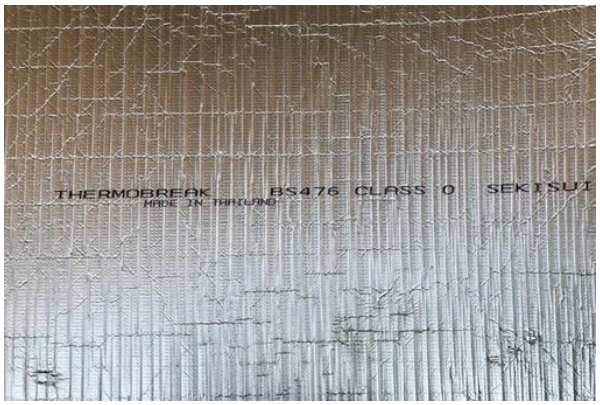

Figure 3.7: Insulation.

3.2.5 Water Storage Tank

The tank of water storage was mounted to provide water to heat exchangers as a water delivery source. The tank is in the cubic form of one m^3. It is made from plastic and insulated by fiberglass 2cm (thickness). Figure 3.8 shows the water storage tank.

Figure 3.8: Water storage tank.

3.2.6 Glazing

Figure 3.9 shows the glass – type (hardening window glass) fixed on the wooden box front face. It is 6 mm thick and has dimensions of 1.25m X 0.98m with a reflection percentage or poor refraction and a high degree of transparency.

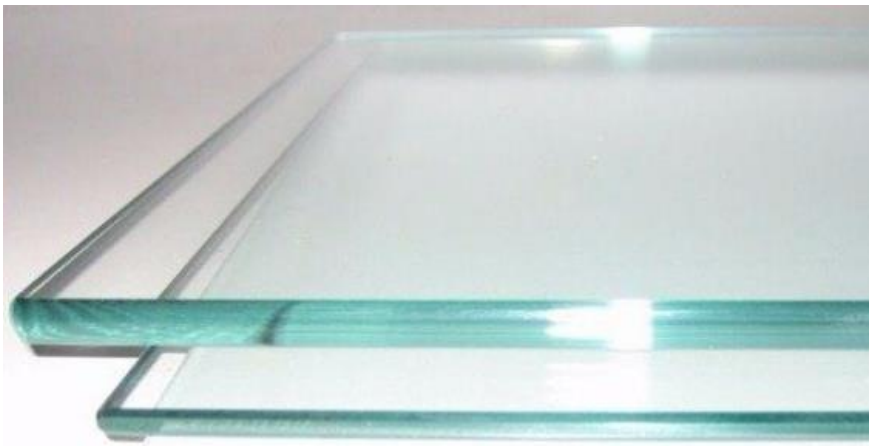

Figure 3.9: Hardening window glass.

3.2.7 Pump

Figure 3.10 exhibits the pump with two speeds work, frequency (50HZ) and voltage (230V) that is employed in this research. The pump has been employed for continuity of flow into the heat exchanger of the integral solar collector storage at a fixed flow average.

Figure 3.10: The pump.

3.2.8 The Heat Exchangers

Two heat exchangers are used. The first heat exchanger is the straight tube, while the second model is the coiled tube. The tubes of the heat exchanger used in the present research are made from copper material with thermal conductivity of386 W/m.oC for each heat exchanger type. The straight tube configuration consists of a horizontal and two vertical tubes mounted into the enclosure. The horizontal tube is 1000 mm (long) × 23mm (inner diameter) × 25mm (outer diameter) and each vertical tubes is 11.6 cm (long) × 23mm (inner diameter) × 25mm (outer diameter). The coiled tube configuration consists of a horizontal coil tube and two vertical tubes mounted inside the enclosure. The horizontal tube is 1000 mm (long), the diameter of the roll is 80

mm, and the outer and inner diameter of the pipe of the coil is 9.2 mm and 8.7 mm respectively. Each vertical tubes is 11.6 cm (long) and the outer and inner diameters are 9.2 mm, 8.7 mm respectively as seen in Figures 3.11 & 3.12.

Figure 3.11: Straight tube.

Figure 3.12: Coiled tube.

3.3 Measurements and Instruments

3.3.1 Temperature Measurements

Figure 3.13 exhibited the chromel-constantan known Type–K thermocouple employed for measuring the temperatures of the inlet & outlet water flowing inside

heat exchangers as well as temperatures of water stored inside the ISCS set-ups. The thermocouples are distributed as flows:

Figure 3.13: Type – K thermocouple.

1. (21) Ports with a diameter of 5 mm are distributed at the bottom face of the enclosure for insertion of thermocouples inside of the enclosure for measuring temperatures of water at various points. 9 thermocouples are situated in the midline (y-z) in enclosure (x=0), while twelve thermocouples are located along horizontal lines in a mid-plane (y-z) (x = 0) of (z= 47 cm) as shown in Figures 3.14 & 3.15. To prevent water leakage from the ports of thermocouples, epoxy resin is used.

Figure 3.14: How to put thermocouples.

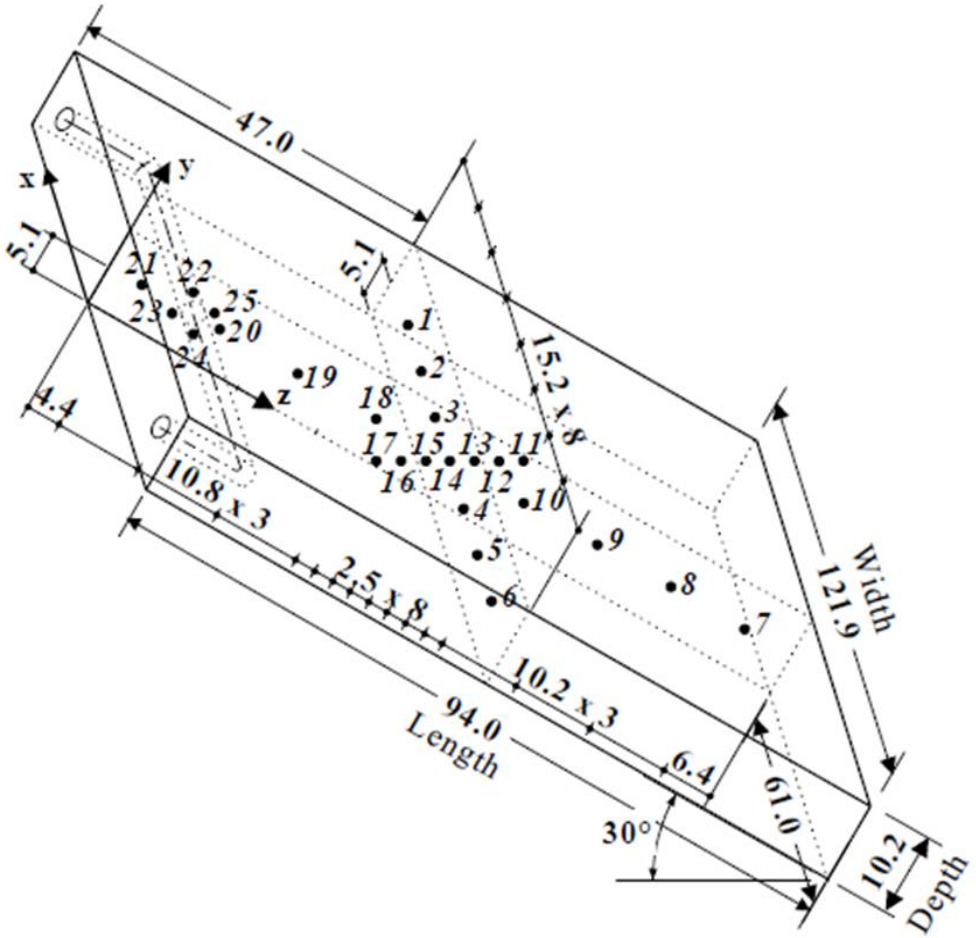

Figure 3.15: Thermocouples are located along horizontal lines in a mid-plane(y-z) (x=0) of (z= 47 cm).

2. Temperatures of water surrounding the tube heat exchanger are assumed with two thermocouples probes placed at (180˚) increment (120 mm) on outside tube walls. However, to calculate the wall tube temperature (Tw), 2 thermo-couples are fixed at (180˚) increment in (1.1 mm) deep on the wall of the tube. As shown in Figure 3.16.

Figure 3.16: Water temperatures surrounding the tube heat exchanger.

3. Two thermocouples are employed for measuring the water temperature at the outlet and inlet water flows within the tube heat exchanger.
4. Thermo-couple employed for calculating temperatures for surrounding.
5. Thermo-couple employed for calculating temperatures of the enclosure from bake.
6. Thermocouple used to calculate temperatures of insulation.
7. Thermocouple used to calculate temperatures of the first glass.
8. Thermocouple used to measure the temperature of the second glass.

3.3.2 Temperature Recorder

Thermo-couple measurements were taken and transmitted to a computer via the temperature recorder (Appellant AT4532x) 32-128 channels (USB disk storage), the specifications of it shown in Figure 3.17 and table3.1.

Figure 3.17: Temperature recorder.

Table 3.1: The specifications of the temperature recorder.

Graduation	Thermo-couple /K /T /E /S /N /B /R
Ranges	-200 °C to~1300 °C （Varying depends on the graduation）
Accuracy	0.2%+1℃
Channel	32channels; Can be expanded to 128channels
The resolution	0.1°C
The speed	Fast100 MS/ channel Medium：500 MS/ channel Low：1second/channel
Comparator	High/low beep Individual setting high/low value for all channels
The correction	Autocorrect for all channels (Auto Calibration)
The interface	ATS45 data acquisition software
	RS232C interface U-disc interface USB communication interface
Cold Junction	Accuracy:0.5℃
	Power：10 VA, Frequency：50 Hz/ 60 Hz, Voltage 85 VAC to～260 VAC
	Broken thermo-couple checking function, TFT-LCD True-color LCD
	ATS45 data acquisition software, AT4532: K thermocouple 32 teams(2m/team)
	21.6cm(Width)x30cm(Depth) x8.8cm(Height) , 3 kg

3.3.3 Flow Meter

The flow meter seen in Figure 3.18 during the experimental work was employed to calculate the water flow rate. With a precision of ±5 percent, the range flow meter is 0.5-4Lpm.

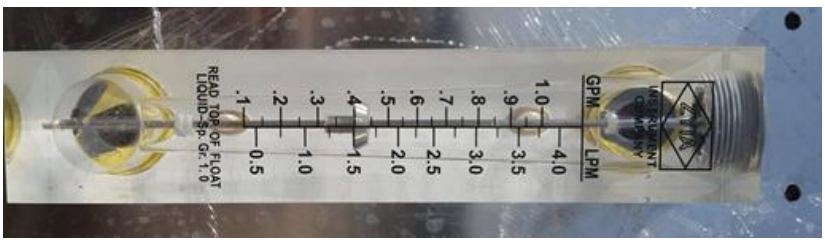

Figure 3.18: Flow meter.

3.3.4 Solar Power Meter

Figure 3.19 exhibits the measuring device of solar radiation intensity (digital meters of solar powers), (sp216 model, Make –EZDO -Electronical Electronics), accuracy (± 5 %), Range 12000 (w⁄m²). The solar collector was positioned at the same angle (45 °) to measure the strength of radiation over the length of the test.

Figure 3.19: Solar power meter.

3.4 The Calibration of Measuring Devices

3.4.1 Thermocouples Calibration

Both thermo-couples have been measured for comparison at the boiling point by attaching 1 end of the thermocouple to the digital thermometer & the other end within water & deionized water. The wapter has been put in the bowl and the heat source has been concentrated on bowls. When water starts to boil, the thermo-couple has been put to calculate boiling degrees. It must be noticed that degrees of deionized water boiling (100 ° C) & degrees of inertia of water (zero ° C) has been employed and degrees of boiling of water were (one hundred ° C) from experimental tests, and

then the relation is provided between thermo-couples and it has been observed that for thermocouples there is no temperature difference.

3.4.2 Calibration of Flow Meter

The used flow meter to calculate the rate of liquid flow (Lpm) was calibrated by the stopwatch and graded glass cylinder. The rate of volume 0.5,1 and 2 L /min was employed in the calibration of the flow meter as seen in Figure 3.20 below with the next steps:

After passing the flow meter, the volume of water has collected in the graded cylinder reads 1 Lpm, recorded by the watch during the known time reaches 60 sec. By dividing the volume by time, the rate of volume flow is given.

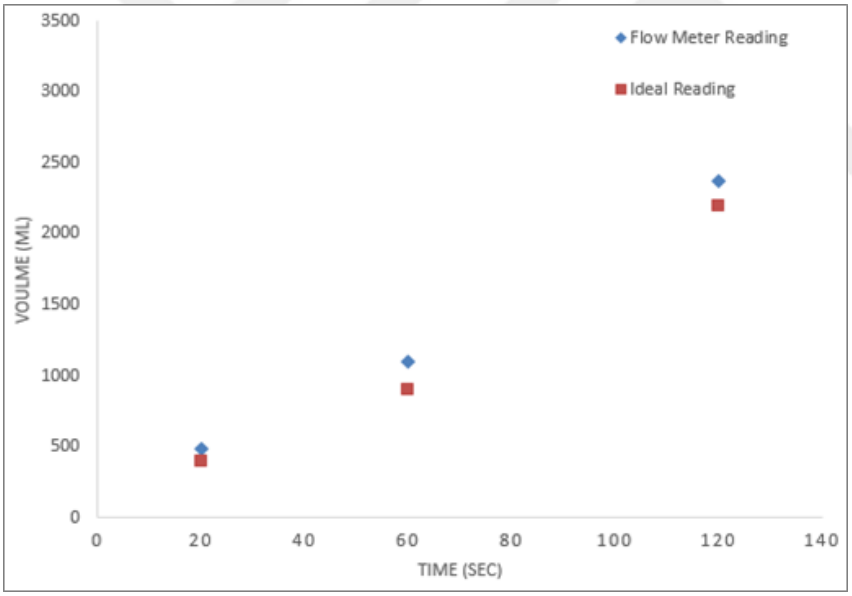

Figure 3.20: Calibrating the flow meter.

3.5 Experimental Procedure

However, before completing the tests, the next preparations have been done as below:

1) The (ISCS) has been filled with deionized water and it has been oriented to the south (by the compass) with the tilt angle reached β=45° in the city of Baghdad at 44.3° longitudes and 33.2° latitude.
2) The pump was linked from 2 sides, exterior from the lower of storage tanks and interior to the flow meter then to the solar collectors for ensuring that the rate of flow isn't altered
3) The thermo-couples have been linked to a temperature recording device to measure the temperature at various points through tests.
4) The thermocouples were connected to a temperature recording device to measure the temperature at various points through tests.

At the current stage, the setup of the test is ready for completion with the next test shown in the chart below.

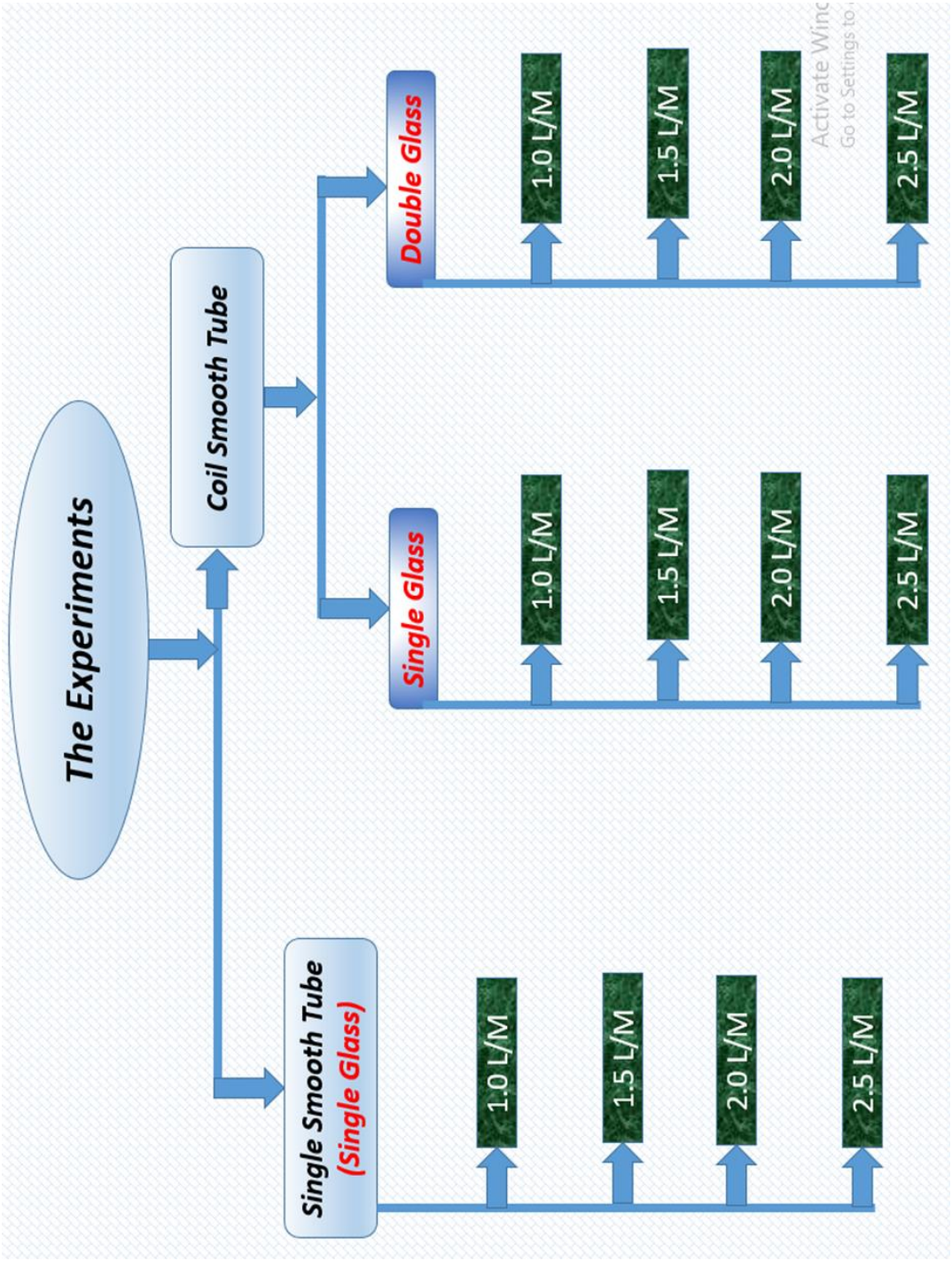

Figure 3.21: Chart of all experiments.

3.6 Summary

The current chapter aims to illustrate details of the work of tests that involves the assembly setups of tests, the devices calibration, preparation of nanofluid, and procedures of tests. Finally, a detailed illustration of how to complete the tests has been reported. The experiments plan involves:

1) The main aim of the current study is to check the natural-convection heat transfer performance of the integral solar-collector storage, in which the heat exchangers in the straight/coiled tube form is integrated immersed in the solar collector, which is tilted at 45 degrees, and filled with a base fluid (water).
2) Study the impact of the change of flow rates inside heat exchangers.
3) Study the effect of single & double-glazing.
4) Developing dimensionless, empirical heat transfer relationships for water heating and solar energy storage systems.
5) Rationalize the use of electrical power.

CHAPTER 4

THEORY OF ISCS FORMULATION

4.1 Introduction

The practical experiments conducted in this research aim for studying heat transfer using natural convection through a single smooth tube and smooth coiled tube heat exchangers, which are immersed separately in a tilted enclosure. The efficiency of each heat exchanger was evaluated at different values of thermal flux and the non-dimensionless relations were determined based on the following calculations.

4.2 Calculations

4.2.1 Calculate Total Heat Rate Transmitted to The Heat Exchanger

$$Q_U = \dot{m}\, C_p(T_O - T_i) \tag{4-1}$$

All properties of water have been completed at the average temperatures

$$T_{ave} = \frac{(T_o + T_i)}{2} \tag{4-2}$$

4.2.2 Calculate The Reynolds Number For The Heat Exchanger

$$R_e = \frac{\rho\, U_{in}\, D_i}{\mu} \tag{4-3}$$

The water velocity within the FPSC can be determined using the next formulae:

$$u_{in} = \frac{q}{A_s} \tag{4-4}$$

$$q = \frac{\dot{m}}{\rho} \tag{4-5}$$

$$A_s = \frac{\pi}{4} D_{in}{}^2 \quad (4\text{-}6)$$

4.2.3 Calculate The Heat Transfer Coefficient

$$h = \frac{Q_u}{\pi D_{ave} L(T_s - T_w)} \quad (4\text{-}7)$$

$$D_{ave} = \frac{(D_o + D_i)}{2} \quad (4\text{-}8)$$

4.2.4 Calculate The Nusselt Number

The number of Nusselt represented the heat transfer enhancement during the fluid layer as a result of convection relative to conduction across a similar fluid layer.

$$Nu = \frac{h\, D_{ave}}{K} \quad (4\text{-}9)$$

4.2.5 Calculate The Rayleigh Number

The number of Rayleigh was the number of dimensionless, which described the relationship between viscosity and between buoyancy within the fluid

$$R_a = \frac{g\, \beta (d_{ave})^3 \Delta T_{sw} cos\Theta}{v\alpha} \quad (4\text{-}10)$$

4.2.6 ISCS Thermal Efficiency

Thermal efficiencies of SCSI is the useful heat gain ratio to total input energies. It can be determined from the next formula [45-46]:

$$\eta = \left[\frac{Energy\ Gaind}{Stord\ Heat}\right] \quad (4\text{-}11)$$

$$Q_i = \dot{m}_{\boldsymbol{En.}}\, C_p(\Delta \boldsymbol{T}_{\boldsymbol{ave-En.}}) \quad (4\text{-}12)$$

4.2.7 Collector Energy Losses

Most of the solar radiation in systems of the solar thermal was absorbed using solar collectors and converted to the working fluids then employed as usable energy, although some of the absorbed heat was typically lost to the atmosphere by various modes of heat transfer (convection, conduction, and radiation) as seen in Figure 4.1A. The ISCS back temperature was(T_b), the plate temperature is (T_p) and the absorbed solar radiation was *S*. Figure 4.1B exhibited the losses of heat from the solar collectors can be collected into the simple resistanceR_L, so that the losses in energy from collectors can be done as below:

$$Q_{Loss} = \frac{T_p - T_a}{R_L} = U_L A_c (T_p - T_a) \quad (4\text{-}13)$$

$$U_{Loss} = U_{to} + U_{bo} + U_{ed} \quad (4\text{-}14)$$

It must be noticed that each heat-transfer loss coefficient was separately calculated and Figure 4.1 didn't exhibit the edge losses.

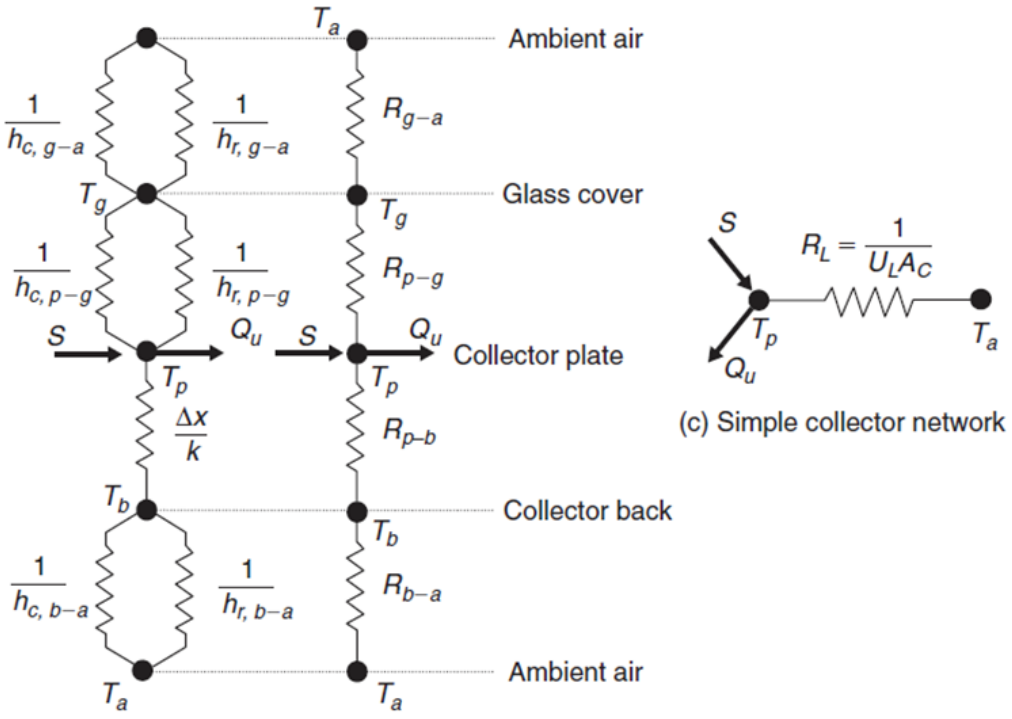

(A) heat transfer network (B) resistance network

Figure 4.1: Thermal networks of the single cover SCIS in terms of (A) convection, conduction, and radiation (B) resistances among the plates, and (C) the simple collector networks [43].

4.2.8 Calculate The Top Losses Energy of The ISCS

$$Q_{top\ loss} = U_t\, A_c (T_p - T_a) \tag{4-15}$$

For designing the aims with sufficient accuracy, the (U_t) coefficient of top heat-transfer loss can be evaluated using the next empirical formula (Klein, 1975) [43]

$$U_{to.} = \frac{1}{\frac{Ng}{\frac{c}{T_p}}\left[\left[\frac{T_p - T_a}{Ng+f}\right]^{0.33}\right] + \frac{1}{h_w}} + \frac{\sigma(T_p^2+T_a^2)(T_p+T_a)}{\left[\frac{1}{\varepsilon_p+0.05\,Ng(1-\varepsilon_p)}\right]+\left[\frac{2Ng+f-1}{\varepsilon_g}\right]-Ng} \tag{4-16}$$

The correction factor (*f*) of the coefficient of heat transfer using wind was evaluated using the next equation:

$$f = (1 - 0.040\ h_{wi} + 0.00050\ h_{wi}^2)\ (1 + 0.090\ Ng) \quad (4\text{-}17)$$

The correction factor (c) of the tilt angle coefficient was evaluated using the next equation:

$$C = 365.90\ (1 - 0.00830\ \beta + 0.00012980\ \beta^2) \quad (4\text{-}18)$$

According to the literature, there was no well-established research work done on the evaluation of the coefficient of wind-heat transfer, thus, the equation of (4-19) can be written as the following formula (h_w = 5 W/m^2. °C).

$$h_w = \frac{8.6 * V^{0.6}}{L^{0.4}} \quad (4\text{-}19)$$

4.2.9 Calculate The Bottom Losses Energy of The ISCS

$$Q_{bo.} = U_{bo.}\ A_c(T_p - T_a) \quad (4\text{-}20)$$

It must be remembered that the loss of energy was only transmitted using the combination of infrared radiation and convection during the insulation material via conduction and into the ambient air. The loss of energy can therefore be determined by the next formula, assuming that the radiation term ($h_{c,b-a}$) is ignored since the casing bottom temperature is low :

$$U_{bot.} = \frac{1}{\frac{t_{ba.}}{k_{ba.}} + \frac{1}{h_{c,bo-a}}} \quad (4\text{-}21)$$

4.2.10 Calculate The Edge Losses Energy of The ISCS

$$Q_{ed.} = U_{ed}\ A_c(T_p - T_a) \quad (4\text{-}22)$$

The loss of energy from the collector plate's back surface has been recorded to rarely surpass 10 percent of the upward loss [43]. Typical values are 0.3-0.6 W/m^2 K for

the coefficient of back surface heat loss. Likewise, the heat loss coefficient of the collector edges was expressed as below:

$$U_{ed} = \frac{1}{\frac{t_{ed.}}{k_{ed.}} + \frac{1}{h_{c,ed.-a}}} \quad (4\text{-}23)$$

CHAPTER 5

RESULTS & DISCUSSION

5.1 Introduction

The current chapter presents experimental results of the performance of integral solar collector storage (ISCS) system using two types of heat exchanger (straight tube and coiled tube) with single and double glass layers of the enclosure. The effect of the rate of fluid flow (1.0, 1.5, 2.0, and 2.5 LPM) on the efficiency of ISCS is evaluated during the day and night times, and the non-dimensional relationships are formulated for the following cases:

1- Heat exchanger (straight tube) with single glass layer of the enclosure STSG.

2- Heat exchanger (coiled tube) with single glass layer of the enclosure CTSG.

3- Heat exchanger (coiled tube) with double glass layer of the enclosure CTDG.

5.2 The ISCS System Temperatures

Temperature is the measure of kinetic energy produced by the motion of particles. However, temperature differences of working fluids at the outlet and inlet of heat exchangers and the temperature distribution in the enclosure are experimentally studied as follows:

5.2.1 The Temperature Difference (ΔT)

The difference of temperature of the outlet & inlet water to the submerged heat exchanger in the enclosure depends mainly on the flow rate of water entering (to be heated) within heat exchangers; the lower the quantity, the greater the temperature difference gained. That is, the average temperature difference will be the higher rate

at low flow (1 LPM) in all experiments for all studied cases due to longer residence time of water inside the heat exchanger as shown in Figures 5.1 and 5.2. . The CTDG exhibited higher temperature difference (28 C and 19.9 C) during the day and night times, respectively) then (19.4 to 11.4 C) for CTSG and (12 to 7.3 C) for STSG during the day and night times, respectively. From Figure 5.2, it was noticed that in the evening times, the temperature difference continues for late nights. This indicates that the thermal storage capacity varies from case to case. The highest thermal storage capacity was given by the CTDG case where the temperature difference was (11.7 C) for the rate of flow reached (1 LPM) at (02:20) compared to 0.5 C and 2.6 C for CTSG and STSG, respectively. This is because the CTDG uses double glasses with a distance of 10 mm between them, this gives a high thermal resistance that is used as an insulator [50], so the heat loss from the upper face is slow compared to other cases, and although the heat exchange is good in that case, the temperatures around the enclosure were high. The thermal performance of CTSG was better than that of STSG since the length of the coiled tube was larger than that of a straight tube, which makes water acquiring more heat from the hot water stored in the enclosure that is heated by the sun.

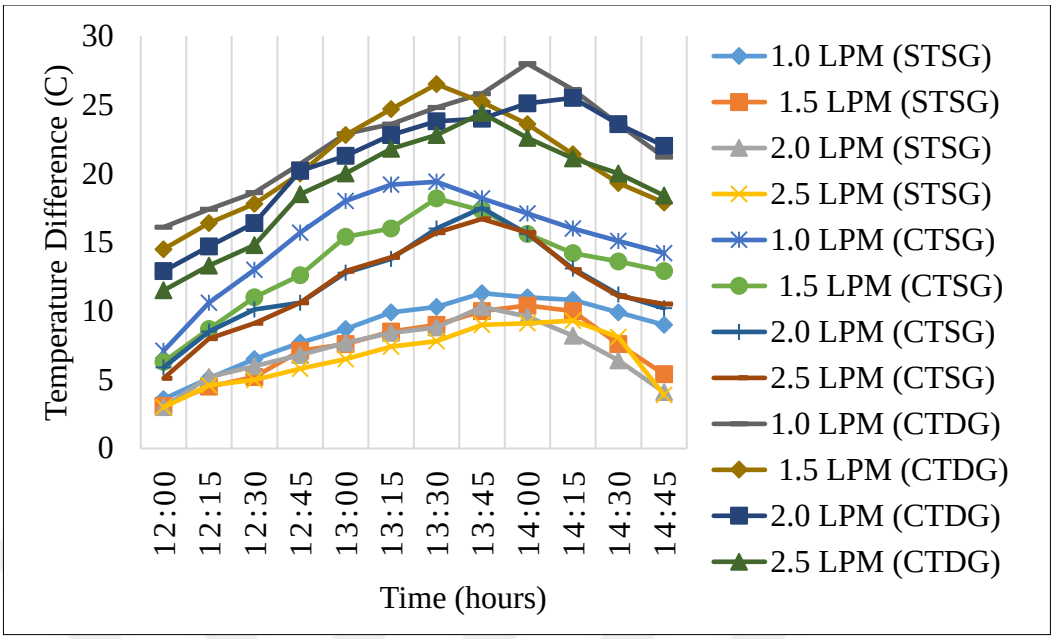

Figure 5.1: Temperature difference with time during the discharge test from 12:00 to 14:45 Daytime for all cases STSG, CTSG, and CTDG at various rates of flow (1.0, 1.5, 2.0, and 2.5 LPM).

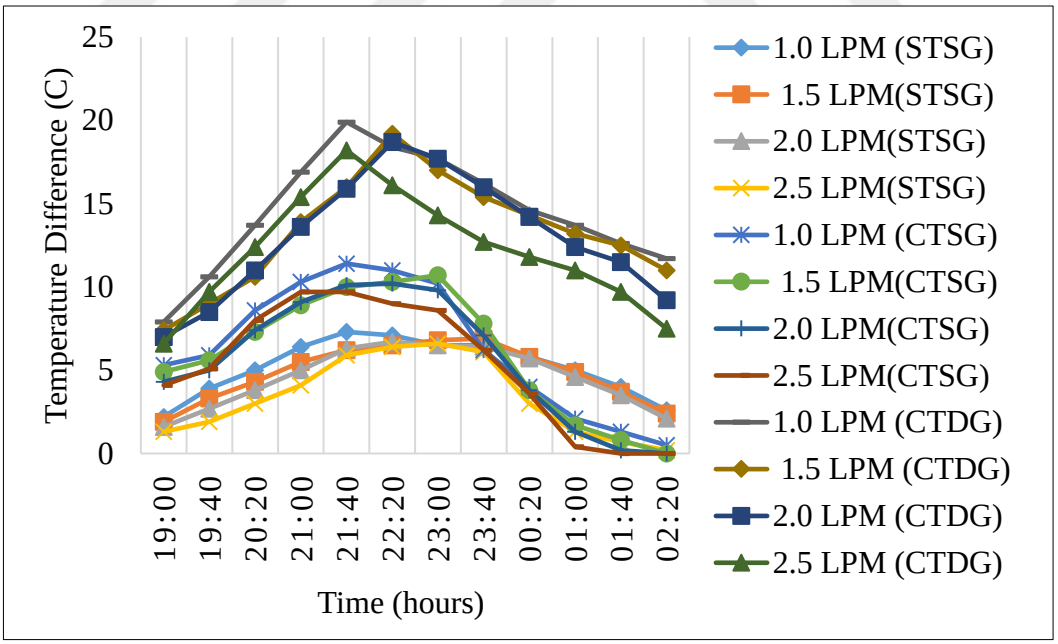

Figure 5.2: Temperature difference with time during the discharge test from 19:00 to 02:20 Nighttime for all cases STSG, CTSG, and CTDG at various rates of flow (1.0, 1.5, 2.0, and 2.5 LPM).

5.2.2 The Temperature Distribution (T1-T10 and T18-T20) in the Enclosure

Figure 5.3: showing placement of the thermocouples, indicated by solid circles and identified by number. Figures 5.4 to 5.9 presents the temperature distribution for the water inside the enclosure. Since the temperature difference was highest at 1 LPM flow rate, the temperature distribution will be studied all over the enclosure for all cases at this flow rate.

Figure 5.4 involves the obtained data from all thermo-couples in enclosures as a time function for the STSG case. However, the temperatures were somewhat uniform except near the straight tube within the thermocouple reading (T20). This uniformity is near the back of the enclosure within the two thermocouples reading (T7, T8), where the temperature difference range was (1-3 C) for the water temperature inside the enclosure for all cases.

Compared to the STSG case, the CTSG and CTDG cases also showed uniform temperature distribution except for a relative irregularity for the thermocouples tube (T20) located near the heat exchanger as well as (T7) and (T8) as shown in Figures 5.5 and 5.6. The irregularity for the STSG case is less than the CTSG and CTDG cases due to the difference in temperatures surrounding the tube from the water temperature entering the tube; the greater differences, the greater the heat transfer from the enclosure to the tube. This is due to differences in the density of the water surrounding the tube from another experiment. The change in density leads to a greater buoyancy force, which causes the water to circulate the tube and the part of the fluid with heavy density (cold water) descends to the bottom, which causes irregularities near the back of the enclosure.

Figure 5.7 reveals that the heat exchange continues with high efficiency when using the case CTDG, and its continuation until after 02:00, and this indicates that the thermal storage, in that case, is much higher than in other cases due to the use of double glass as mentioned in the previous paragraph 5.2.1.

From Figures 5.8 and 5.8, it was noticed the same temperature gradient during the draining process at daytime, but the observation that can be seen is that the time it took for the CTSG case to reach a steady-state is less than the time for the STSG case.

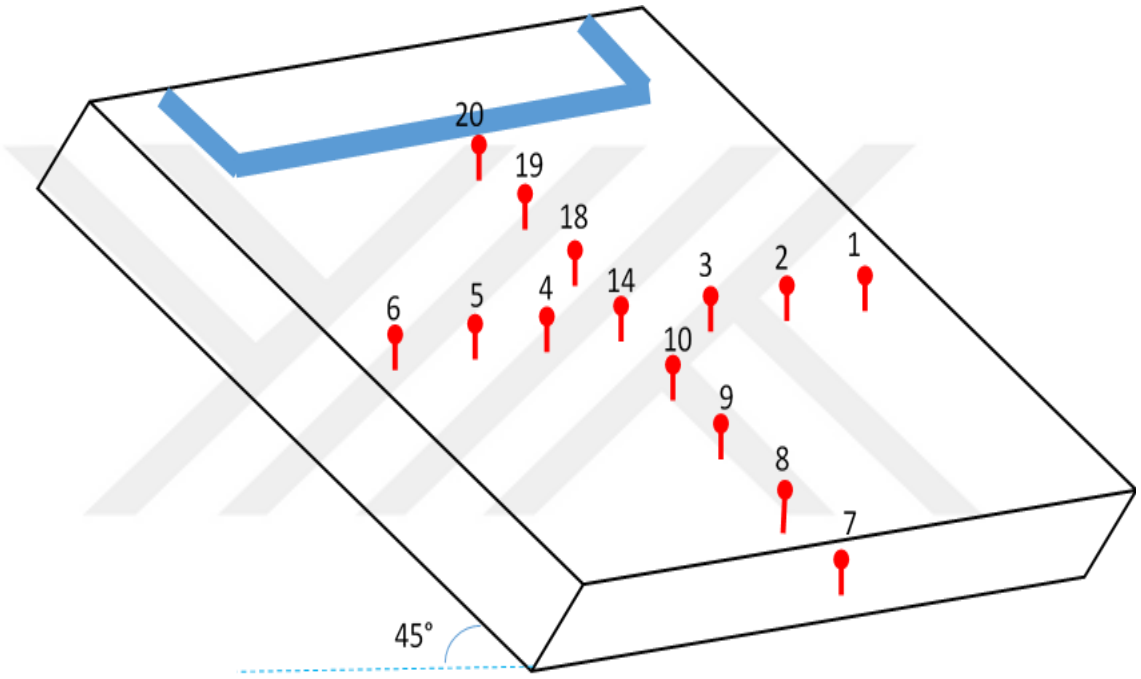

Figure 5.3: Showing placement of the thermocouples (T1-T10 and T18-T20), indicated by solid circles and identified by number.

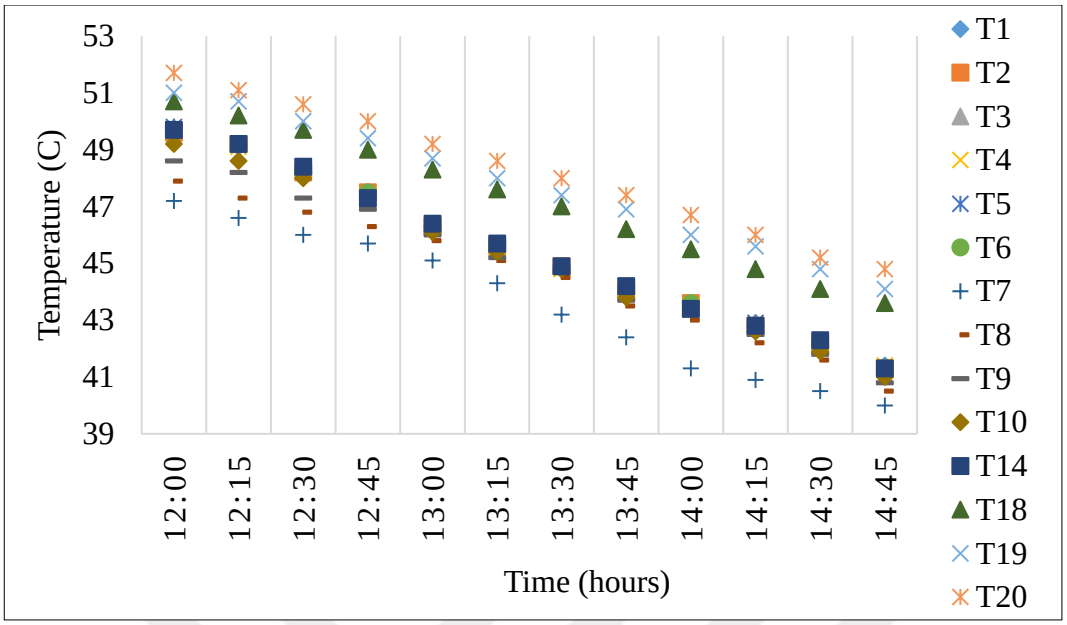

Figure 5.4: The temperature distribution (T1-T10 and T18-T20) in the enclosure with time for the case STSG. During the discharge at Daytime from 12:00 to 14:45, at a flow rate of 1 LPM.

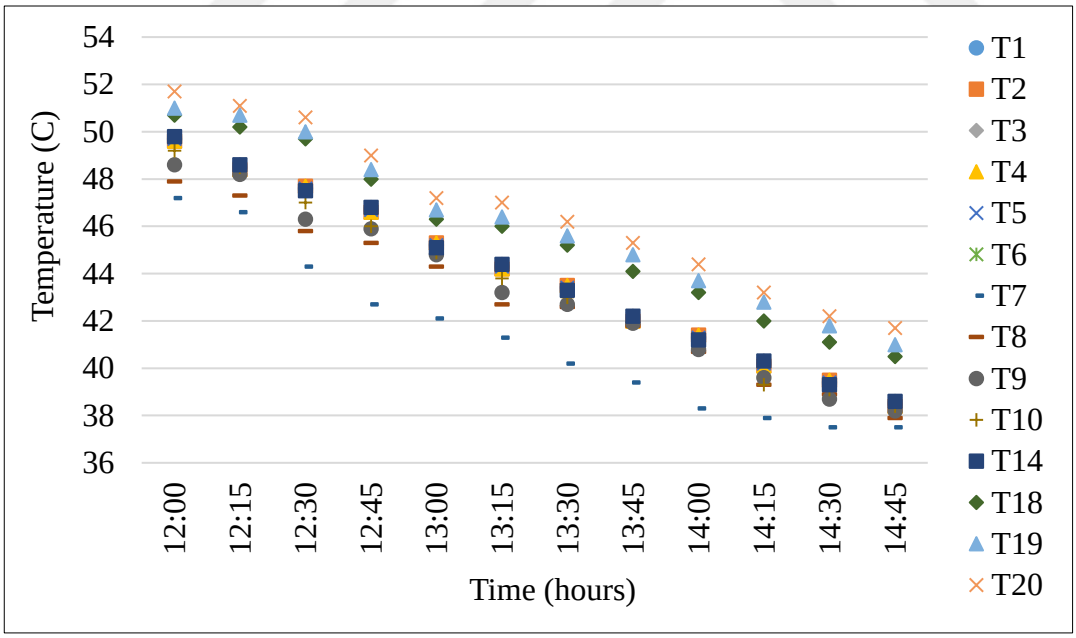

Figure 5.5: The temperature distribution (T1-T10 and T18-T20) in the enclosure with time for the case CTSG. During the discharge at Daytime from 12:00 to 14:45, at a flow rate of 1 LPM.

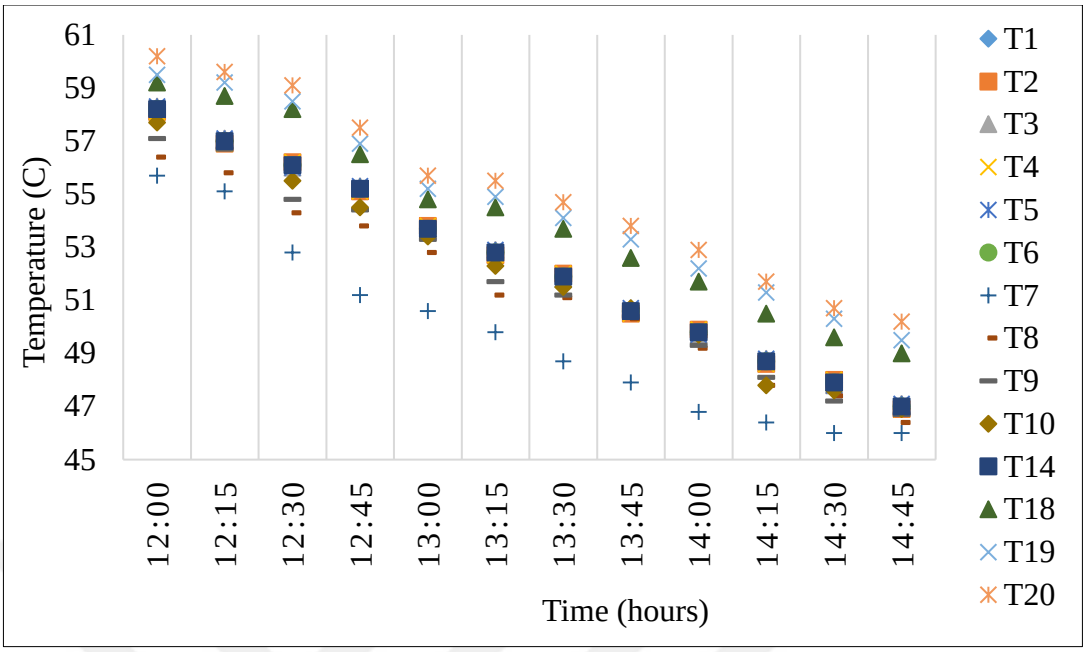

Figure 5.6: The temperature distribution (T1-T10 and T18-T20) in the enclosure with time for the case CTDG. During the discharge at Daytime from 12:00 to 14:45, at a flow rate of 1 LPM.

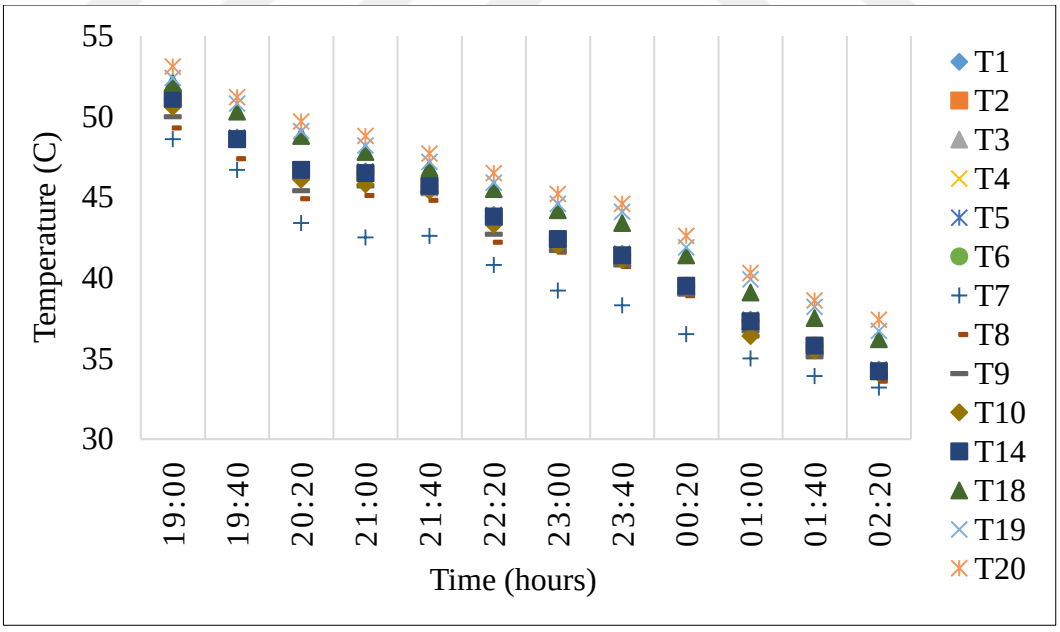

Figure 5.7: The temperature distribution (T1-T10 and T18-T20) in the enclosure with time for the case CTDG. During the discharge at Nighttime from 19:00 to 02:20, at a flow rate of 1 LPM.

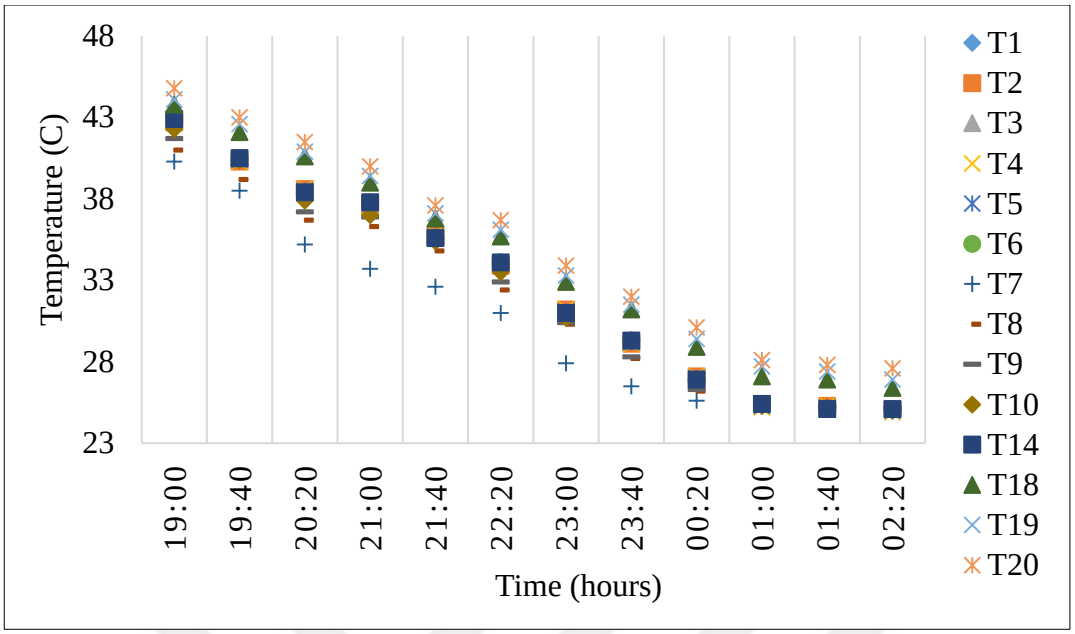

Figure 5.8: The temperature distribution (T1-T10 and T18-T20) in the enclosure with time for the case CTSG. During the discharge at Nighttime from 19:00 to 02:20, at a flow rate of 1 LPM.

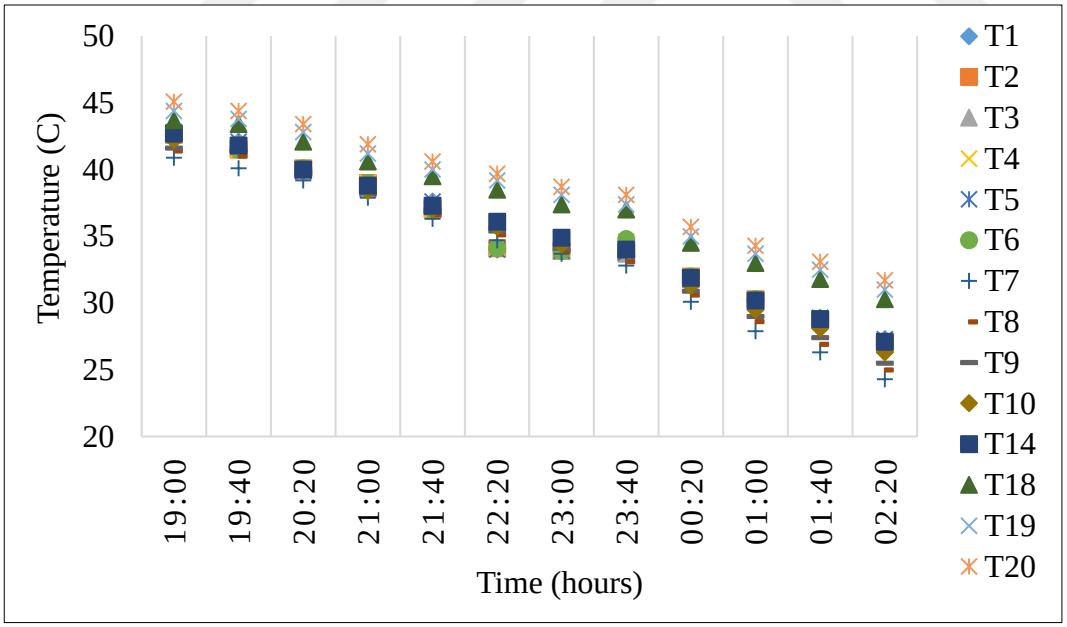

Figure 5.9: The temperature distribution (T1-T10 and T18-T20) in the enclosure with time for the case STSG. During the discharge at Nighttime from 19:00 PM to 02:20, at a flow rate of 1 LPM.

5.2.3 The Temperatures Near the Heat Exchanger (Ts1 and Ts2)

Figure 5.10: Showing placement of the thermocouples near the heat exchanger. Figures 5.11 and 5.12 show the temperature distribution near the heat exchanger STSG. The data indicate the lightly hot area above the heat exchanger and the cold plume coming down from heat exchangers. It was noted that the measured water temperature below the exchanger of heat (The thermocouple Ts2) is (1.5 C) cooler than the thermocouple above heat exchanger (Ts1) during the day and (0.6 C) at night, and it was (0.1 C) hotter than the temperature of the water near the heat exchanger (T20) during the day and night times. This indicates that there is a slight gradient in the density of water near the exchanger of heat due to changes in temperatures near the exchanger of heat and, thus the heat exchange between the enclosure water and the heat exchanger. Temperatures near the heat exchanger are higher by (4 C) during the day and (3 C) at night times, from those that were calculated in the bottom and middle part of the enclosure. This indicates that there is a good gradient of water density in enclosures due to the temperature change at the top, middle, and bottom, which leads to coming down of the cold plumes from the tube heading towards the bottom, which works to circulate the water in the enclosure, and the water at the top, bottom and sides of tubes maintains its relative temperature throughout the experiment [44]. In comparison with the use of CTSG and CTDG, it was found that the residence time of the hot zone located in the heat exchanger increases from the case of CTSG to CTDG due to the finding of double glazing layer, which increases the rate of heat transfer as shown in e Figures 5.13, 5.14, 5.15 and 5.16.

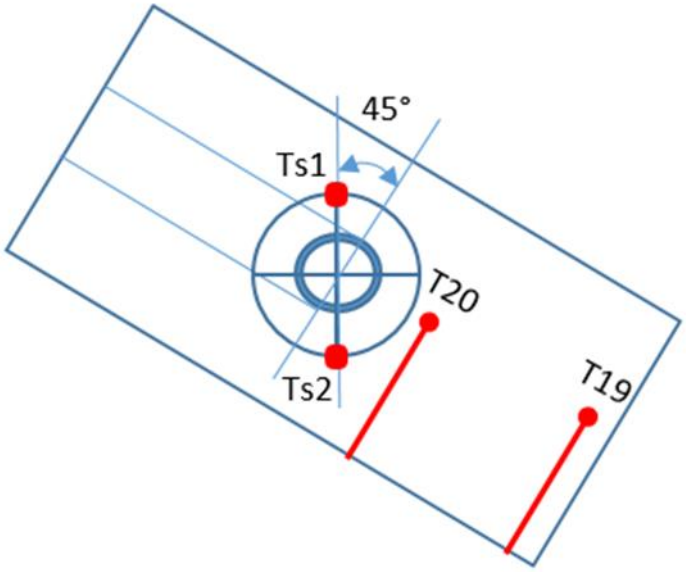

Figure 5.10: Showing placement of the thermocouples near the heat exchanger.

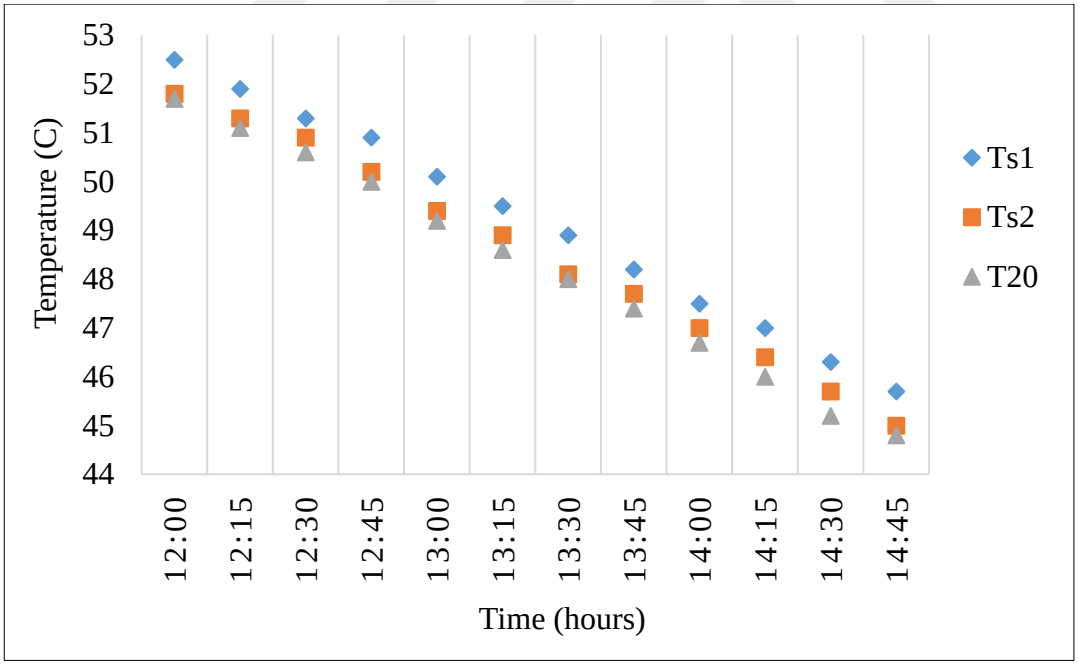

Figure 5.11: The temperatures near the heat exchanger (Ts1, Ts2, & T20) with time for the case STSG, during the discharge at Daytime from 12:00 to 14:45, at a flow rate of 1 LPM.

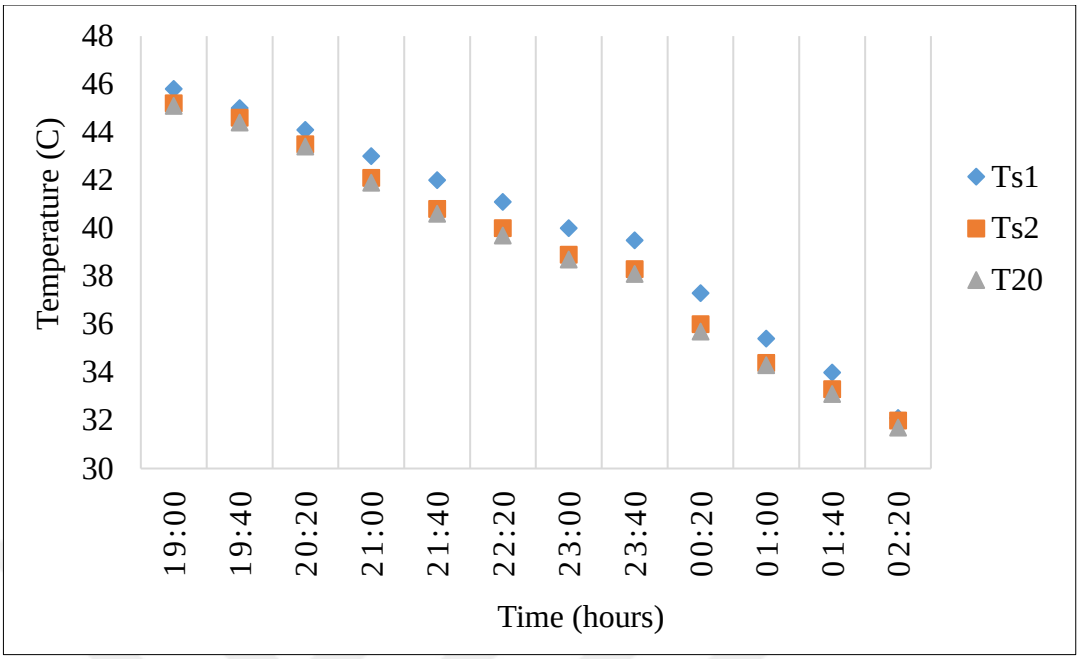

Figure 5.12: The temperatures near the heat exchanger (Ts1, Ts2, & T20) with time for the case STSG, during the discharge at Nighttime from 19:00 to 02:20, at a flow rate of 1 LPM.

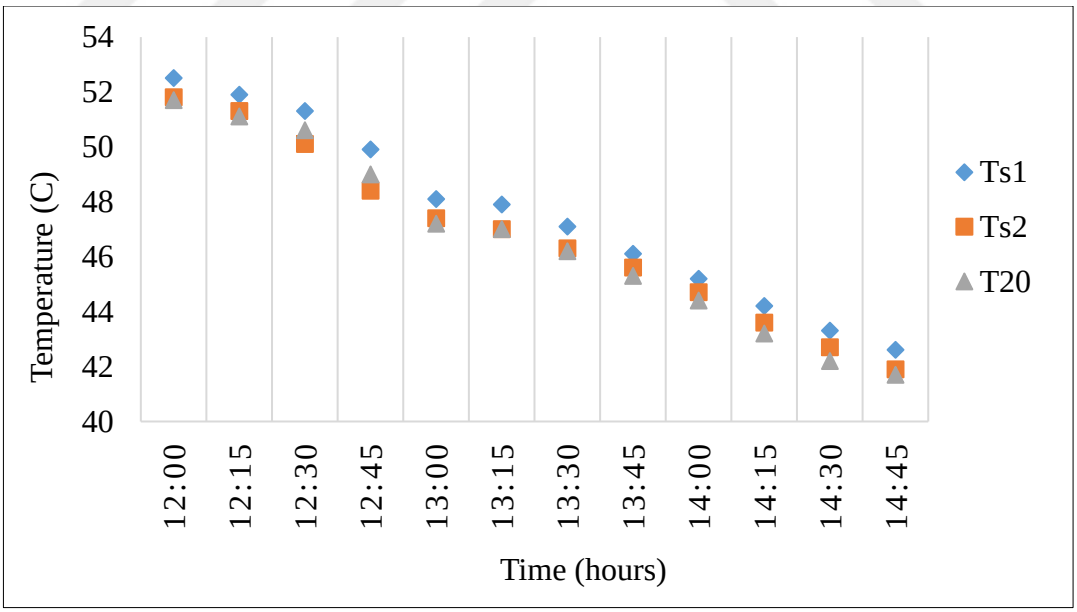

Figure 5.13: The temperatures near the heat exchanger (Ts1, Ts2, & T20) with time for the case CTSG, during the discharge at Daytime from 12:00 to 14:45, at a flow rate of 1 LPM.

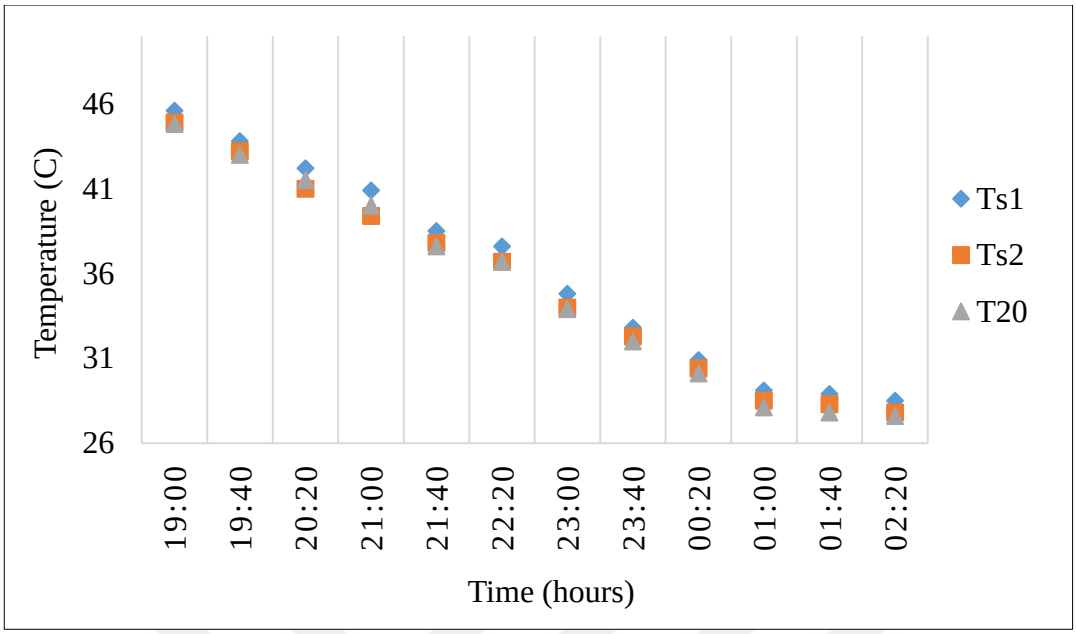

Figure 5.14: The temperatures near the heat exchanger (Ts1, Ts2, & T20) with time for the case CTSG, during the discharge at Nighttime from 19:00 to 02:20, at a flow rate of 1 LPM.

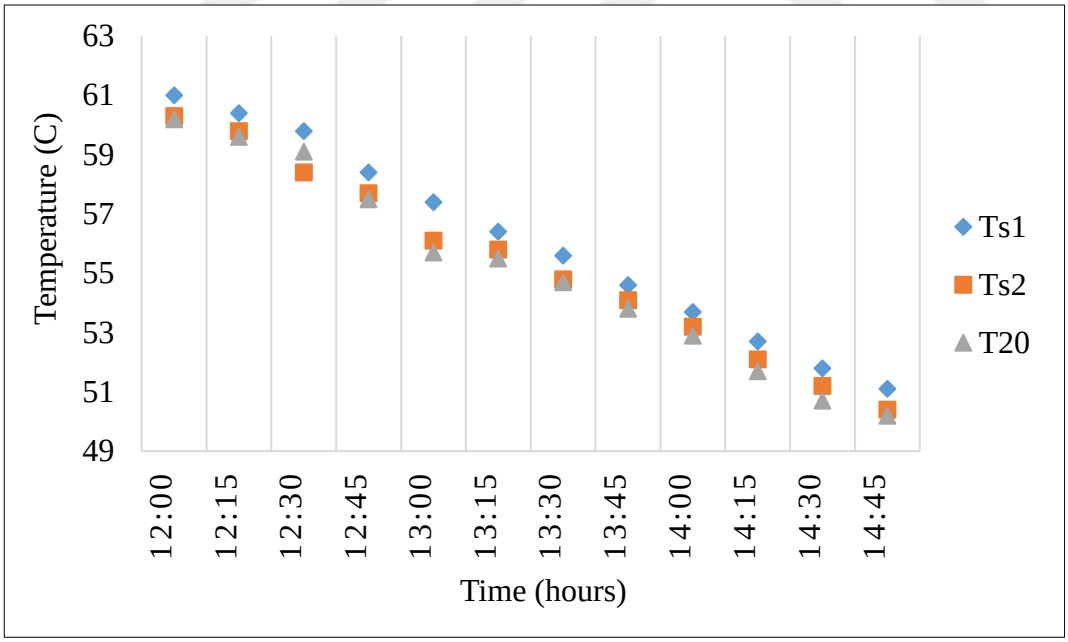

Figure 5.15: The temperatures near the heat exchanger (Ts1, Ts2, & T20) with time for the case CTDG, during the discharge at Daytime from 12:00 to 14:45, at a flow rate of 1 LPM.

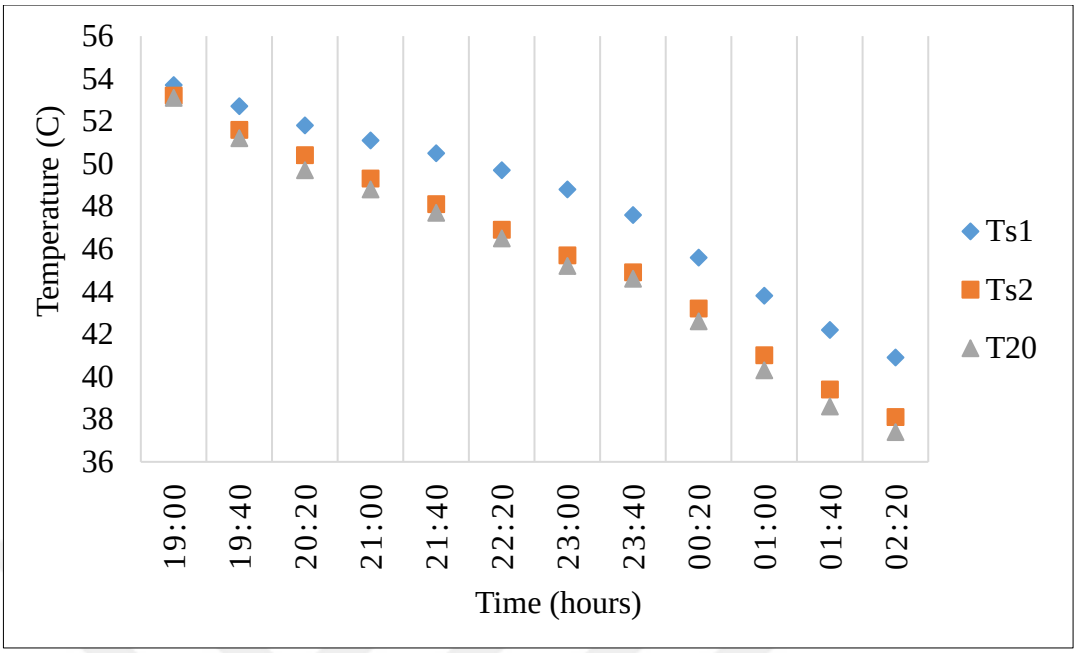

Figure 5.16: The temperatures near the heat exchanger (Ts1, Ts2, & T20) with time for the case CTDG, during the discharge at Nighttime from 19:00 to 02:20, at a flow rate of 1 LPM.

5.2.4 The Temperatures along the Horizontal Line at the Center of the Enclosure (T11-T17)

Figure 5.15 exhibits the site of the thermo-couples (T11-T17) in the middle of the enclosure. These thermocouples have been placed to find out the details of the natural convection heat transfer and how the fluid is effectively circulated with buoyancy force. Since the largest temperature difference was at the flow (1 LPM), so these temperatures will be studied with all cases at this flow during day and night times.

Figures 5.16, 5.17 shows a graph of the readings of the seven thermocouples (T11-T17) along the horizontal line in the enclosure center during the day and night times, respectively for the case STSG, where it is noticed that the water on the bottom surface (T17) of the enclosure is slightly colder than other locations indicating the

coming down of cold plumes to the bottom as the highest temperature difference between the thermocouple readings at the nearest location from the bottom (T17) and the rate of the other six thermocouples (from T11 to T16) is less than (2 C) & the rate difference was (1 C). From this difference, it is concluded that the cold water coming from tubes runs along the enclosure's bottom surface heading towards the enclosure back. Compared to the CTSG and CTDG cases as shown in Figures 5.18 5.19, 5.20, and 5.21 it is noted that the water on the bottom surface of the enclosure is colder than other locations in the enclosure, but the difference is that the amount of coldness compared to the total liquid in the enclosure is greater concerning the case CTDG than other cases, and the result of the cold plume descending is faster in the current case. Temperature differences and the gradient of water density in the enclosure lead to the formation of a vortex in the enclosure middle (due to the heat transfer in natural convection). The highest temperature differences were between the thermocouple readings near the surface OF bottom for the enclosure (T17) & the readout of the other thermocouples (T11 to T16) is (2 C) for the CTSG case, while it is about (2.5 C) for the CTDG case. The conclusion can be drawn as that cold water coming from a tube is heading towards the bottom with different natural convection rates for all cases.

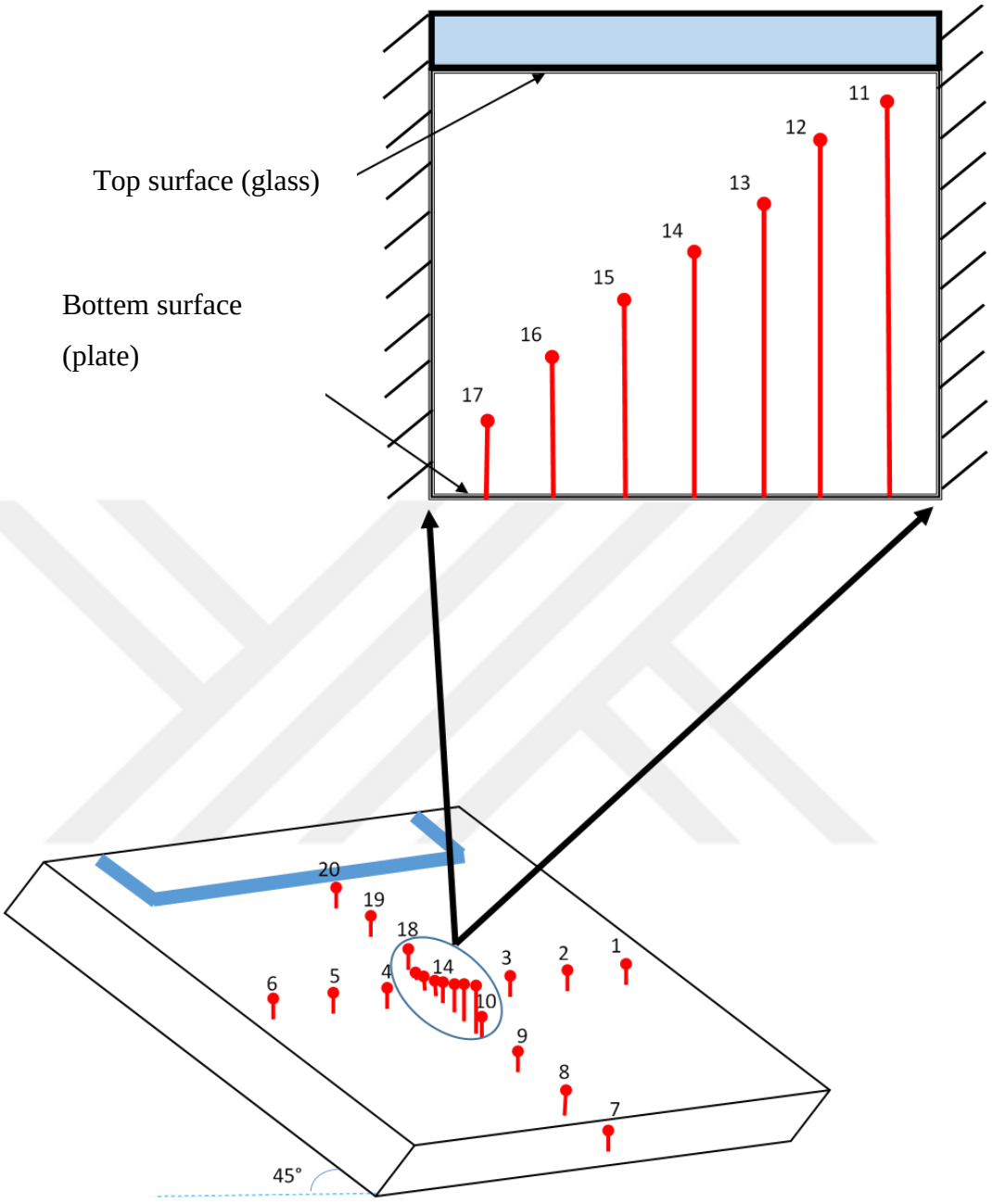

Figure 5.17: The location of the thermocouples at the center of the enclosure (T11-T17).

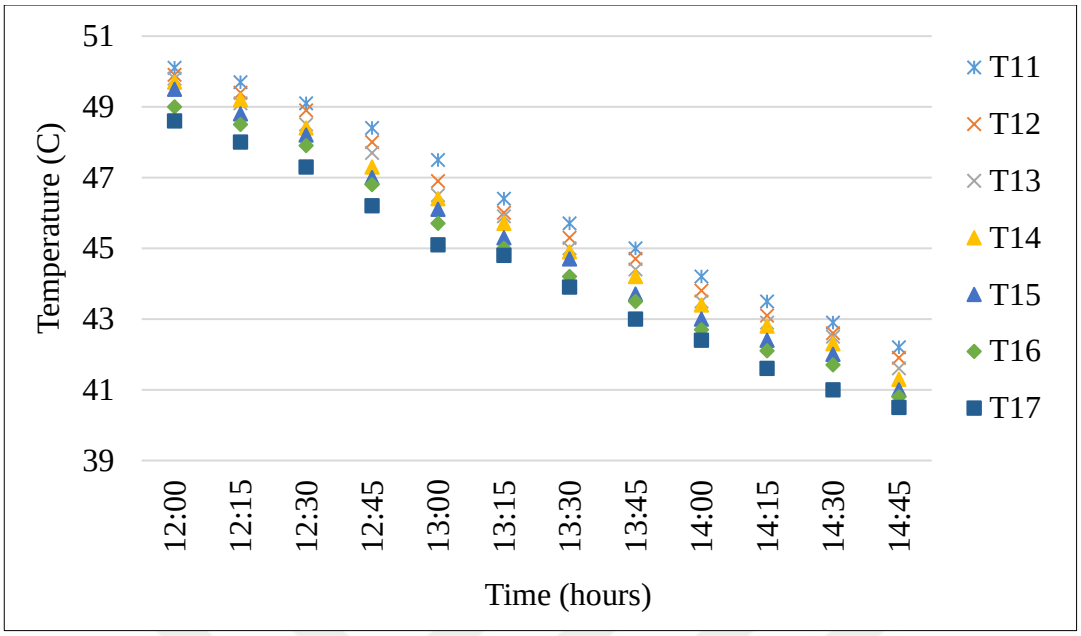

Figure 5.18: The measured temperatures at the center of the enclosure (T11 to T17) with time for the case STSG, during the discharge at Daytime from 12:00 to 14:45, at a flow rate of 1 LPM.

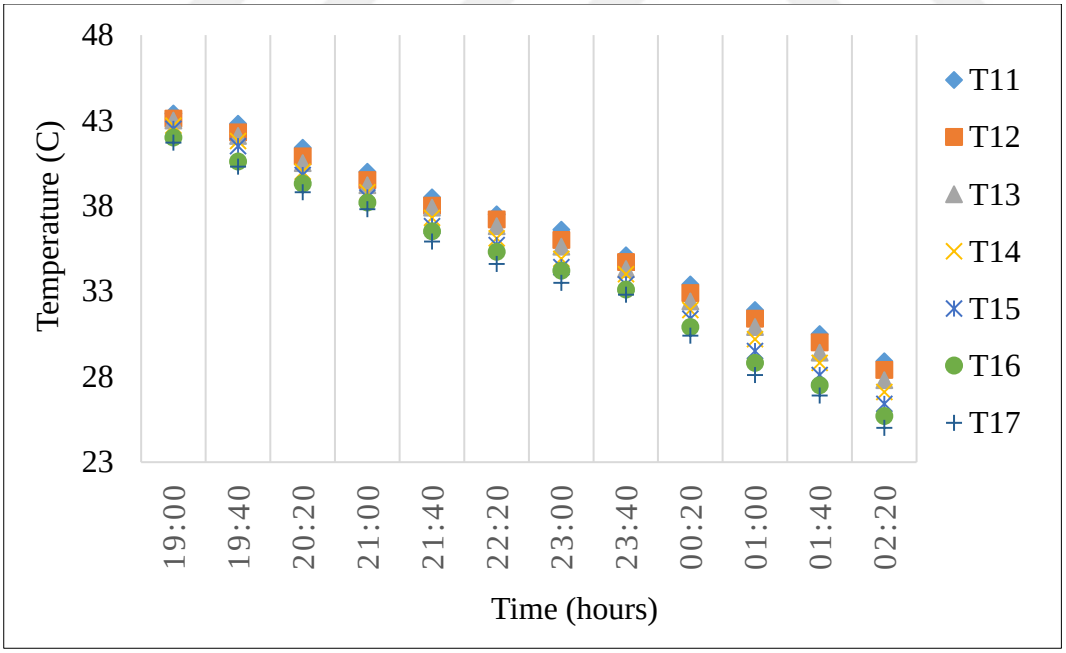

Figure 5.19: The measured temperatures at the center of the enclosure (T11 to T17) with time for the case STSG, during the discharge at Nighttime from 19:00 to 02:20, at a flow rate of 1 LPM.

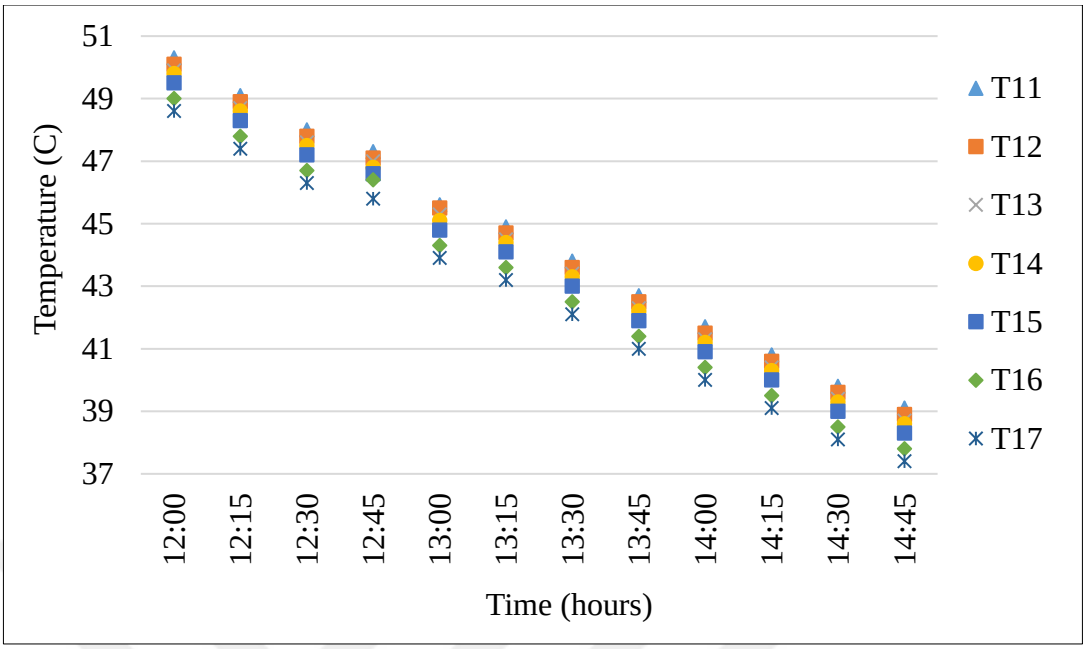

Figure 5.20: The measured temperatures at the center of the enclosure (T11 to T17) with time for the case CTSG, during the discharge at Daytime from 12:00 to 14:45, at a flow rate of 1 LPM.

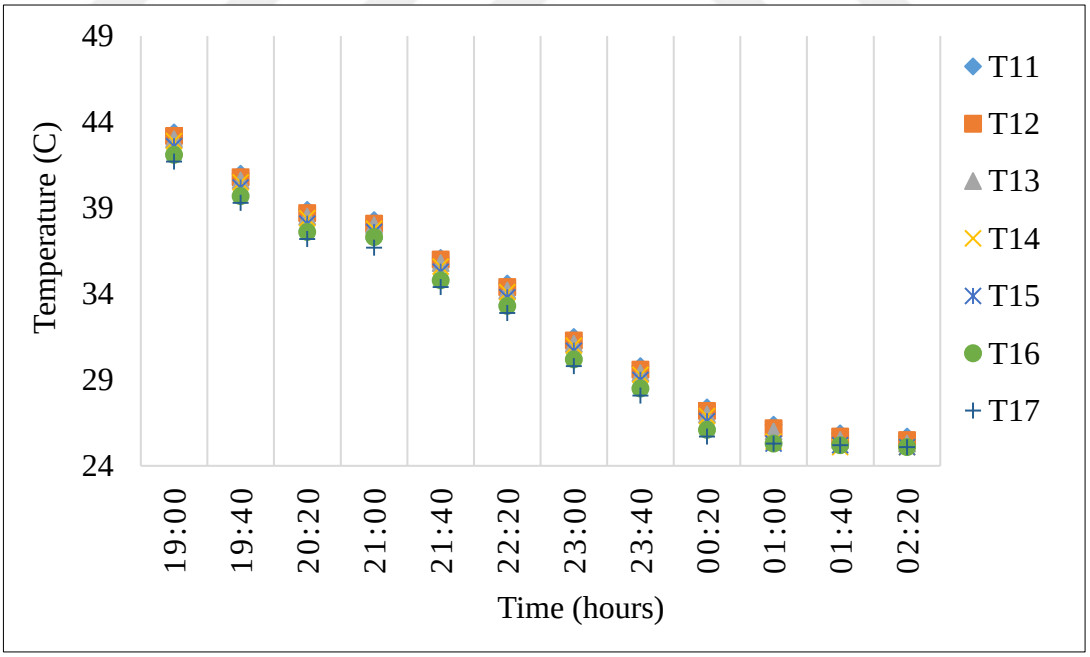

Figure 5.21: The measured temperatures at the center of the enclosure (T11 to T17) with time for the case CTSG, during the discharge at Nighttime from 19:00 to 02:20, at a flow rate of 1 LPM.

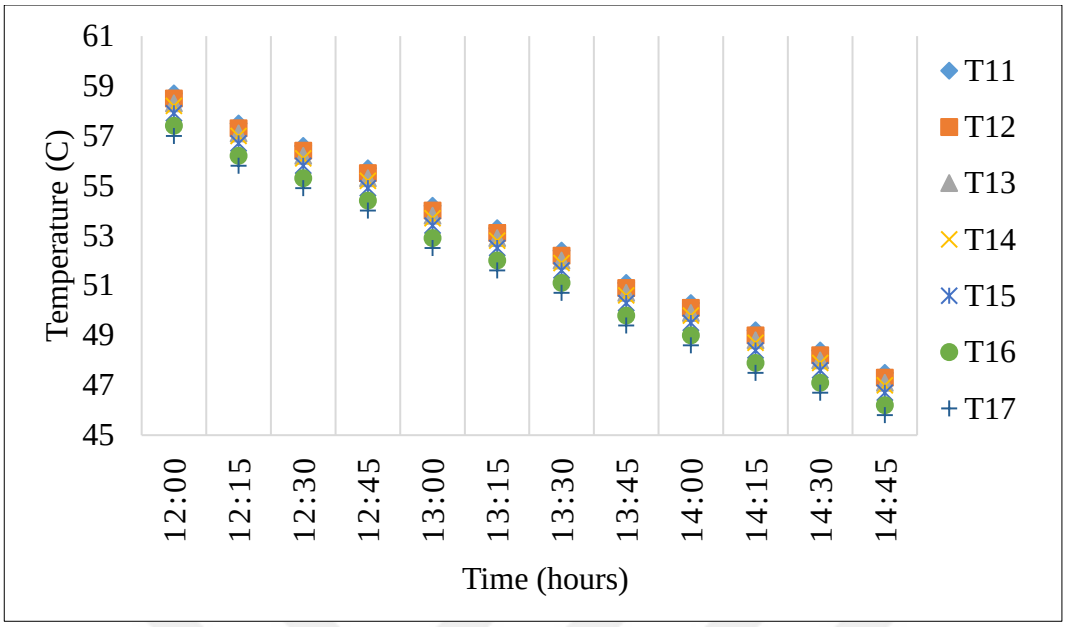

Figure 5.22: The measured temperatures at the center of the enclosure (T11 to T17) with time for the case CTDG, during the discharge at Daytime from 12:00 to 14:45, at a flow rate of 1 LPM.

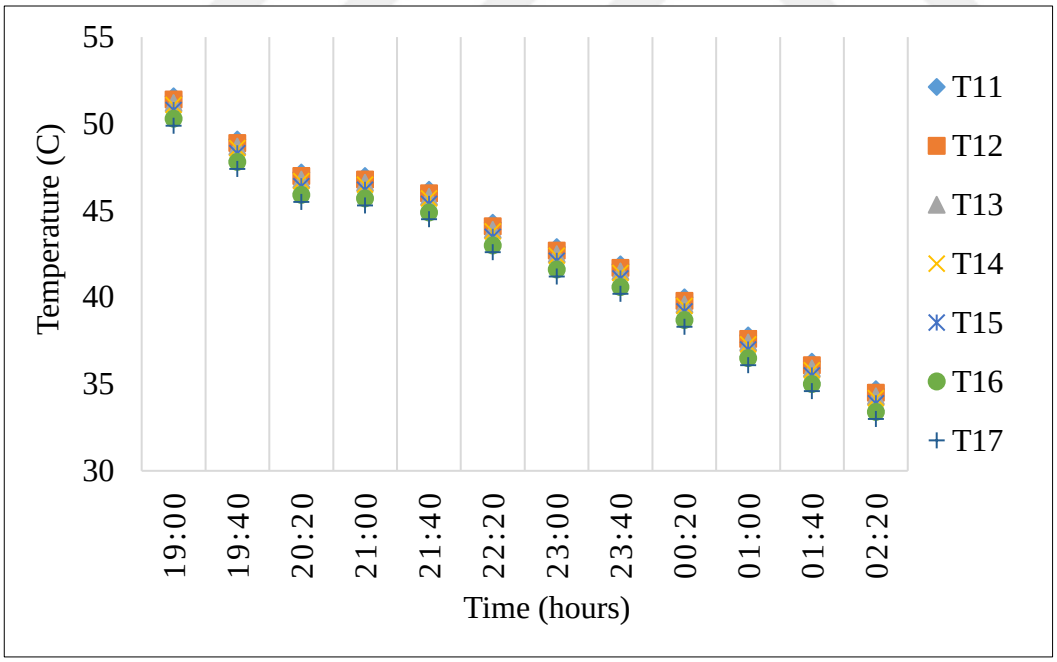

Figure 5.23: The measured temperatures at the center of the enclosure (T11 to T17) with time for the case CTDG, during the discharge at Nighttime from 19:00 to 02:20, at a flow rate of 1 LPM.

5.2.5 Glass Temperature

The temperature distribution of the glass layer for all cases during the daytime at the discharge rate of flow of 1 LPM is presented as in Figure 5.22. The results show that the glass temperature for the STSG case is close to the glass temperature of the CTSG and CTDG cases. It must be noticed that the temperature of the inner glass is higher than the outer one (8 C) for CTDG case because there is a resistance from the outer glass that allows the entry of the solar rays and prevents the expulsion of the heat outside, meaning that it acts as an insulator to prevent heat escaping outside the collector from the upper face [51]. Which is led to an increase in the temperatures inside the enclosure consequently. This leads to improvement of heat transfer by natural convection, which reflects positively on preserving/storing heat for long period during night times.

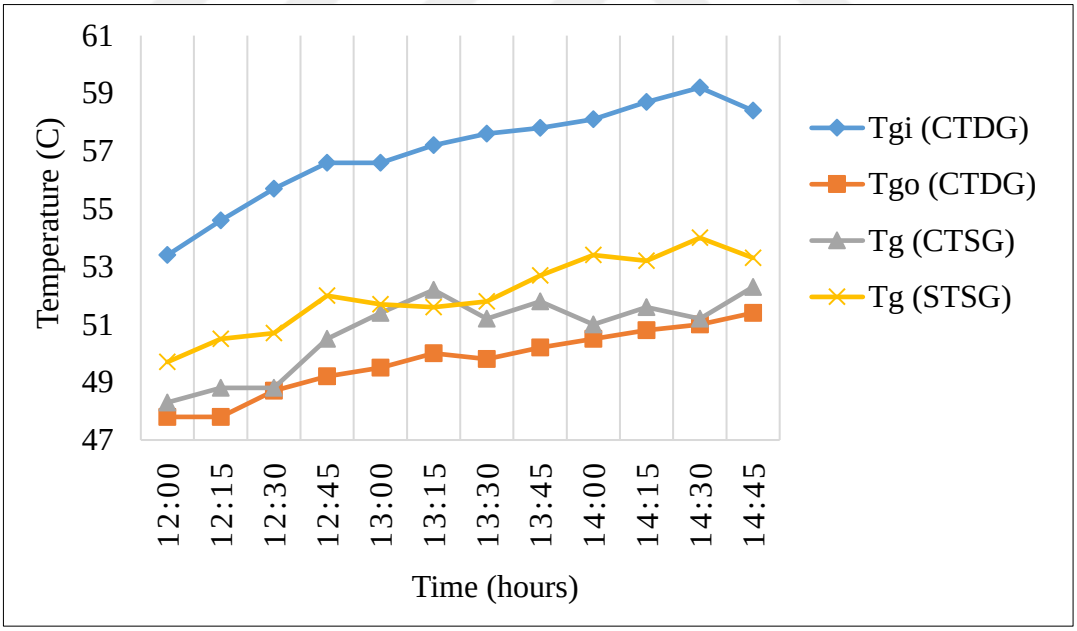

Figure 5.24: The temperatures of the glass layer for all cases during the daytime at a discharge flow rate of (1 LPM).

5.2.6 The Ambient Temperatures (Ta)

The variation of the ambient temperatures with time at the discharge water flow rates of (1.0, 1.5, 2.0, and 2.5 LPM) from 12:00 to 14:45 & from 19:00 to 02:20 of the all cases STSG, CTSG, & CTDG was shown in Figures 5.23 & 5.24. The ambient temperatures for all experiments are very close, which makes the comparison relatively fair for all the experiments.

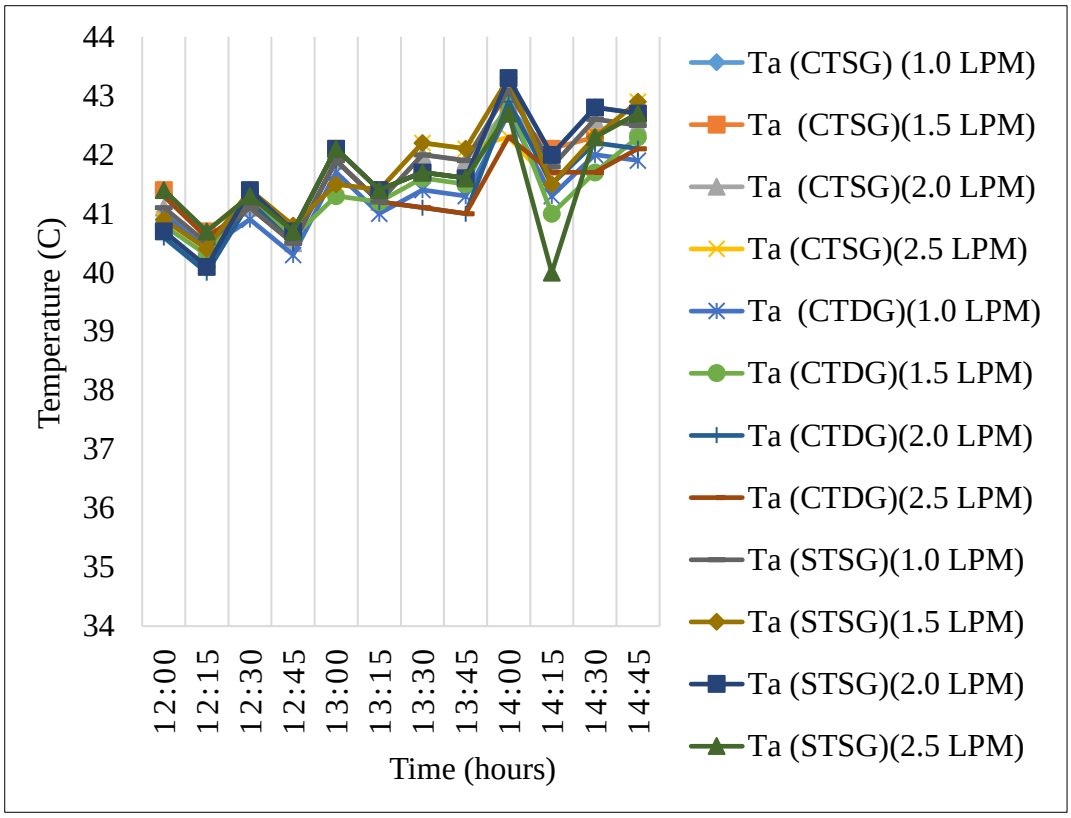

Figure 5.25: Temperatures of ambient with time for all cases during the Daytime (1.0, 1.5, 2.0, and 2.5 LPM).

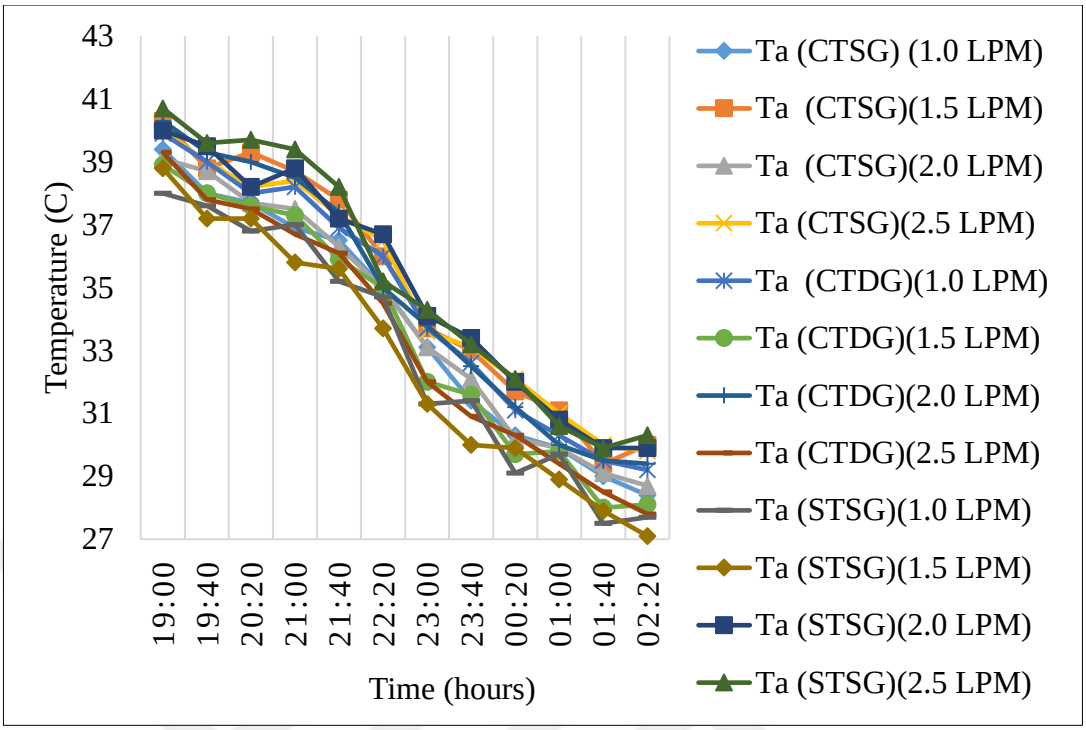

Figure 5.26: Temperatures of ambient with time for all cases during the Nighttime (1.0, 1.5, 2.0, and 2.5 LPM).

5.3 Heat Rates (Q)

The amount of heat is a measurement of the total internal energies of an object, that is, it measures the kinetic energy resulting from the movement of particles in addition to the energy stored in the bonds between the particles. The amount of heat depends on the amount of water that enters the heat exchanger, as the higher the flow rate, the greater the exchange of heat between the water surrounding the heat exchanger and the water inside it, and this depends on the thermal gradient inside the enclosure resulting from a change in the density of water as a result of exposure to solar energy and the appearance of a temperature gradient on top and the bottom of enclosures made the upper area hot, the middle cold, & the lower area cool. This works to move the heat to the water inside heat exchangers. Although the temperature difference for the high rate of flow is low, the increase in the rate of flow is much higher than the

decrease in the temperature difference, which increases the amount of heat with the increase in the flow.

The amount of heat varies from experiment to experiment and from case to case as the amount of heat is higher in all flow rates for CTDG case because the amount of heat gained from solar energy is higher than in the rest of the cases due to the greenhouse impact from double glazing as shown in the Figures below 5.25 & 5.26, where it was found that the highest amount of heat is at the flow of 2.5 LPM for CTDG case (4282 J/s in the day & 3194 J/s in the night), while CTSG case gives (2930 J/s in the day & 1702 J/s in the night) and the STSG case provides (1632 J/s in the day & 1158 J/s in the night).

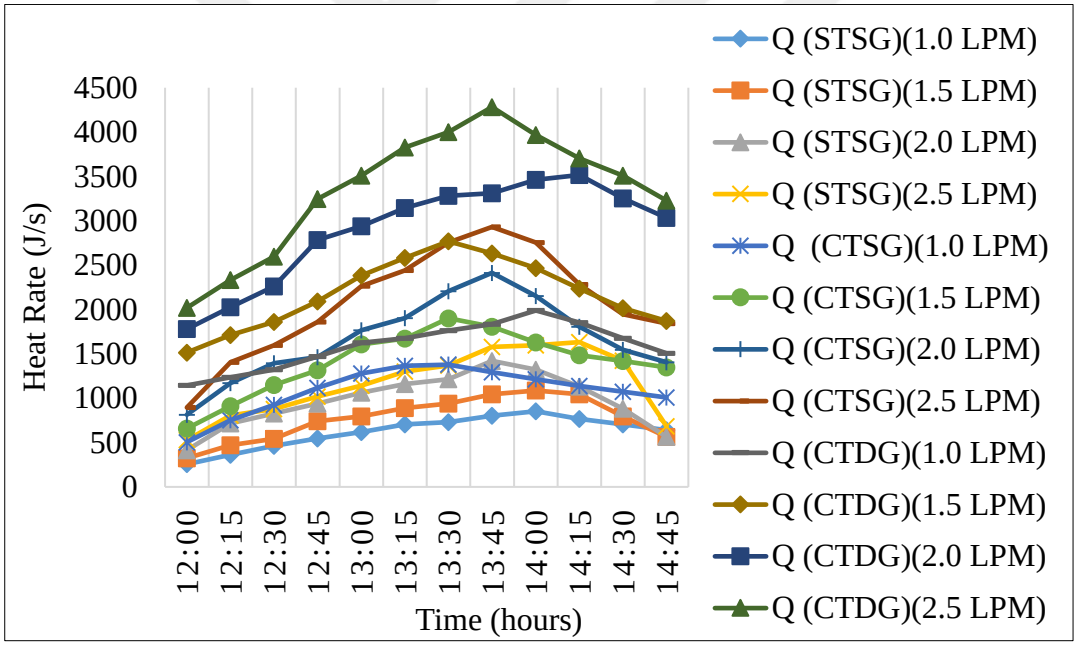

Figure 5.27: The heart rate with time for all cases during the Daytime at water flow rates of (1.0, 1.5, 2.0, and 2.5 LPM).

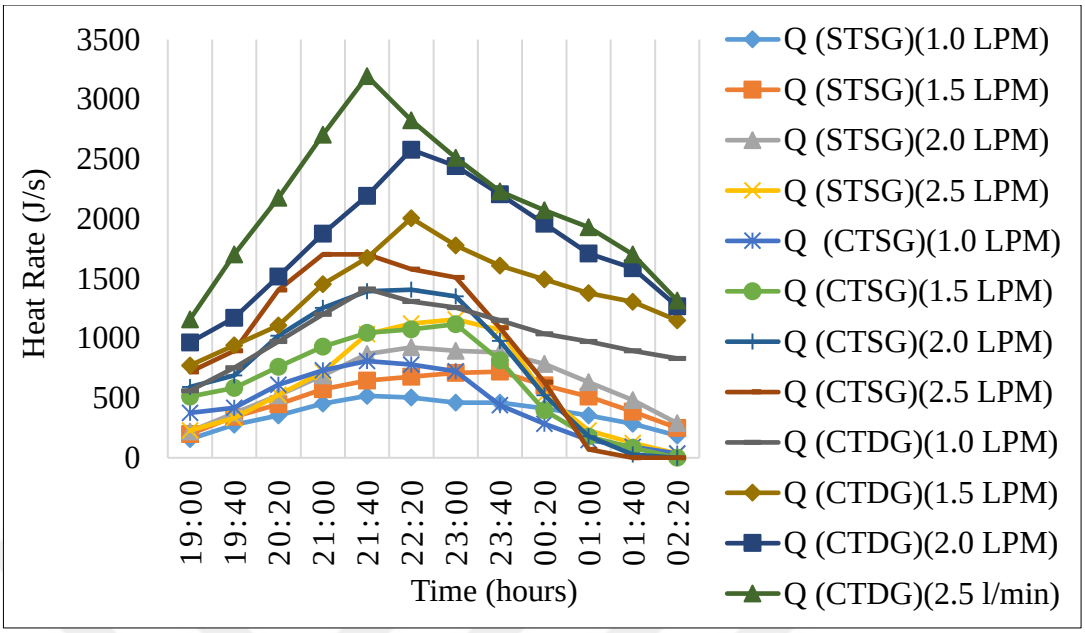

Figure 5.28: The heart rate with time for all cases during the Nighttime at water flow rates of (1.0, 1.5, 2.0, and 2.5 LPM).

5.4 Natural Convection Heat Transfer Coefficient (h)

The coefficient of film or, coefficient of heat transfer or efficacy of film, in thermodynamics and mechanics, is the constant of proportionality between heat flow and thermodynamic driving force of heat flow (like the difference of temperature, ΔT) [53]. Through the definition of the heat transfer coefficient, it depends on the heat amount transferred and the temperature differences between the surrounding layer of the heat exchanger and its wall (Ts & Tw), where the lower the difference, the higher values of the heat transfer factor. However, the difference depends on the mechanism of circulation of the water inside the enclosure, which depends on the raised temperature inside the enclosure resulting from exposure to solar radiation & on the amount of water entering the heat exchangers. As the water flow rate, the heat transfer becomes higher and thus the rotation enhances and thus reduces the temperature difference for the layer near the heat exchanger. This indicates that the

difference is in a state of more convergence because the rapid density of water layers varies with increasing temperatures, and this generates something like a plume that circulates water in enclosures from the top to bottom and vice versa. Figures 5.27 and 5.28 show that the highest amount of natural convection heat transfer coefficient records at the flow of 2.5 LPM for CTDG case (8473 W/m².C Daytime & 5591 W/m².C Nighttime), while the heat transfer coefficients reach (5799 W/m².C Daytime & 3368 W/m².C Nighttime), and (3125 W/m².C Daytime & 2373 W/m².C Nighttime) were reported for CTSG and STSG cases, respectively.

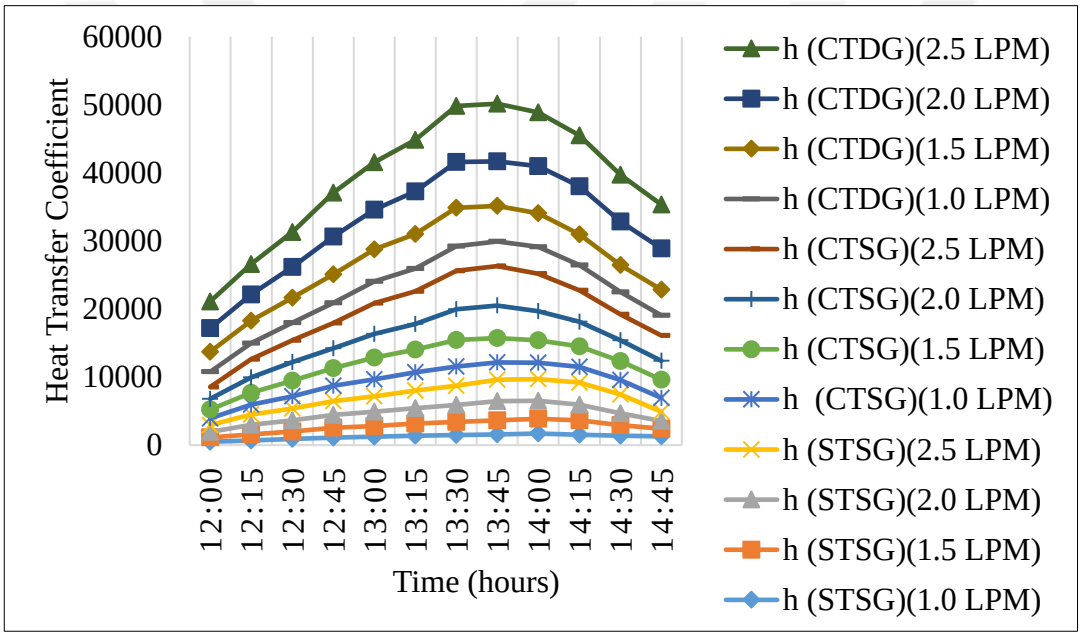

Figure 5.29: The natural Convection Heat Transfer Coefficient with time for all cases during the Daytime at water flow rates of (1.0, 1.5, 2.0, and 2.5 LPM).

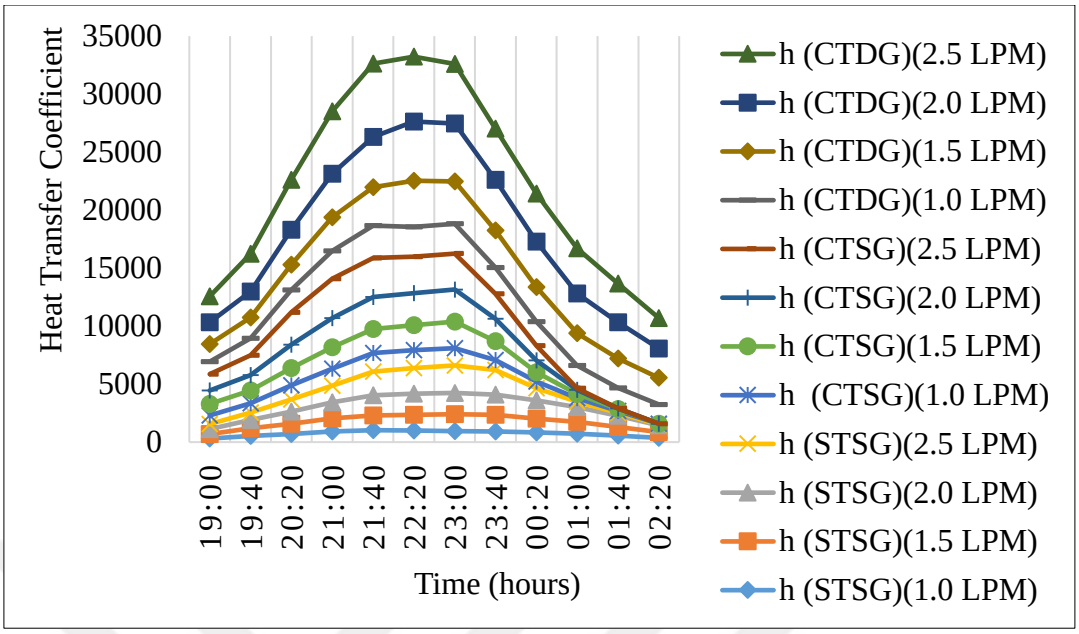

Figure 5.30: The natural Convection Heat Transfer Coefficient with time for all cases during the Nighttime at water flow rates of (1.0, 1.5, 2.0, and 2.5 LPM).

5.5 The Results of Solar Radiation and Internal Energy

The internal energy of the water inside the enclosure is the intermediate source that drives the condensed energy to the heat exchanger contained within the enclosure. This energy was provided due to the solar energy applied to the solar collector SCIS during the morning period from sunrise to the moment the discharge process began, and since the collector is isolated from all sides, so the amount of the internal heat of the water increased to reach twice the instantaneous solar energy, which is stored energy we use for heat exchange [56]. Figures 5.29-5.40 show the amount of solar energy, the temperature difference, and the amount of input energy for the STSG and CTSG cases, where it is observed that the internal energy is close for both cases because they were conducted using a single glazing layer and at the same operating conditions. The CTDG case exhibited higher internal energy than the instantaneous solar energy as well as higher than the internal energy of the two above cases because

this case uses double glass that makes the two thermal resistors of the glasswork to intensively trap the heat from the sun throughout the morning period.

Through the tests, it is evident that the incident solar radiation rises during the time (12:00 - 14:45) with some fluctuations because of the finding clouds from time to another time. After obtaining the temperature difference results, the highest temperature difference in each case and at each flow rate coincides roughly with the highest solar flood and the highest internal energy in most of the experiments.

Figure 5.41 shows the internal energy gradient at the discharge process during the evening times, where the internal energy decreases as time passes for all cases due to the absence of solar energy and the heat exchange continues. The internal energy of the CTDG case is higher than the other cases due to the effectiveness of the double glass where the largest energy was stored during the day. It was also found that the continued presence of energy until 02:20 and indicates the large amount of energy stored during the day times.

As for the internal energy of other cases, where the internal energy of the case CTSG was observed to drop more rapidly than the internal energy of the STSG case, especially after 12:20, due to that rates of exchange of heat are faster and higher for CTSG, this made the energy storage of the case STSG continues more than CTSG.

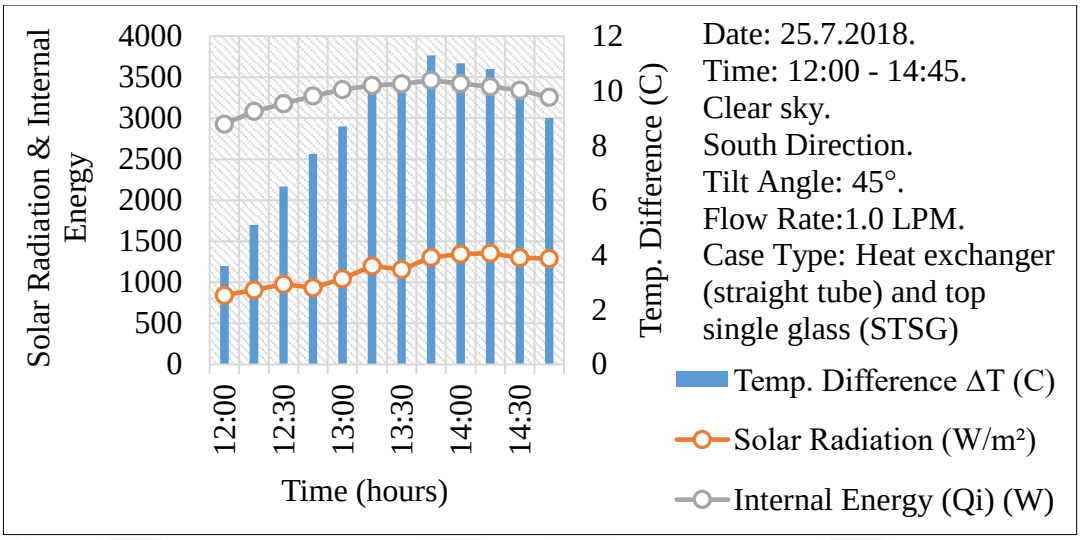

Figure 5.31: Show internal energy, solar energy, and temperature difference with time on July 25, 2018, during the discharge time at a rate of 1.0 LPM, for the case STSG.

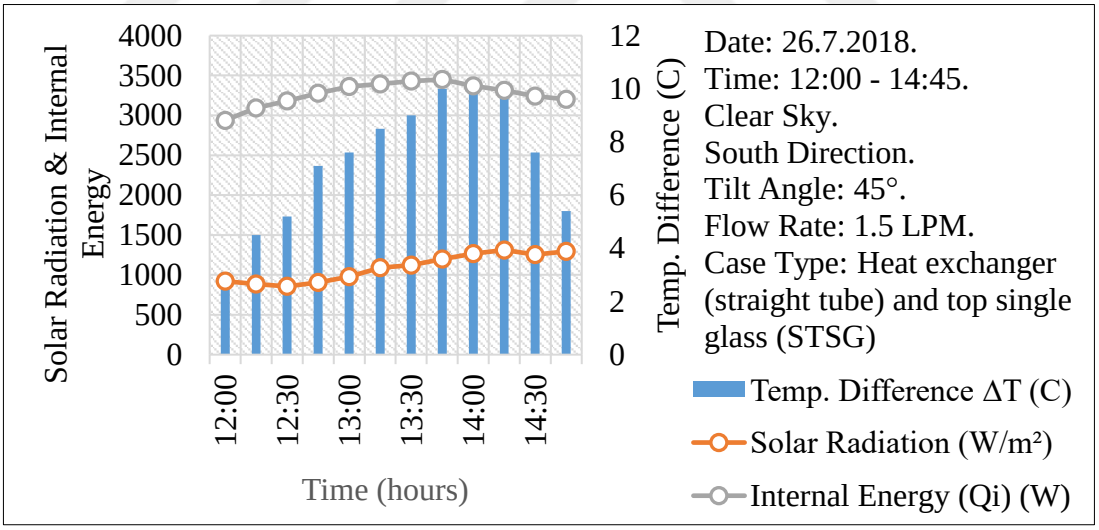

Figure 5.32: Show internal energy, solar energy, and temperature difference with time on July 26, 2018, during the discharge time at a rate of 1.5 LPM, for the case STSG.

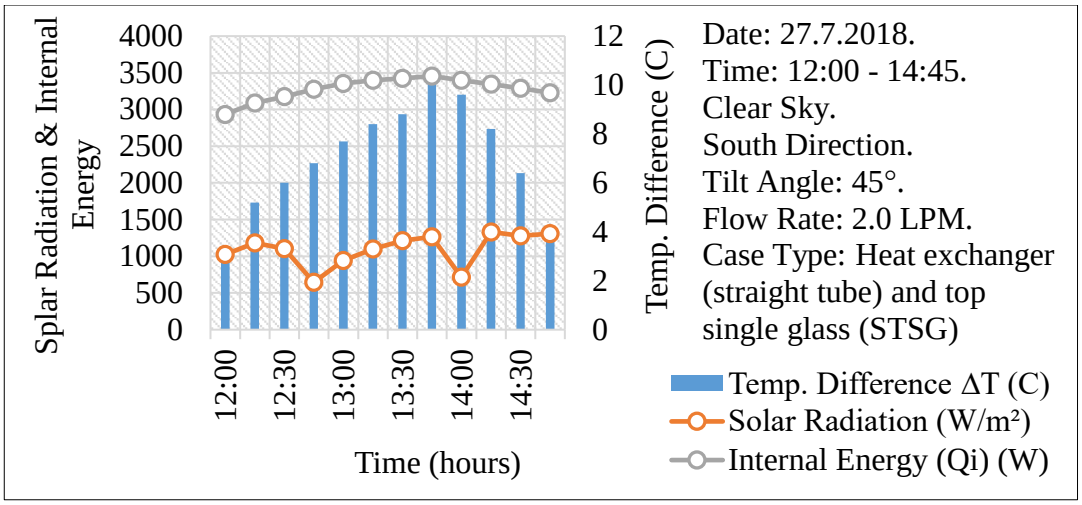

Figure 5.33: Show internal energy, solar energy, and temperature difference with time on July 27, 2018, during the discharge time at a rate of 2.0 LPM, for the case STSG.

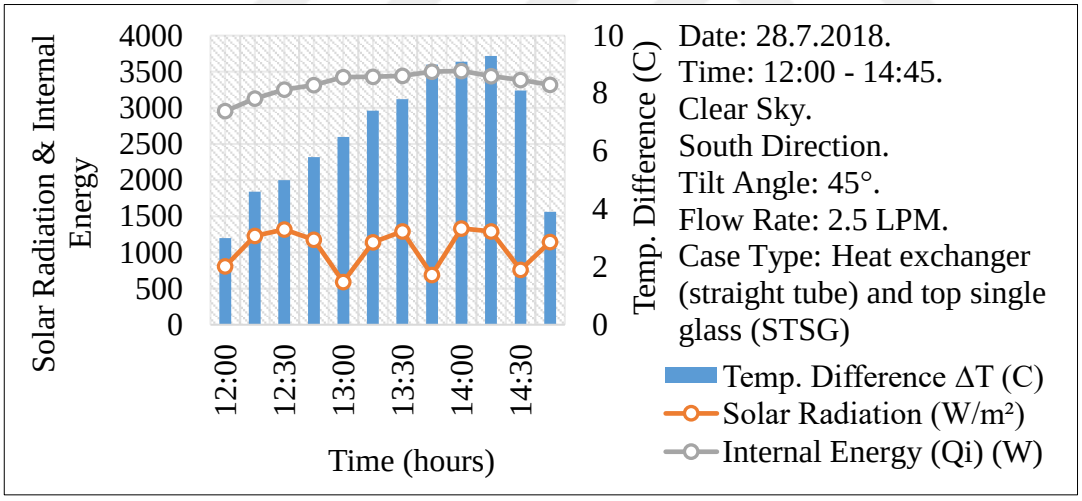

Figure 5.34: Show internal energy, solar energy, and temperature difference with time on July 28, 2018, during the discharge time at a rate of 2.5 LPM, for the case STSG.

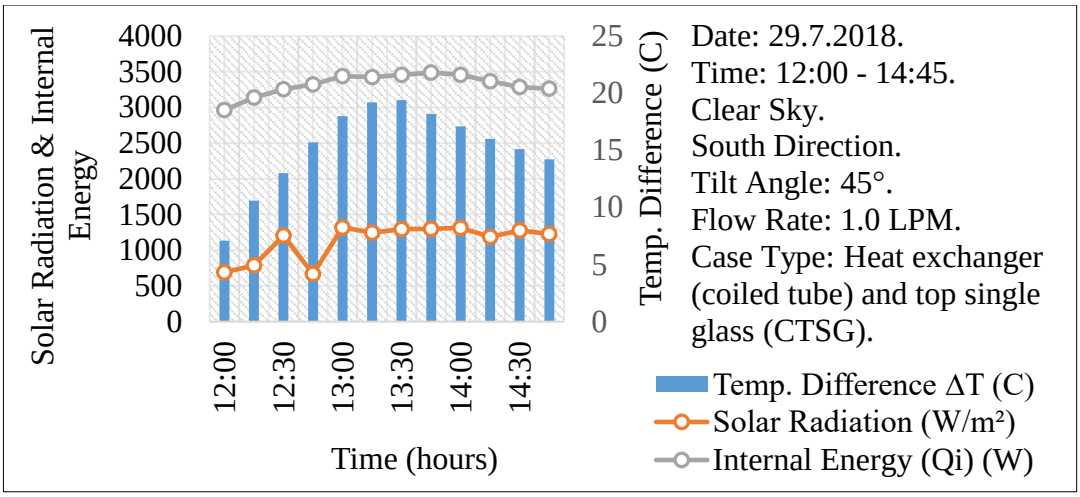

Figure 5.35: Show internal energy, solar energy, and temperature difference with time on July 29, 2018, during the discharge time at a rate of 1.0 LPM, for the case CTSG.

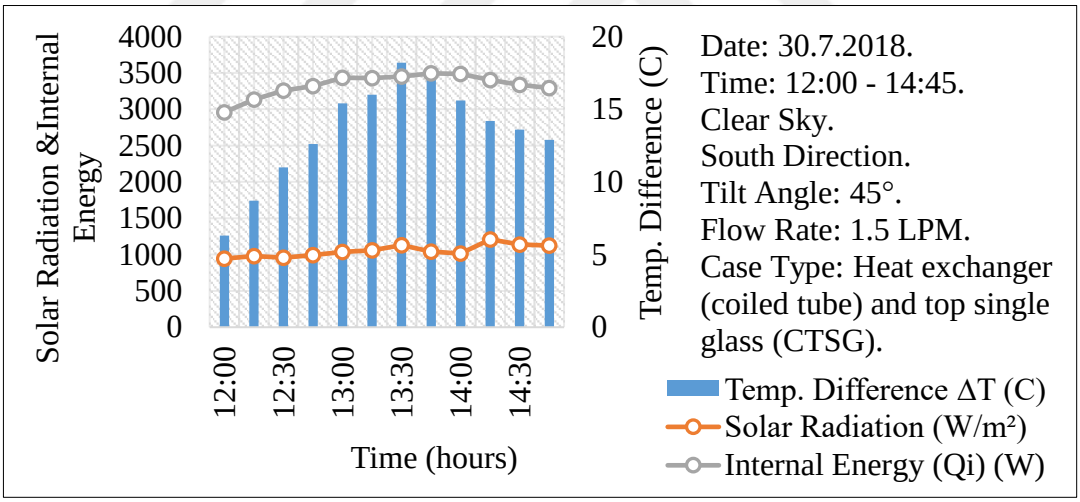

Figure 5.36: Show internal energy, solar energy, and temperature difference with time on July 30, 2018, during the discharge time at a rate of 1.5 LPM, for the case CTSG.

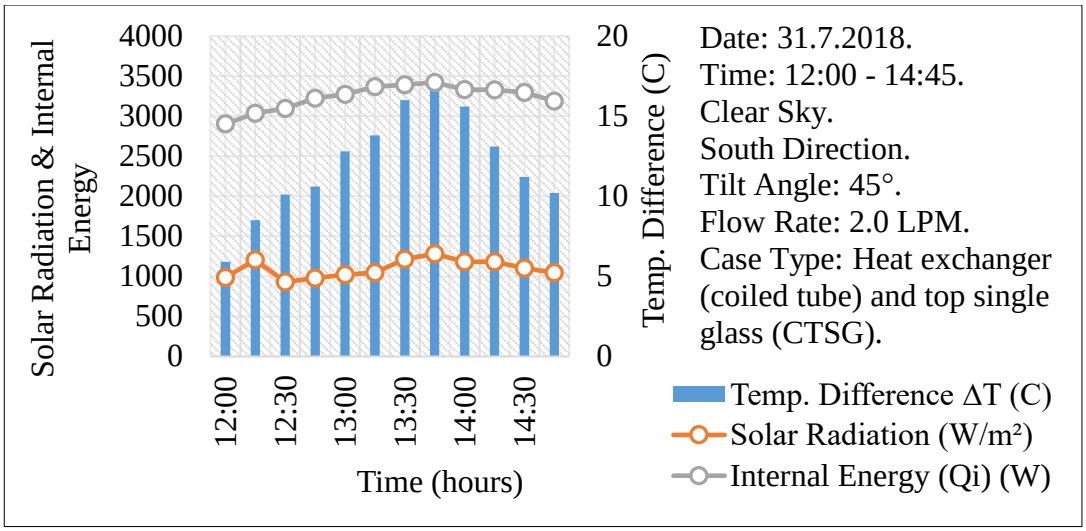

Figure 5.37: Show internal energy, solar energy, and temperature difference with time on July 31, 2018, during the discharge time at a rate of 2.0 LPM, for the case CTSG.

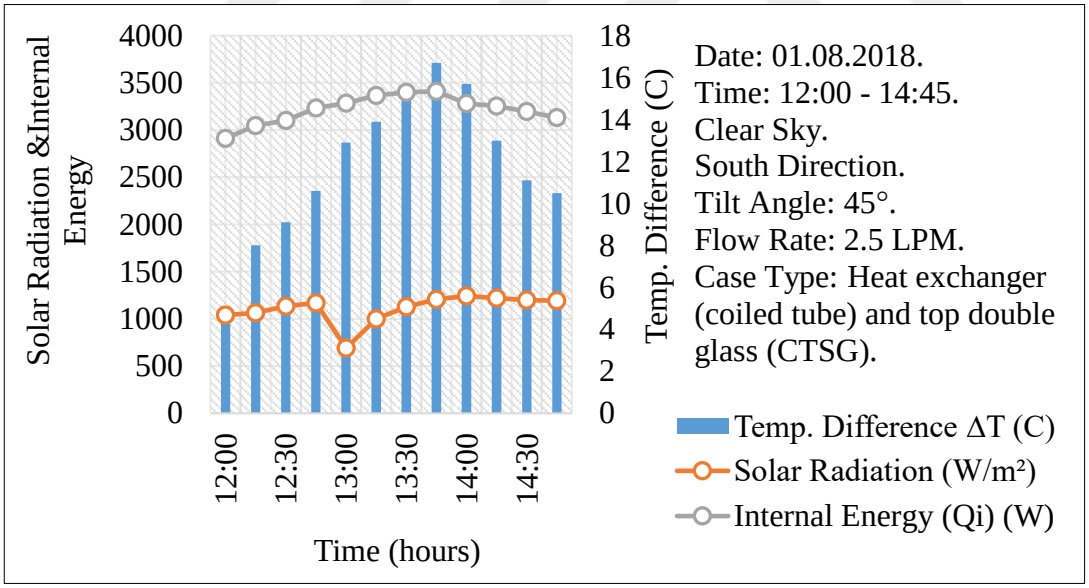

Figure 5.38: Show internal energy, solar energy, and temperature difference with time on August 01, 2018, during the discharge time at a rate of 2.5 LPM, for the case CTSG.

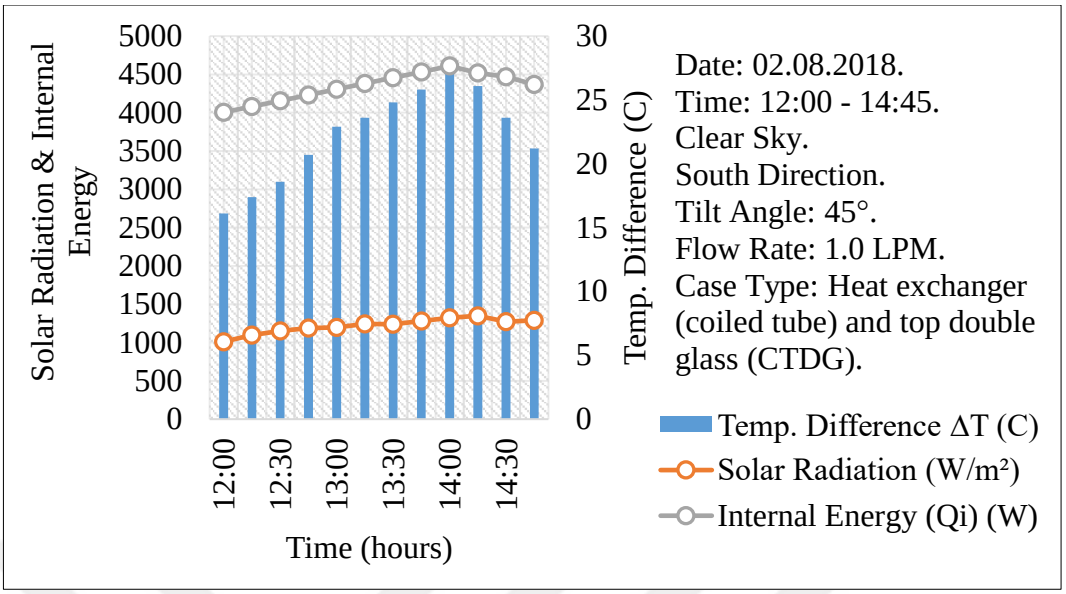

Figure 5.39: Show internal energy, solar energy, and temperature difference with time on August 02, 2018, during the discharge time at a rate of 1.0 LPM, for the case CTDG.

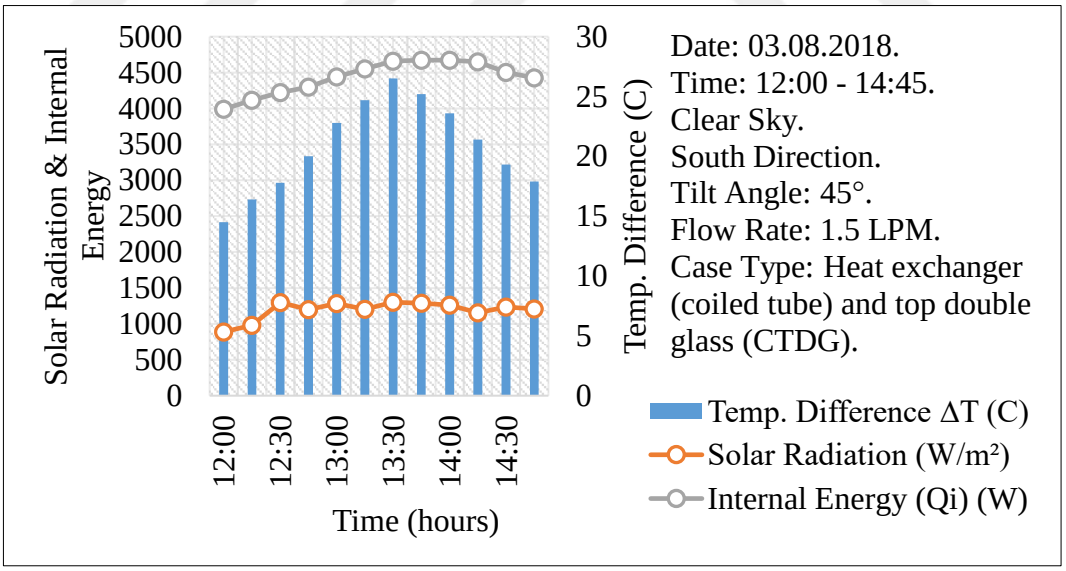

Figure 5.40: Show internal energy, solar energy, and temperature difference with time on August 03, 2018, during the discharge time at a rate of 1.5 LPM, for the case CTDG.

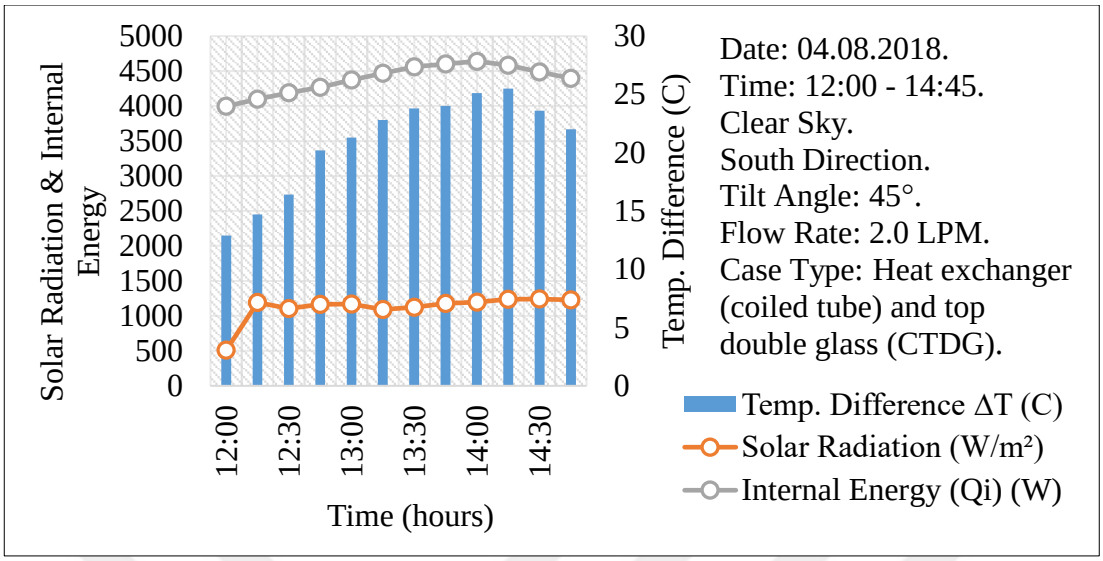

Figure 5.41: Show internal energy, solar energy, and temperature difference with time on August 04, 2018, during the discharge time at a rate of 2.0 LPM, for the case CTDG.

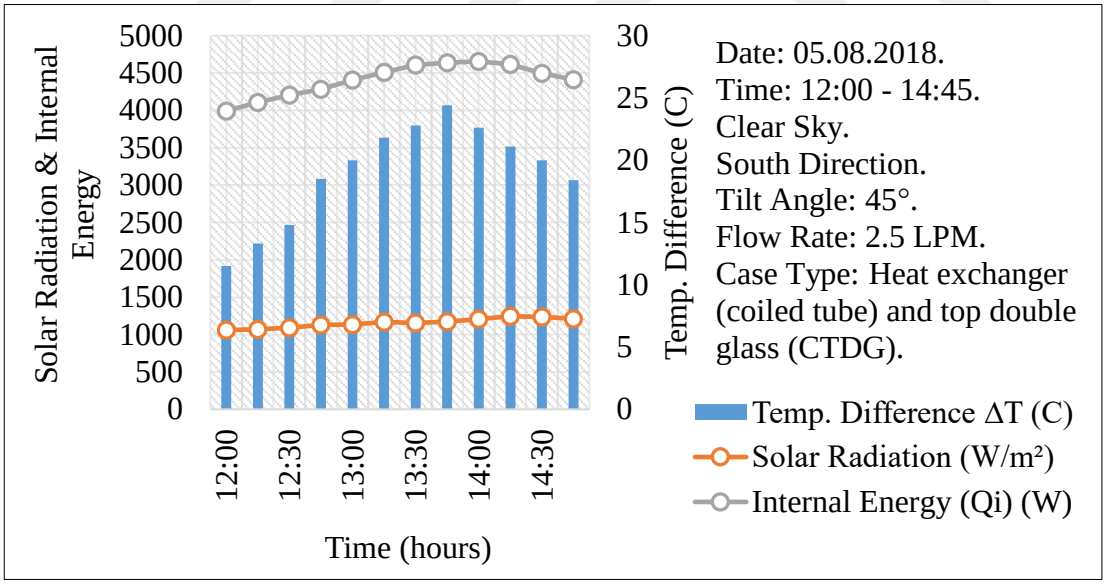

Figure 5.42: Show internal energy, solar energy, and temperature difference with time on August 05, 2018, during the discharge time at a rate of 2.5 LPM, for the case CTDG.

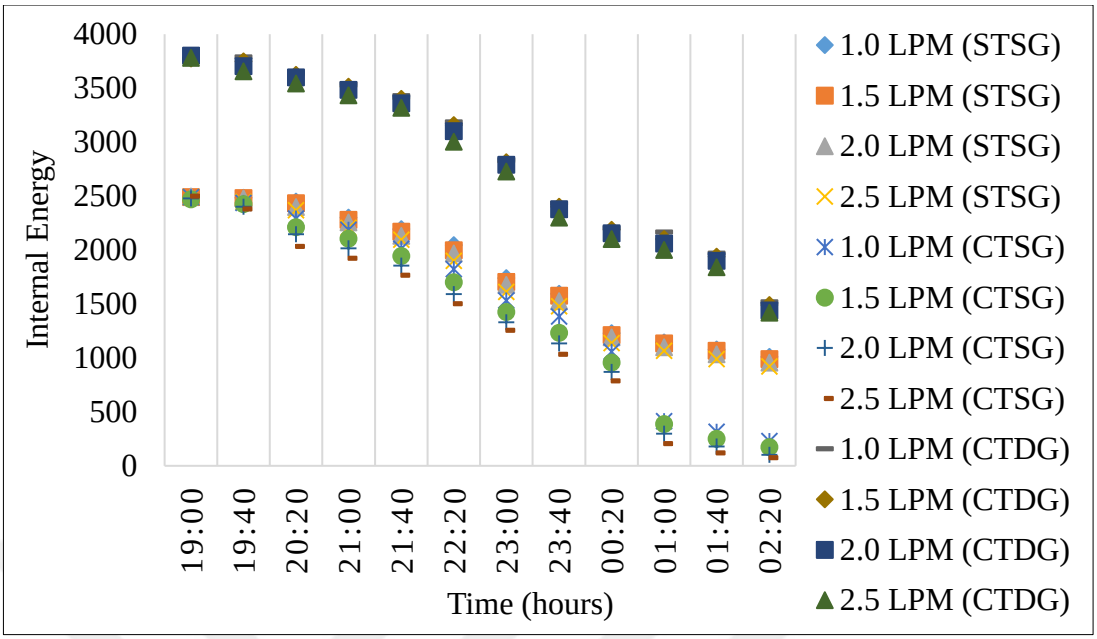

Figure 5.43: Show internal energy with time on 25,26,27,28,29,30,31 July & 01.02, 03, 04, 05 August, 2018, respectively during the discharge time at a rate of 1.0, 1.5, 2.0, and 2.5 LPM, for the all cases. (Nighttime)

5.6 Efficiency

The Efficiency depends on the amount of solar energy-absorbing by the SCIS system which is then stored and used at the need to heat the water flowing inside the heat exchanger, taking in to account thermal losses from each side of collectors. . The efficiency is evaluated for all cases during the day and night times. The day time shows how efficient is the collector in acquiring the solar radiation, while the efficiency evaluation during night time reflects the storage capacity as well as the thermal efficiency.

In all classic solar water heating collectors (which use a copper sheet painted black and welded to the tube that is used as a heat exchanger) depend on the fact that solar energy is the energy entering the collector because it works to heat the water directly by heating the plate and thus the amount of energy entering is the same as solar energy.

In our current research, a medium was used to store heat during the times when the drain was not used, and this medium was the water inside the enclosure, where this water in an isolated collector is exposed to solar radiation & its temperature increases and remains to store the thermal energy until the start of the discharge. Therefore, the energy entering the collector is the energy stored in the water because the heat exchanger is immersed inside it, so it will be adopted in the efficiency law mentioned in Chapter Four, through the relationship (4-5), internal energies of water inside the collector was calculated using determining the average temperature difference distributed inside the enclosure [56].

From Figure 5.42, it was observed that the coiled heat exchangers efficiency with the use of double glass CTDG is higher than in other cases, reaching 84.5% at a flow rate of 2.5 LPM, this indicates that the heat losses were less than the other cases and the internal energy was high. On the other hand, the efficiency of the CTSG case was calculated to be 68.8%, which higher than 41% for the STSG case at the rate of flow of 2.5 LPM due to the use of a coiled tube instead of the straight tube heat exchanger.

From Figure 5.43, it was found that all the cases have thermal storage that lasts for varying hours during the evening depending on the used heat exchanger type. Results exhibit that the thermal efficiency (77.8%) of the CTDG case at a water flow rate of 2.5 LPM was higher than the efficiency (56.6%) for the CTSG case and that (39.7%) for STSG case. This gives two impressions: the first impression is that the heat storage capacity of the double glass enclosure is higher than single glass, and the second impression is that the heat transfer is better for the CTDG case compared to other cases. The decrease in efficiency for all types is due to the solar radiation absence and the increasing in losses due to the low ambient temperatures surrounding the ISCS system.

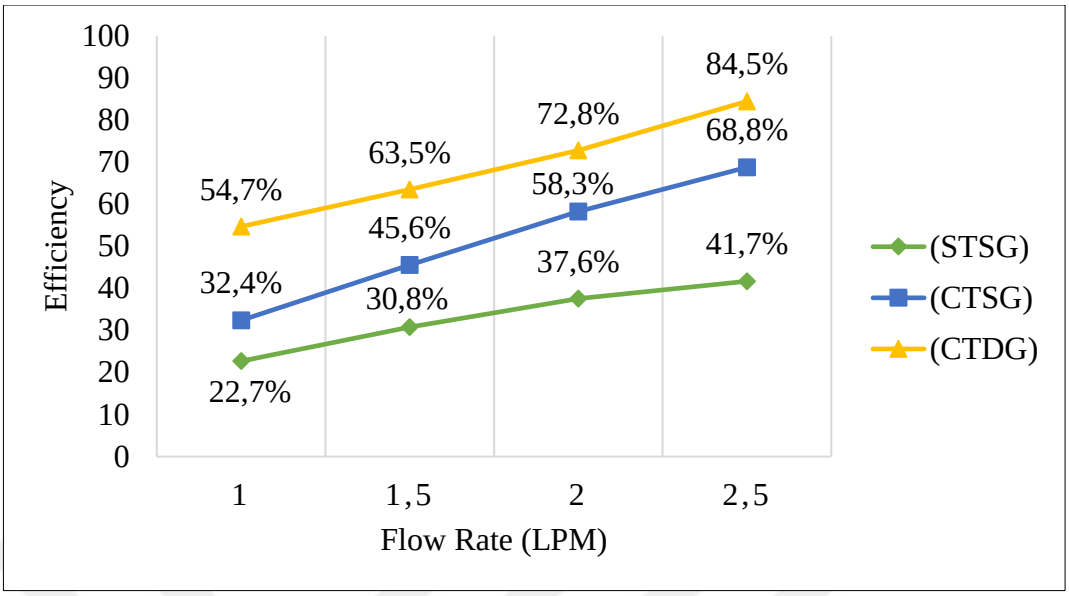

Figure 5.44: The Thermal Efficiency at a flow rate of (1.0, 1.5, 2.0, and 2.5 LPM) during the Daytime for all cases.

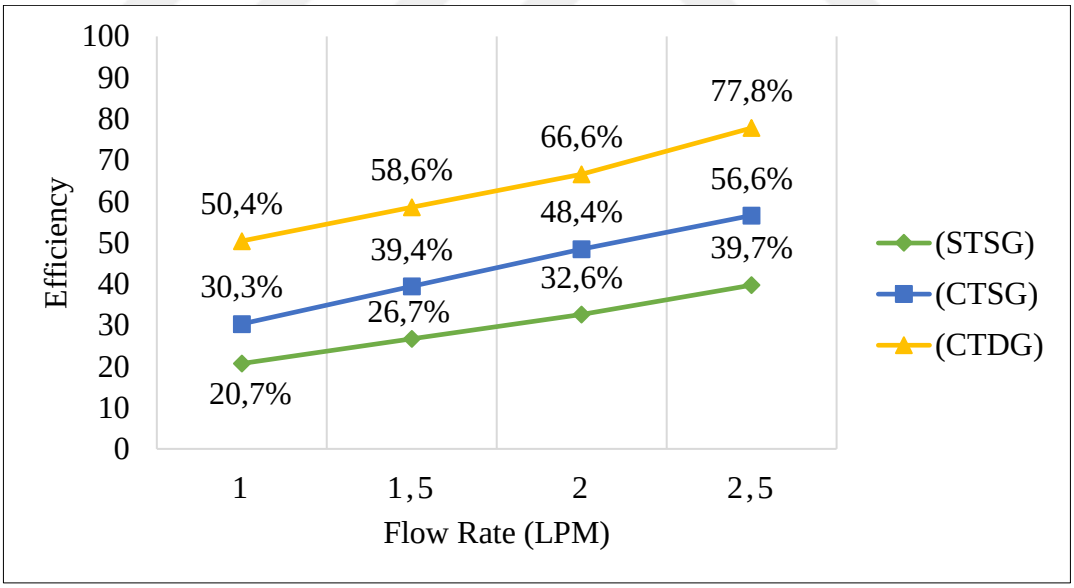

Figure 5.45: The Thermal Efficiency at a flow rate of (1.0, 1.5, 2.0, and 2.5 LPM) during the Nighttime for all cases.

5.7 Non-Dimensionless Relationship between the Nusselt & Rayleigh Number

The non-dimensional relationship is considered as one of the pillars of the design of the heat transfer systems, which expresses the effectiveness of the system and its response/behavior to heat transfer. The dimensional relationship of the free natural heat transfer system is expressed by the number of Nusselt as a function of the number of Rayleigh.

Where the number of Nusselt is heat transfer ratio using the convection to heat transfer by conducting water atoms [48], and it gives an indication of improved heat transfer by free convection of water layers concerning heat transfer by conduction. The results exhibit that the Nusselt number of the case of CTDG is better than that of the CTSG case, and the last was better than the STSG case. This behavior indicates that the transfer of heat using the natural convection overcomes the heat transfer by conduction, meaning that the layers of water transfer heat faster and larger than the heat transfer between the water atoms.

The Rayleigh number depends on the flow driven by the force of buoyancy, which is produced in the case of transfer of heat by the natural convection & it is defined as a ratio between the force of buoyancy to the strength of viscosity [49], that is, raising the water temperatures inside the enclosure leads to a change in the densities of the water layers that work to reduce the viscosity of hot regions, which in turn to has the high buoyancy force that moves water layers in a circular motion inside the enclosure. The increase in heat of the layer surrounding the heat exchanger enhances the heat transfer to the heat exchanger. I was noticed that the Rayleigh numbers of CTDG case are higher than those of other cases because the thermal confinement is high, which leads to an increase in the temperatures inside the enclosure with the presence of the Coiled Tube model that accelerates the transfer of heat (due to increase in its surface area), that makes the presence of a circular movement inside the enclosure due to the high buoyancy force possessed by the hot layers due to the weak strength of the viscosity.

To find this dimensionless relationship, the Statistica program is used the data is filled in. The “Advanced Linear/Nonlinear” is activated from which the “Nonlinear Estimation” is chosen. After that, the shape of the relationship to be drawn Nu=C*Ra^n [36] was expressed, then the “Gauss-Newton” method was chosen. Finally, the relationship is plotted to find the resolution ratio R.

The results exhibited that the highest compatibility between the number of Nusselt and the Rayleigh number is was determined for CTDG case as shown in Figures 5.46-5.47, which show that number of Nusselt increases with an increasing number of Rayleigh, where the resolution ratio was 96.6% during the day and 92.7% at night. This gives a clear indication of the preference for the natural convection heat transfer, i.e. whenever natural convection heat transfer overcomes conduction heat transfer, it is matched by overcomes of buoyancy forces over viscosity. Whereas, the weakest compatibility between the number of Nusselt and the number of Rayleigh was observed for the STSG case as shown in Figures 5.48-5.49 where the resolution ratio was 72.7% during the day and 60.9% at night. In addition to that, the compatibility began to improve for the CTSG case as shown in Figures 5.50-5.51, where the resolution ratio was 88.5% during the day and 79.9% at night.

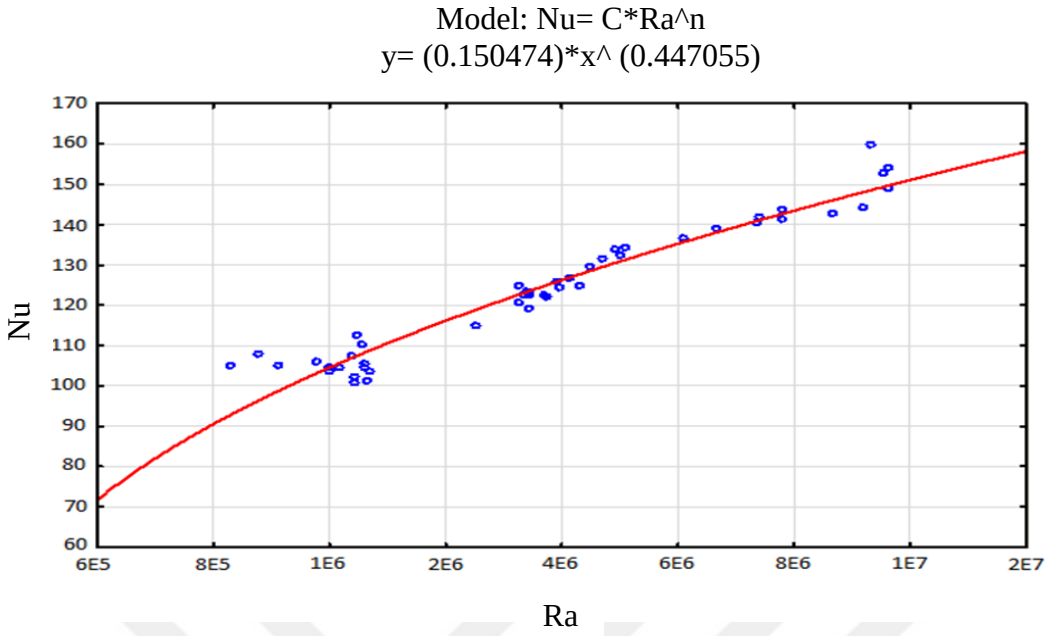

Figure 5.46: Non Dimensionless relationship of CTDG at Daytime. Where the form of relationship is: $Nu = 0.150474Ra^{0.447055}$ $6X10^5$ Ra $2X10^7$ R= 96.6%.

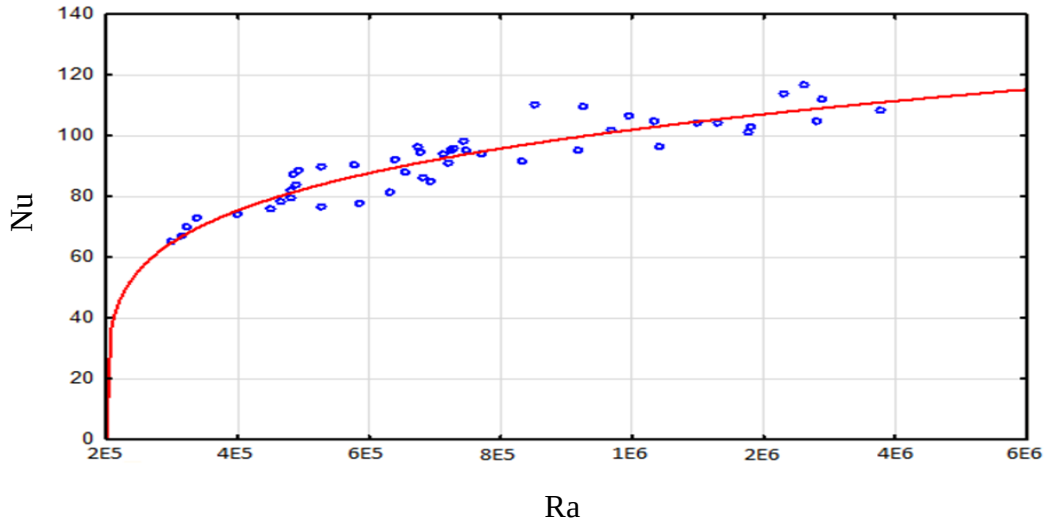

Figure 5.47: Non Dimensionless relationship of CTDG at Nighttime. Where the form of relationship is: $Nu = 6.121Ra^{0.218}$ $2X10^5$ Ra $6X10^6$ R= 92.7%.

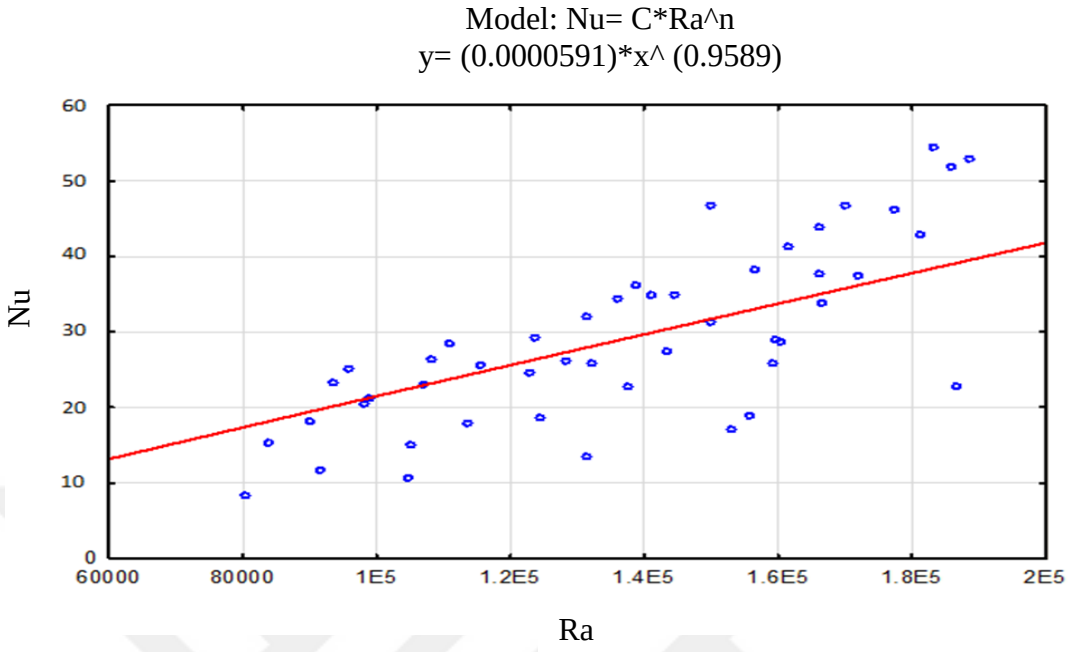

Figure 5.48: Non Dimensionless relationship of STSG at Daytime. Where the form of relationship is: $Nu = 0.0000691Ra^{0.9589}$ $6X10^4$ Ra $2X10^5$ R= 72.7%.

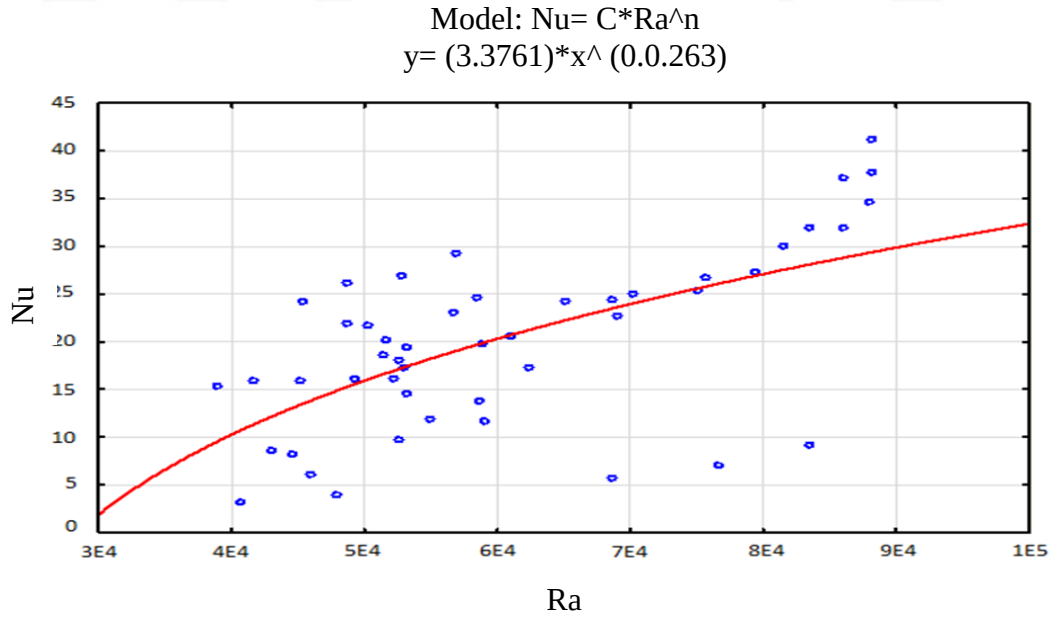

Figure 5.49: Non Dimensionless relationship of STSG at Nighttime. Where the form of relationship is: $Nu = 3.3761Ra^{0.263}$ $3X10^4$ Ra $1X10^5$ R= 60.9%.

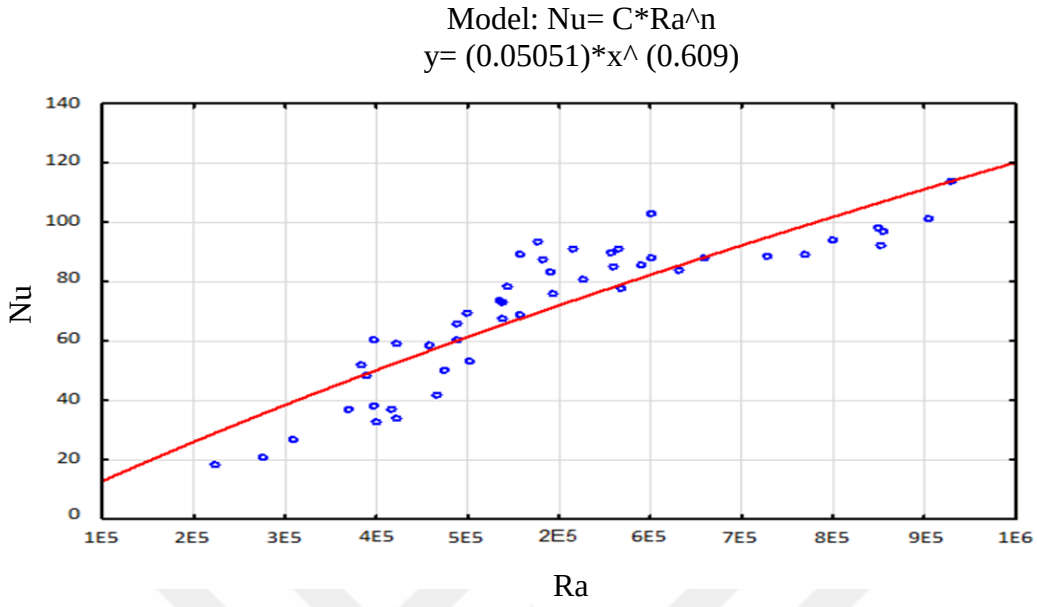

Figure 5.50: Non Dimensionless relationship of CTSG at Daytime. Where the form of relationship is: $Nu = 0.05051Ra^{0.609}$ $1X10^5$ Ra $1X10^6$ R= 88.5%.

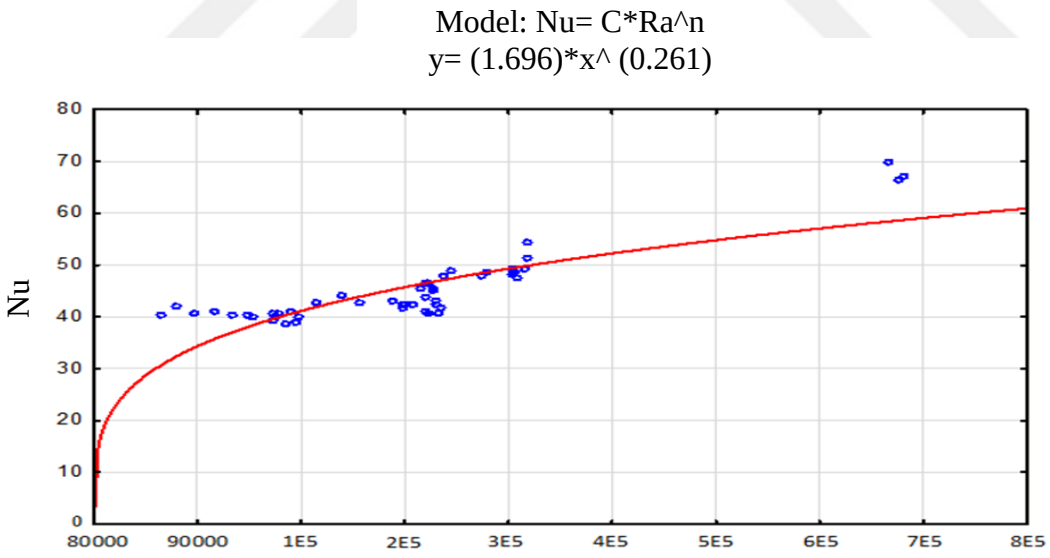

Figure 5.51: Non Dimensionless relationship of CTSG at Nighttime. Where the form of relationship is: $Nu = 1.696Ra^{0.261}$ $8X10^4$ Ra $8X10^5$ R= 79.9%.

CHAPTER 6

CONCLUSIONS & RECOMMENDATIONS

This study presents the initial measurements of transfer of heat using the natural convection in different types of heat exchanges that are immersed in a rectangular, slanted, and thermally insulated enclosure employed for systems of solar water heating. . The effects of heat exchanger types, the rate of water flow inside heat exchangers, and the glassing layer are experimentally studied. The results are represented by temperature distribution, efficiency, and empirical groups for all cases (STSG, CTSG, and CTDG).

6.1 Conclusions

1. The temperature measurements of the water in enclosures allow the identification of the free-convective heat transfer field from enclosures to heat exchangers. The highest temperature difference with using CTDG 28 C in the daytime and 19.9 C at nighttime.
2. The amount of heat transported to a tube within any level of the initial thermal alignment leads to the descent of a cold feather from the tube to the back of the enclosure that this feather leads to a rotational movement in the fluid, which helps to fully mix in the middle part of the enclosure.
3. Using water as a medium for transmission and heat-storing in this type of solar water heaters gives a high preference over traditional heating collectors.
4. The internal energy of the water inside the enclosure is much higher than the solar energy, and this is what raises the donor energy to the heat exchanger and provides thermal storage for evening times.

5. The efficiency of the collector using the heat exchangers in the coiled tube and double glass (CTDG) form is higher than those in other cases (STSG and CTSG). The efficiency is 84.5% at daytime and 77.5% at nighttime.
6. The temperature measurements near the heat exchangers allow the calculation of the Rayleigh number during the heat transfer process, and non-dimensional, empirical relationships have been deduced between the number of Nusselt and the number of Rayleigh for each group of experiments. The empirical relationships of CTDG are:

$Nu = 0.150474Ra^{0.447055}$ $6X10^5$ Ra $2X10^7$ R= 96.6% (Daytime)

$Nu = 6.121Ra^{0.218}$ $2X10^5$ Ra $6X10^6$ R= 92.7% (Nighttime)

6.2 Recommendations

1. Using a double coiled heat exchanger with the double glass and knowing its effect on the free convection heat transfer.
2. Studying impacts of finned heat exchangers on the thermal performances of ISCS systems.
3. Putting small tubes with the coiled heat exchanger and becoming one group for increasing the exposure of water to be heated to the heat stored inside the enclosure.
4. A theoretical study using the (FLUENT) program needs to be performed to know the thermal behavior inside the enclosure and compare the results with the experimental work.
5. Using nanotechnology and mixing nanoparticles with the fluid in the enclosure may enhance the thermal properties of the fluid and thus increasing the thermal storage capability and the transfer of heat by the natural convection from the enclosure to the heat exchanger.

REFERENCES

[1] H. R. Roomi, "Natural convection from single finned tube immersed in a tilted enclosure", Journal of Engineering, vol. 13, No. 3, September 2006.

[2] D. L. Turcotte, G. Schubert, "Geodynamics", Cambridge University Press, 2002.

[3] W. M. Kays, "Convective Heat and Mass Transfer", 4th Edition, McGraw-Hill Professional, 2004.

[4] W. McCabe, J. Smith, "Unit Operations of Chemical Engineering", McGraw Hill, 1956.

[5] O. B. Carroll, O. Carroll, & J. O. Bennett, "Momentum, heat, and mass transfer", McGraw-Hill, 1982, 1962.

[6] M. R. Rajkumar, G. Venugopal, S. Anil Lal, "Natural convection from free standing tandem planar heat sources in a vertical channel", Applied Thermal Engineering, vol. 50, pp. 1386-1395, 2013.

[7] J. Banaszek, Y. Jaluria, T. A. Kowalewski, & M. Rebow, "Semi-Implicit Fem Analysis of Natural Convection in Freezing Water", Numerical Heat Transfer, Part A: Applications, 36 no. 5, pp. 449–472, 2010.

[8] "Water - Density, Specific Weight and Thermal Expansion Coefficient", Www.engineeringtoolbox.com. 2018.

[9] P. G. Stanley, H. Eugene, "Supercooled and Glassy Water", Physics Today, June 2003.

[10] T. Kowalewski, "Phase change problems with free convection: fixed grid numerical simulation", December 1999.

[11] W. Tong, J. N. Koster, "Natural convection of water in a rectangular cavity including density inversion", International Journal of Heat and Fluid Flow, vol. 14 no. 4, pp. 366–375, December 1993.

[12] M. A. Ezan, & M. Kalfa, “Numerical investigation of transient natural convection heat transfer of freezing water in a square cavity”, International Journal of Heat and Fluid Flow, vol. 61, pp. 438–448, October 2016.

[13] E. B. Moore & V. Molinero, “Structural transformation in supercooled water controls the crystallization rate of ice”, Nature. 479, pp. 506–508, November 2011.

[14] C. Marken, “Solar collectors: Behind the glass”, Home Power, vol. 133, pp. 70–76, 2009.

[15] A. Verma, & V. Kumar, “Solar water heating”, International Journal of Research in Aeronautical and Mechanical Engineering, vol.3, no. 1, pp. 53-63, January 2015.

[16] W. Li, T. H. Rubin, & P. A. Onyina “Comparing Solar Water Heater Popularization Policies in China Israel and Australia: The Roles of Governments in Adopting Green Innovations”, vol. 21, no. 3, pp. 160-170, August 2012.

[17] RS. Tang, Y. Etzio, & I. A. Meir, “Estimates of clear night sky emissivity in the Negev Highlands”, Energy Convers Manag vol. 45, no. 11-12, pp.1831–1843, 2004.

[18] RS. Tang, Z. Sun, Z. Li, Y. Yu, H. Zhong, & C. Xia “Experimental investigation on the thermal performance of flat-plate collectors at night”, Energy Convers Manag vol. 49, part 4, pp. 2642–2646, 2020.

[19] RS. Tang, & Y. Etzion, “Comparative studies on water evaporation rate from a wetted surface and that from a free water surface”, vol. 39, no. 1, pp. 77–86, 2004.

[20] X. Y. Liu, & RS. Tang, “Design optimization of SS-AlN cermet solar selective coatings”, Applied Mechanics and Materials vol. 261, pp. 40-45, 2013.

[21] RS. Tang, W. Gao, Y. Yu, H. Chen, “Optimal tilt-angle of all-glass evacuated tube solar collectors”, Energy vol. 34, no. 9, pp. 1387-1395, September 2009.

[22] RS. Tang, T. Wu, “optimal tilt-angles for solar collectors used in China”, vol. 79, no. 3, pp. 239-248, November, 4rtn 2004.

[23] RS. Tang, Y. Cheng, M. Wu, Z. Li, Y. Yu, “Experimental and modeling studies on thermosiphon domestic solar water heaters with flat-plate collectors at clear nights”, Energy Convers Manag, vol. 51, no. 12, pp. 2548-2556, December 2010.

[24] RS. Tang, Y. Yang, W. Gao, “Comparative studies on the thermal performance of water-in- glass evacuated tube solar heaters with different collector tilt-angles”, Sol Energy, vol. 85, no. 7, pp. 1381-1389, July 2011.

[25] Y. Q. Yang, R. S. Tang, “Effects of tube space on the thermal performance of water-in-glass evacuated tube solar water heaters”, Adv Mater Res, vol. 860–863, pp. 81–87, 2014.

[26] RS. Tang, Y. Yang, “Nocturnal reverse flow in water-in-glass evacuated tube solar water heaters”, Energy Convers Manag, vol. 80, pp. 173-177, April 2014.

[27] L. J. Shah, S. Furbo, “Theoretical flow investigations of an all-glass evacuated tubular collector”, Solar Energy vol. 81, no. 6, pp. 822-828, June 2007,

[28] R. S. Tang, N. Y. Liu, “Shading effect and optimal tilt-angle of collectors in a collector array”, Adv. Mater. Res, vol. 588–589, pp. 2078–2082, 2005.

[29] T. Doerr, “Passive Solar Simplified (1st Ed.)” vol. 11, pp. 11361-11373, 2012.

[30] B. Norton, “Harnessing Solar Heat”, vol. 1, pp. 75-87, 2014.

[31] W. Liu, J. H. Davidson, F. A. Kulacki, and S. C. Mantell, “Natural convection from a horizontal tube heat exchanger immersed in a tilted enclosure”, International Solar Energy Conference, vol. 16893, pp. 65-74, 2002.

[32] S. Kakaç, H. Liu, and A. Pramuanjaroenkij, “Heat Exchangers: Selection, Rating and Thermal Design”, (2nd ed.), CRC Press, 2002.

[33] W. Liu, J. H. Davidson, F. A. Kulacki, S. C. Mantell, “Natural Convection

from a Horizontal Tube Heat Exchanger Immersed in a Tilted Enclosure", Journal of Solar Energy Engineering, vol. 125 (1), pp. 67 -75, 2003.

[34] W. Liu, J. H. Davidson, and F. A. Kulacki, " Natural Convection From a Tube Bundle in a Thin Inclined Enclosure", vol. 126(2), pp. 702 – 709, 2004.

[35] Y. Su, and J. H. Davidson, " Natural Convective Flow and Heat Transfer in a Collector Storage with an Immersed Heat Exchanger: Numerical Study", International Solar Energy Conference, vol. 47373, pp. 165-174 2005.

[36] W. Liu, J. H. Davidson, and F. A. Kulacki, "Thermal Characterization of Prototypical Integral Collector Storage Systems with Immersed Heat Exchangers", Journal of Solar Energy Engineering, vol. 127(1), pp. 21-28,2005.

[37] W. Logie, E. Frank, M. Y. Haller, and M. Rommel, " Investigation of Immersed Coil Heat Exchangers regarding Heat Transfer and Storage Stratification", Graz, Austria. 2010.

[38] R. Andrzejczyk, and T. Muszyński, "Performance analyses of helical coil heat exchangers. The effect of external coil surface modification on heat exchanger effectiveness", archives of thermodynamics 37, 2016.

[39] A. S. A. Ghias, S. V. Ananth1, M. D. Anand, and G. G. Devadhas, "Experimental Study of Thermal Performance of Coil in Shell Heat Exchanger", Indian Journal. Sci. Technol, vol. 9, pp.1-17, 2016.

[40] H. Vettrivel, and P. Mathiazhagan, "Experimental Investigation of Solar Flat Plate Collector with Double Glazing System", European Journal of Advances in Engineering and Technology, vol. 3(12), pp. 51-55, 2016.

[41] J. Manikandan, and B. Sivaraman, "Comparative studies on the thermal efficiency of single and double glazed flat plate solar water heater", ARPN Journal of engineering and applied sciences, vol. 11(9), pp. 5521-5526, 2016.

[42] H. Vettrivel, and P. Mathiazhagan, "Comparison Study of Solar Flat Plate Collector with Single and Double Glazing Systems", International Journal of Renewable Energy Research (IJRER), vol. 7(1), pp. 266-274. 2017.

[43] A. A. M. SAYIGH, “ Solar Energy engineering, Academic Press”, Elsevier Inc., 2009.

[44] J. Banaszek, Y. Jaluria, T. A. Kowalewski, and M. Rebow, “Semi-Implicit Fem Analysis of Natural Convection in Freezing Water”, Numerical Heat Transfer, Part A: Applications. vol. 36(5) pp. 449–472, 1999.

[45] Vulcanic, “Calculatıon of the Power Requıred for Heatıng a Volume of Liquid,” https://www.vulcanic.com/en/heating-volume-liquid, 2015.

[46] The Engineering ToolBox “Thermal Energy Stored in Heated Water,” https://www.engineeringtoolbox.com/energy-storage-water-d_1463.html, 2009.

[47] T. Li, Y. Liu, D. Wang, K. Shang, and J. Liu, “Optimization analysis on storage tank volume in the solar heating system “, Procedia Engineering, vol. 121, pp.1356-1364, 2015.

[48] Y. A. Çengel, “Heat and Mass Transfer”, Second ed., McGraw-Hill. pp. 466. 2002.

[49] L. Rayleigh, “On convection currents in a horizontal layer of fluid, when the higher temperature is on the underside”, The London, Edinburgh, and Dublin Philosophical Magazine and Journal of Science, vol. 32(192), pp. 529-546, 1916.

APPENDIX

A: The Result of case STSG

Table A.1: The results for case STSG at 1.0 LPM on 25– 07 – 2018 (Daytime)

NO.	Time	Flow Rate (Kg/s)	ΔT (C)	Re	Qu (w)	(h) (W/m^2*C)	Nu	Ra
1	12:00	0.017	3.6	1395.076463	255.6936	505.9921197	16.8085479	413349.5706
2	12:15	0.017	5.1	1397.886067	362.2326	704.7747382	23.40513069	583985.294
3	12:30	0.017	6.5	1400.707011	461.669	929.4855243	30.86465876	779506.7398
4	12:45	0.017	7.7	1406.383193	546.9002	1110.741473	36.86391888	938300.2197
5	13:00	0.017	8.7	1406.383193	617.9262	1244.080625	41.29124471	1056228.205
6	13:15	0.017	9.9	1409.23857	703.1574	1415.677952	46.96847597	1208256.419
7	13:30	0.017	10.3	1409.23857	731.5678	1525.953712	50.63201556	1306796.336
8	13:45	0.017	11.3	1412.105566	802.5938	1615.874835	53.57950117	1386304.685
9	14:00	0.017	12	1417.874696	852.312	1731.025673	57.40046002	1489659.417
10	14:15	0.017	10.8	1414.98425	767.0808	1571.710036	52.0699391	1345559.645
11	14:30	0.017	9.9	1429.555539	703.1574	1403.473832	46.4985982	1195641.732
12	14:45	0.017	9	1432.505884	639.234	1298.269255	43.00064247	1101912.429

Table A.2: The results for case STSG at 1.0 LPM on 25– 07 – 2018 (Nighttime)

NO.	Time	Flow Rate (Kg/s)	ΔT (C)	Re	Qu (w)	(h) (W/m^2*C)	Nu	Ra
1	19:00	0.017	2.2	1395.076463	156.2572	309.2174065	1.03E+01	3.83E+04
2	19:40	0.017	3.9	1397.886067	277.0014	538.945388	1.79E+01	5.73E+04
3	20:20	0.017	5	1400.707011	355.13	714.9888649	2.38E+01	1.68E+05
4	21:00	0.017	6.4	1406.383193	454.5664	923.2136922	3.07E+01	4.44E+05
5	21:40	0.017	7.3	1406.383193	518.4898	1043.883743	3.48E+01	7.09E+05
6	22:20	0.017	7.1	1409.23857	504.2846	1015.284188	3.38E+01	6.38E+05
7	23:00	0.017	6.5	1409.23857	461.669	962.9804982	3.21E+01	5.22E+05
8	23:40	0.017	6.5	1412.105566	461.669	929.4855243	3.10E+01	4.56E+05
9	0:20	0.017	5.8	1417.874696	411.9508	836.6624085	2.79E+01	3.06E+05
10	1:00	0.017	5	1414.98425	355.13	727.643535	2.42E+01	1.80E+05
11	1:40	0.017	4	1429.555539	284.104	567.0601342	1.89E+01	6.98E+04
12	2:20	0.017	2.6	1432.505884	184.6676	375.0555624	1.25E+01	1.45E+04

Table A.3: The results for case STSG at 1.5 LPM on 26– 07 – 2018 (Daytime)

NO.	Time	Flow Rate (Kg/s)	ΔT (C)	Re	Qu (w)	(h) (W/m^2*C)	Nu	Ra
1	12:00	0.025	3.1	2051.583034	323.795	640.7579948	2.13E+01	7.66E+05
2	12:15	0.025	4.5	2055.714805	470.025	914.5000928	3.04E+01	9.24E+05
3	12:30	0.025	5.2	2059.863251	543.14	1093.512382	3.63E+01	1.29E+06
4	12:45	0.025	7.1	2068.210578	741.595	1506.162044	5.00E+01	1.37E+06
5	13:00	0.025	7.6	2068.210578	793.82	1598.210404	5.30E+01	1.54E+06
6	13:15	0.025	8.5	2072.409662	887.825	1787.472162	5.93E+01	1.70E+06
7	13:30	0.025	9	2072.409662	940.05	1960.820019	6.51E+01	1.83E+06
8	13:45	0.025	10	2076.625832	1044.5	2102.908426	6.97E+01	1.92E+06
9	14:00	0.025	10.4	2085.109847	1086.28	2206.209191	7.32E+01	1.86E+06
10	14:15	0.025	10	2080.859192	1044.5	2140.128044	7.09E+01	1.36E+06
11	14:30	0.025	7.6	2102.287558	793.82	1584.432728	5.25E+01	9.67E+05
12	14:45	0.025	5.4	2106.6263	564.03	1145.531695	3.79E+01	7.66E+05

Table A.4: The results for case STSG at 1.5 LPM on 26– 07 – 2018 (Nighttime)

NO.	Time	Flow Rate (Kg/s)	ΔT (C)	Re	Qu (w)	(h) (W/m^2*C)	Nu	Ra
1	19:00	0.025	1.9	2051.583034	198.455	392.722642	1.31E+01	1.72E+04
2	19:40	0.025	3.3	2055.714805	344.685	670.6334014	2.23E+01	1.32E+05
3	20:20	0.025	4.3	2059.863251	449.135	904.2506232	3.01E+01	4.10E+05
4	21:00	0.025	5.5	2068.210578	574.475	1166.745245	3.88E+01	1.08E+06
5	21:40	0.025	6.2	2068.210578	647.59	1303.803224	4.34E+01	1.65E+06
6	22:20	0.025	6.5	2072.409662	678.925	1366.890477	4.55E+01	1.98E+06
7	23:00	0.025	6.8	2072.409662	710.26	1481.508459	4.93E+01	2.69E+06
8	23:40	0.025	6.9	2076.625832	720.705	1451.006814	4.83E+01	2.48E+06
9	0:20	0.025	5.8	2085.109847	605.81	1230.385895	4.10E+01	1.33E+06
10	1:00	0.025	4.9	2080.859192	511.805	1048.662742	3.49E+01	7.23E+05
11	1:40	0.025	3.7	2102.287558	386.465	771.3685649	2.57E+01	2.25E+05
12	2:20	0.025	2.4	2106.6263	250.68	509.1251979	1.70E+01	4.64E+04

Table A.5: The results for case STSG at 2.0 LPM on 27– 07 – 2018 (Daytime)

NO.	Time	Flow Rate (Kg/s)	ΔT (C)	Re	Qu (w)	(h) (W/m^2*C)	Nu	Ra
1	12:00	0.033	3	2708.089605	413.622	818.5166643	2.72E+01	6.83E+05
2	12:15	0.033	5.2	2713.543543	716.9448	1394.917475	4.63E+01	1.19E+06
3	12:30	0.033	6	2719.019492	827.244	1665.503473	5.53E+01	1.43E+06
4	12:45	0.033	6.8	2730.037962	937.5432	1904.12824	6.32E+01	1.65E+06
5	13:00	0.033	7.7	2730.037962	1061.6298	2137.396124	7.09E+01	1.86E+06
6	13:15	0.033	8.4	2735.580754	1158.1416	2331.704863	7.74E+01	2.03E+06
7	13:30	0.033	8.8	2735.580754	1213.2912	2530.765038	8.40E+01	2.22E+06
8	13:45	0.033	10.3	2741.146098	1420.1022	2859.114296	9.48E+01	2.52E+06
9	14:00	0.033	9.6	2752.344998	1323.5904	2688.181045	8.91E+01	2.36E+06
10	14:15	0.033	8.2	2746.734133	1130.5668	2316.474595	7.67E+01	2.02E+06
11	14:30	0.033	6.4	2775.019577	882.3936	1761.222064	5.84E+01	1.52E+06
12	14:45	0.033	4.1	2780.746716	565.2834	1148.077321	3.80E+01	9.69E+05

Table A.6: The results for case STSG at 2.0 LPM on 27– 07 – 2018 (Nighttime)

NO.	Time	Flow Rate (Kg/s)	ΔT (C)	Re	Qu (w)	(h) (W/m^2*C)	Nu	Ra
1	19:00	0.033	1.6	2708.089605	220.5984	436.542221	1.45E+01	2.57E+04
2	19:40	0.033	2.7	2713.543543	372.2598	724.2840735	2.41E+01	1.76E+05
3	20:20	0.033	3.8	2719.019492	523.9212	1054.818867	3.51E+01	7.37E+05
4	21:00	0.033	5	2730.037962	689.37	1400.094294	4.66E+01	2.16E+06
5	21:40	0.033	6.3	2730.037962	868.6062	1748.778647	5.82E+01	5.04E+06
6	22:20	0.033	6.7	2735.580754	923.7558	1859.812212	6.19E+01	6.37E+06
7	23:00	0.033	6.5	2735.580754	896.181	1869.315085	6.23E+01	6.50E+06
8	23:40	0.033	6.4	2741.146098	882.3936	1776.537038	5.92E+01	5.36E+06
9	0:20	0.033	5.7	2752.344998	785.8818	1596.107495	5.32E+01	3.57E+06
10	1:00	0.033	4.6	2746.734133	634.2204	1299.485748	4.33E+01	1.63E+06
11	1:40	0.033	3.5	2775.019577	482.559	963.1683162	3.21E+01	5.23E+05
12	2:20	0.033	2.1	2780.746716	289.5354	588.0396036	1.96E+01	8.02E+04

Table A.7: The results for case STSG at 2.5 LPM on 28– 07 – 2018 (Daytime)

NO.	Time	Flow Rate (Kg/s)	ΔT (C)	Re	Qu (w)	(h) (W/m^2*C)	Nu	Ra
1	12:00	0.042	3	3446.659498	526.428	1041.748482	3.46E+01	8.78E+05
2	12:15	0.042	4.6	3453.600872	807.1896	1570.501493	5.22E+01	1.35E+06
3	12:30	0.042	5	3460.570262	877.38	1766.443078	5.87E+01	1.52E+06
4	12:45	0.042	5.8	3474.59377	1017.7608	2067.048303	6.86E+01	1.79E+06
5	13:00	0.042	6.5	3474.59377	1140.594	2296.376001	7.62E+01	2.00E+06
6	13:15	0.042	7.4	3481.648232	1298.5224	2614.335755	8.67E+01	2.29E+06
7	13:30	0.042	7.8	3481.648232	1368.7128	2854.953947	9.47E+01	2.51E+06
8	13:45	0.042	9	3488.731398	1579.284	3179.59754	1.05E+02	2.81E+06
9	14:00	0.042	9.1	3502.984543	1596.8316	3243.127511	1.08E+02	2.87E+06
10	14:15	0.042	9.3	3495.843442	1631.9268	3343.736056	1.11E+02	2.96E+06
11	14:30	0.042	8.1	3531.843097	1421.3556	2836.968495	9.40E+01	2.49E+06
12	14:45	0.042	3.9	3539.132185	684.3564	1389.91179	4.60E+01	1.18E+06

Table A.8: The results for case STSG at 2.5 LPM on 28– 07 – 2018 (Nighttime)

NO.	Time	Flow Rate (Kg/s)	ΔT (C)	Re	Qu (w)	(h) (W/m^2*C)	Nu	Ra
1	19:00	0.042	1.3	3446.659498	228.1188	451.4243421	1.50E+01	2.92E+04
2	19:40	0.042	1.9	3453.600872	333.4044	648.6853992	2.16E+01	1.16E+05
3	20:20	0.042	3	3460.570262	526.428	1059.865847	3.53E+01	7.50E+05
4	21:00	0.042	4.1	3474.59377	719.4516	1461.189318	4.86E+01	2.54E+06
5	21:40	0.042	5.9	3474.59377	1035.3084	2084.402832	6.94E+01	9.83E+06
6	22:20	0.042	6.4	3481.648232	1123.0464	2261.04714	7.53E+01	1.34E+07
7	23:00	0.042	6.6	3481.648232	1158.1416	2415.730263	8.05E+01	1.72E+07
8	23:40	0.042	6.1	3488.731398	1070.4036	2155.060555	7.18E+01	1.12E+07
9	0:20	0.042	3	3502.984543	526.428	1069.162916	3.56E+01	7.78E+05
10	1:00	0.042	1.3	3495.843442	228.1188	467.4039649	1.56E+01	3.35E+04
11	1:40	0.042	0.7	3531.843097	122.8332	245.1701168	8.17E+00	2.88E+03
12	2:20	0.042	0.2	3539.132185	35.0952	71.2775277	2.38E+00	2.63E+01

B: The Result of case CTSG

Table B.1: The results for case CTSG at 1.0 LPM on 29– 07 – 2018 (Daytime)

NO.	Time	Flow Rate (Kg/s)	ΔT (C)	Re	Qu (w)	(h) (W/m^2*C)	Nu	Ra
1	12:00	0.017	7.1	8761.08019	504.2846	203.3557342	2.90E+00	1.39E+05
2	12:15	0.017	10.6	8778.724503	752.8756	127.9281309	1.82E+00	6.48E+04
3	12:30	0.017	13	8796.440029	923.338	162.3501382	2.31E+00	9.59E+04
4	12:45	0.017	15.7	8832.086451	1115.1082	197.7889167	2.81E+00	1.32E+05
5	13:00	0.017	18	8832.086451	1278.468	224.7924991	3.20E+00	1.63E+05
6	13:15	0.017	19.2	8850.018221	1363.6992	239.7786657	3.41E+00	1.82E+05
7	13:30	0.017	19.4	8850.018221	1377.9044	251.0070398	3.57E+00	1.96E+05
8	13:45	0.017	18.2	8868.022953	1292.6732	227.2901935	3.23E+00	1.66E+05
9	14:00	0.017	17.1	8904.25309	1214.5446	215.426145	3.06E+00	1.52E+05
10	14:15	0.017	16	8886.101092	1136.416	203.3521133	2.89E+00	1.38E+05
11	14:30	0.017	15.1	8977.608787	1072.4926	186.9502752	2.65E+00	1.20E+05
12	14:45	0.017	14.2	8996.136953	1008.5692	178.8918865	2.54E+00	1.12E+05

Table B.2: The results for case CTSG at 1.0 LPM on 29– 07 – 2018 (Nighttime)

NO.	Time	Flow Rate (Kg/s)	ΔT (C)	Re	Qu (w)	(h) (W/m^2*C)	Nu	Ra
1	19:00	0.017	5.3	8761.08019	376.4378	151.8007593	2.17E+00	3.83E+03
2	19:40	0.017	5.9	8778.724503	419.0534	166.1456543	2.37E+00	5.41E+03
3	20:20	0.017	8.6	8796.440029	610.8236	250.6020083	3.58E+00	2.61E+04
4	21:00	0.017	10.3	8832.086451	731.5678	302.7724182	4.32E+00	5.39E+04
5	21:40	0.017	11.4	8832.086451	809.6964	332.1933598	4.74E+00	7.70E+04
6	22:20	0.017	11	8850.018221	781.286	320.5374524	4.57E+00	6.72E+04
7	23:00	0.017	10.2	8850.018221	724.4652	307.9364715	4.40E+00	5.76E+04
8	23:40	0.017	6.2	8868.022953	440.3612	180.6665641	2.58E+00	7.47E+03
9	0:20	0.017	4	8904.25309	284.104	117.5815216	1.68E+00	1.44E+03
10	1:00	0.017	2.1	8886.101092	149.1546	62.27658468	8.89E-01	1.26E+02
11	1:40	0.017	1.3	8977.608787	92.3338	37.55513255	5.36E-01	1.82E+01
12	2:20	0.017	0.5	8996.136953	35.513	14.6976902	2.10E-01	5.01E-01

Table B.3: The results for case CTSG at 1.5 LPM on 30– 07 – 2018 (Daytime)

NO.	Time	Flow Rate (Kg/s)	ΔT (C)	Re	Qu (w)	(h) (W/m^2*C)	Nu	Ra
1	12:00	0.025	6.3	12883.94146	658.035	265.3564883	3.78E+00	1.19E+05
2	12:15	0.025	8.7	12909.88897	908.715	360.2859403	5.13E+00	1.97E+05
3	12:30	0.025	11	12935.94122	1148.95	471.3786065	6.71E+00	3.07E+05
4	12:45	0.025	12.6	12988.36243	1316.07	544.6791075	7.75E+00	3.88E+05
5	13:00	0.025	15.4	12988.36243	1608.53	659.9300491	9.39E+00	5.32E+05
6	13:15	0.025	16	13014.73268	1671.2	685.6416095	9.75E+00	5.66E+05
7	13:30	0.025	18.2	13014.73268	1900.99	808.0224598	1.15E+01	7.42E+05
8	13:45	0.025	17.3	13041.21022	1806.985	741.3499903	1.05E+01	6.43E+05
9	14:00	0.025	15.6	13094.48984	1629.42	674.3646093	9.58E+00	5.51E+05
10	14:15	0.025	14.2	13067.79572	1483.19	619.2769625	8.79E+00	4.78E+05
11	14:30	0.025	13.6	13202.36586	1420.52	577.7712701	8.20E+00	4.27E+05
12	14:45	0.025	12.9	13229.61317	1347.405	557.6476577	7.92E+00	4.02E+05

Table B.4: The results for case CTSG at 1.5 LPM on 30– 07 – 2018 (Nighttime)

NO.	Time	Flow Rate (Kg/s)	ΔT (C)	Re	Qu (w)	(h) (W/m^2*C)	Nu	Ra
1	19:00	0.025	4.9	12883.94146	511.805	206.3883798	2.94E+00	8.27E+04
2	19:40	0.025	5.6	12909.88897	584.92	231.9081914	3.31E+00	1.29E+05
3	20:20	0.025	7.3	12935.94122	762.485	312.8239843	4.46E+00	4.07E+05
4	21:00	0.025	8.9	12988.36243	929.605	384.7336553	5.49E+00	9.01E+05
5	21:40	0.025	10	12988.36243	1044.5	428.5260059	6.12E+00	1.36E+06
6	22:20	0.025	10.3	13014.73268	1075.835	441.3817861	6.30E+00	1.53E+06
7	23:00	0.025	10.7	13014.73268	1117.615	475.0461714	6.78E+00	2.02E+06
8	23:40	0.025	7.8	13041.21022	814.71	334.2502846	4.77E+00	5.26E+05
9	0:20	0.025	3.8	13094.48984	396.91	164.2683023	2.35E+00	3.46E+04
10	1:00	0.025	1.7	13067.79572	177.565	74.13879129	1.06E+00	1.64E+03
11	1:40	0.025	0.8	13202.36586	83.56	33.9865453	4.85E-01	8.28E+01
12	2:20	0.025	0	13229.61317	0	0	0.00E+00	0.00E+00

Table B.5: The results for case CTSG at 2.0 LPM on 31– 07 – 2018 (Daytime)

NO.	Time	Flow Rate (Kg/s)	ΔT (C)	Re	Qu (w)	(h) (W/m^2*C)	Nu	Ra
1	12:00	0.033	5.9	17006.80272	813.4566	328.0311636	4.67E+00	1.69E+05
2	12:15	0.033	8.5	17041.05345	1171.929	464.6446264	6.61E+00	2.99E+05
3	12:30	0.033	10.1	17075.44241	1392.5274	571.3108711	8.13E+00	4.20E+05
4	12:45	0.033	10.6	17144.6384	1461.4644	604.8531804	8.60E+00	4.61E+05
5	13:00	0.033	12.8	17144.6384	1764.7872	724.0375396	1.03E+01	6.20E+05
6	13:15	0.033	13.8	17179.44713	1902.6612	780.6029724	1.11E+01	7.01E+05
7	13:30	0.033	16	17179.44713	2205.984	937.6612281	1.33E+01	9.47E+05
8	13:45	0.033	17.5	17214.3975	2412.795	989.8950737	1.41E+01	1.03E+06
9	14:00	0.033	15.6	17284.72659	2150.8344	890.1612843	1.27E+01	8.69E+05
10	14:15	0.033	13.1	17249.49036	1806.1494	754.1223406	1.07E+01	6.61E+05
11	14:30	0.033	11.2	17427.12294	1544.1888	628.0713571	8.92E+00	4.89E+05
12	14:45	0.033	10.2	17463.08938	1406.3148	582.0285321	8.26E+00	4.32E+05

Table B.6: The results for case CTSG at 2.0 LPM on 31– 07 – 2018 (Nighttime)

NO.	Time	Flow Rate (Kg/s)	ΔT (C)	Re	Qu (w)	(h) (W/m^2*C)	Nu	Ra
1	19:00	0.033	4.3	17006.80272	592.8582	239.0735599	3.41E+00	1.45E+05
2	19:40	0.033	5	17041.05345	689.37	273.3203685	3.90E+00	2.43E+05
3	20:20	0.033	7.4	17075.44241	1020.2676	418.5842026	5.97E+00	1.24E+06
4	21:00	0.033	9.1	17144.6384	1254.6534	519.2607492	7.41E+00	2.84E+06
5	21:40	0.033	10.1	17144.6384	1392.5274	571.3108711	8.15E+00	4.10E+06
6	22:20	0.033	10.2	17179.44713	1406.3148	576.9674144	8.23E+00	4.26E+06
7	23:00	0.033	9.8	17179.44713	1351.1652	574.3175022	8.20E+00	4.19E+06
8	23:40	0.033	7.1	17214.3975	978.9054	401.6145728	5.73E+00	1.06E+06
9	0:20	0.033	3.8	17284.72659	523.9212	216.834159	3.10E+00	1.00E+05
10	1:00	0.033	1.3	17249.49036	179.2362	74.83656815	1.07E+00	1.70E+03
11	1:40	0.033	0.2	17427.12294	27.5748	11.21555995	1.60E-01	1.18E+00
12	2:20	0.033	0	17463.08938	0	0	0.00E+00	0.00E+00

Table B.7: The results for case CTSG at 2.5 LPM on 01– 08 – 2018 (Daytime)

NO.	Time	Flow Rate (Kg/s)	ΔT (C)	Re	Qu (w)	(h) (W/m^2*C)	Nu	Ra
1	12:00	0.042	5.1	21645.02165	894.9276	360.8848241	5.14E+00	1.98E+05
2	12:15	0.042	8	21688.61348	1403.808	556.5796595	7.92E+00	4.03E+05
3	12:30	0.042	9.1	21732.38125	1596.8316	655.1305579	9.32E+00	5.26E+05
4	12:45	0.042	10.6	21820.44888	1860.0456	769.8131386	1.09E+01	6.85E+05
5	13:00	0.042	12.9	21820.44888	2263.6404	928.70156	1.32E+01	9.33E+05
6	13:15	0.042	13.9	21864.7509	2439.1164	1000.693929	1.42E+01	1.05E+06
7	13:30	0.042	15.7	21864.7509	2754.9732	1171.011011	1.67E+01	1.36E+06
8	13:45	0.042	16.7	21909.23318	2930.4492	1202.272562	1.71E+01	1.42E+06
9	14:00	0.042	15.7	21998.74293	2754.9732	1140.194932	1.62E+01	1.30E+06
10	14:15	0.042	13	21953.89682	2281.188	952.4654128	1.35E+01	9.69E+05
11	14:30	0.042	11.1	22179.97465	1947.7836	792.2263709	1.12E+01	7.16E+05
12	14:45	0.042	10.5	22225.75012	1842.498	762.5507505	1.08E+01	6.73E+05

Table B.8: The results for case CTSG at 2.5 LPM on 01– 08 – 2018 (Nighttime)

NO.	Time	Flow Rate (Kg/s)	ΔT (C)	Re	Qu (w)	(h) (W/m^2*C)	Nu	Ra
1	19:00	0.042	4.1	21645.02165	719.4516	290.1230939	4.14E+00	3.05E+05
2	19:40	0.042	5.1	21688.61348	894.9276	354.8195329	5.06E+00	6.60E+05
3	20:20	0.042	8	21732.38125	1403.808	575.938952	8.22E+00	4.22E+06
4	21:00	0.042	9.7	21820.44888	1702.1172	704.4516457	1.01E+01	9.14E+06
5	21:40	0.042	9.7	21820.44888	1702.1172	698.3259793	9.97E+00	8.85E+06
6	22:20	0.042	9	21864.7509	1579.284	647.931321	9.25E+00	6.64E+06
7	23:00	0.042	8.6	21864.7509	1509.0936	641.445522	9.16E+00	6.39E+06
8	23:40	0.042	6.2	21909.23318	1087.9512	446.3526878	6.37E+00	1.59E+06
9	0:20	0.042	3.6	21998.74293	631.7136	261.4459716	3.73E+00	2.05E+05
10	1:00	0.042	0.4	21953.89682	70.1904	29.30662809	4.18E-01	4.69E+01
11	1:40	0.042	0	22179.97465	0	0	0.00E+00	0.00E+00
12	2:20	0.042	0	22225.75012	0	0	0.00E+00	0.00E+00

C: The Result of Case CTDG

Table C.1: The results for case CTDG at 1.0 LPM on 02– 08 – 2018 (Daytime)

NO.	Time	Flow Rate (Kg/s)	ΔT (C)	Re	Qu (w)	(h) (W/m^2*C)	Nu	Ra
1	12:00	0.017	16.1	8761.08019	1143.5186	461.1306085	6.56E+00	1.25E+06
2	12:15	0.017	17.4	8778.724503	1235.8524	489.9888788	6.97E+00	1.44E+06
3	12:30	0.017	18.6	8796.440029	1321.0836	541.9996923	7.71E+00	1.80E+06
4	12:45	0.017	20.7	8832.086451	1470.2382	608.4843744	8.65E+00	2.33E+06
5	13:00	0.017	22.9	8832.086451	1626.4954	667.3006964	9.49E+00	2.86E+06
6	13:15	0.017	23.6	8850.018221	1676.2136	687.6985343	9.78E+00	3.06E+06
7	13:30	0.017	24.8	8850.018221	1761.4448	748.7082837	1.06E+01	3.70E+06
8	13:45	0.017	25.8	8868.022953	1832.4708	751.8060248	1.07E+01	3.73E+06
9	14:00	0.017	28	8904.25309	1988.728	823.0706514	1.17E+01	4.57E+06
10	14:15	0.017	26.1	8886.101092	1853.7786	774.0089811	1.10E+01	3.97E+06
11	14:30	0.017	23.6	8977.608787	1676.2136	681.7700987	9.68E+00	2.99E+06
12	14:45	0.017	21.2	8996.136953	1505.7512	623.1820646	8.85E+00	2.44E+06

Table C.2: The results for case CTDG at 1.0 LPM on 02– 08 – 2018 (Nighttime)

NO.	Time	Flow Rate (Kg/s)	ΔT (C)	Re	Qu (w)	(h) (W/m^2*C)	Nu	Ra
1	19:00	0.017	7.9	8761.08019	561.1054	226.2690564	3.23E+00	5.31E+04
2	19:40	0.017	10.6	8778.724503	752.8756	298.4989721	4.26E+00	1.89E+05
3	20:20	0.017	13.7	8796.440029	973.0562	399.2148271	5.70E+00	7.19E+05
4	21:00	0.017	16.9	8832.086451	1200.3394	496.7819289	7.09E+00	1.96E+06
5	21:40	0.017	19.9	8832.086451	1413.4174	579.8813912	8.28E+00	3.99E+06
6	22:20	0.017	18.4	8850.018221	1306.8784	536.1717386	7.65E+00	2.79E+06
7	23:00	0.017	17.7	8850.018221	1257.1602	534.3603476	7.63E+00	2.74E+06
8	23:40	0.017	16.2	8868.022953	1150.6212	472.0642481	6.74E+00	1.55E+06
9	0:20	0.017	14.6	8904.25309	1036.9796	429.1725539	6.13E+00	1.00E+06
10	1:00	0.017	13.7	8886.101092	973.0562	406.2805763	5.80E+00	7.82E+05
11	1:40	0.017	12.6	8977.608787	894.9276	363.9959001	5.20E+00	4.72E+05
12	2:20	0.017	11.7	8996.136953	831.0042	343.9259508	4.91E+00	3.65E+05

Table C.3: The results for case CTDG at 1.5 LPM on 03– 08 – 2018 (Daytime)

NO.	Time	Flow Rate (Kg/s)	ΔT (C)	Re	Qu (w)	(h) (W/m^2*C)	Nu	Ra
1	12:00	0.025	14.5	12883.94146	1514.525	610.7411238	8.69E+00	2.35E+06
2	12:15	0.025	16.4	12909.88897	1712.98	679.1597035	9.67E+00	2.98E+06
3	12:30	0.025	17.8	12935.94122	1859.21	762.7762906	1.09E+01	3.86E+06
4	12:45	0.025	20	12988.36243	2089	864.570012	1.23E+01	5.11E+06
5	13:00	0.025	22.8	12988.36243	2381.46	977.0392935	1.39E+01	6.71E+06
6	13:15	0.025	24.7	13014.73268	2579.915	1058.459235	1.51E+01	8.02E+06
7	13:30	0.025	26.5	13014.73268	2767.925	1176.516219	1.67E+01	1.02E+07
8	13:45	0.025	25.2	13041.21022	2632.14	1079.885535	1.53E+01	8.38E+06
9	14:00	0.025	23.6	13094.48984	2465.02	1020.192614	1.45E+01	7.38E+06
10	14:15	0.025	21.4	13067.79572	2235.23	933.2765492	1.33E+01	6.03E+06
11	14:30	0.025	19.3	13202.36586	2015.885	819.9254053	1.16E+01	4.52E+06
12	14:45	0.025	17.9	13229.61317	1869.655	773.7901607	1.10E+01	3.97E+06

Table C.4: The results for case CTDG at 1.5 LPM on 03– 08 – 2018 (Nighttime)

NO.	Time	Flow Rate (Kg/s)	ΔT (C)	Re	Qu (w)	(h) (W/m^2*C)	Nu	Ra
1	19:00	0.025	7.4	12883.94146	772.93	311.6885735	4.45E+00	2.31E+05
2	19:40	0.025	9	12909.88897	940.05	372.7095934	5.32E+00	5.24E+05
3	20:20	0.025	10.6	12935.94122	1107.17	454.2375663	6.48E+00	1.30E+06
4	21:00	0.025	13.9	12988.36243	1451.855	600.8761583	8.57E+00	4.69E+06
5	21:40	0.025	16	12988.36243	1671.2	685.6416095	9.79E+00	8.60E+06
6	22:20	0.025	19.2	13014.73268	2005.44	822.7699314	1.17E+01	1.99E+07
7	23:00	0.025	17	13014.73268	1775.65	754.7462537	1.08E+01	1.34E+07
8	23:40	0.025	15.4	13041.21022	1608.53	659.9300491	9.42E+00	7.23E+06
9	0:20	0.025	14.3	13094.48984	1493.635	618.1675586	8.83E+00	5.36E+06
10	1:00	0.025	13.2	13067.79572	1378.74	575.6659088	8.22E+00	3.87E+06
11	1:40	0.025	12.5	13202.36586	1305.625	531.0397703	7.58E+00	2.67E+06
12	2:20	0.025	11	13229.61317	1148.95	475.5135066	6.79E+00	1.61E+06

Table C.5: The results for case CTDG at 2.0 LPM on 04– 08 – 2018 (Daytime)

NO.	Time	Flow Rate (Kg/s)	ΔT (C)	Re	Qu (w)	(h) (W/m^2*C)	Nu	Ra
1	12:00	0.033	12.9	17006.80272	1778.5746	717.2206798	1.02E+01	2.25E+06
2	12:15	0.033	14.7	17041.05345	2026.7478	803.5618834	1.14E+01	2.89E+06
3	12:30	0.033	16.4	17075.44241	2261.1336	927.6730976	1.32E+01	3.99E+06
4	12:45	0.033	20.2	17144.6384	2785.0548	1152.64474	1.64E+01	6.48E+06
5	13:00	0.033	21.3	17144.6384	2936.7162	1204.843718	1.71E+01	7.15E+06
6	13:15	0.033	22.8	17179.44713	3143.5272	1289.691867	1.83E+01	8.32E+06
7	13:30	0.033	23.8	17179.44713	3281.4012	1394.771077	1.98E+01	9.92E+06
8	13:45	0.033	24	17214.3975	3308.976	1357.570387	1.93E+01	9.32E+06
9	14:00	0.033	25.1	17284.72659	3460.6374	1432.246682	2.04E+01	1.05E+07
10	14:15	0.033	25.5	17249.49036	3515.787	1467.948068	2.08E+01	1.11E+07
11	14:30	0.033	23.6	17427.12294	3253.8264	1323.436074	1.88E+01	8.79E+06
12	14:45	0.033	22	17463.08938	3033.228	1255.355657	1.78E+01	7.81E+06

Table C.6: The results for case CTDG at 2.0 LPM on 04– 08 – 2018 (Nighttime)

NO.	Time	Flow Rate (Kg/s)	ΔT (C)	Re	Qu (w)	(h) (W/m^2*C)	Nu	Ra
1	19:00	0.033	7	17006.80272	965.118	389.1895162	5.55E+00	6.39E+04
2	19:40	0.033	8.5	17041.05345	1171.929	464.6446264	6.63E+00	1.44E+05
3	20:20	0.033	11	17075.44241	1516.614	622.2197606	8.88E+00	5.50E+05
4	21:00	0.033	13.6	17144.6384	1875.0864	776.0380427	1.11E+01	1.52E+06
5	21:40	0.033	15.9	17144.6384	2192.1966	899.3903812	1.28E+01	2.99E+06
6	22:20	0.033	18.7	17179.44713	2578.2438	1057.773593	1.51E+01	6.29E+06
7	23:00	0.033	17.7	17179.44713	2440.3698	1037.287734	1.48E+01	5.75E+06
8	23:40	0.033	16	17214.3975	2205.984	905.0469245	1.29E+01	3.08E+06
9	0:20	0.033	14.2	17284.72659	1957.8108	810.2750152	1.16E+01	1.85E+06
10	1:00	0.033	12.4	17249.49036	1709.6376	713.825727	1.02E+01	1.04E+06
11	1:40	0.033	11.5	17427.12294	1585.551	644.894697	9.21E+00	6.51E+05
12	2:20	0.033	9.2	17463.08938	1268.4408	524.9669113	7.50E+00	2.54E+05

Table C.7: The results for case CTDG at 2.5 LPM on 05– 08 – 2018 (Daytime)

NO.	Time	Flow Rate (Kg/s)	ΔT (C)	Re	Qu (w)	(h) (W/m^2*C)	Nu	Ra
1	12:00	0.042	11.5	21645.02165	2017.974	813.7598974	1.16E+01	2.98E+06
2	12:15	0.042	13.3	21688.61348	2333.8308	925.3136839	1.32E+01	3.97E+06
3	12:30	0.042	14.8	21732.38125	2597.0448	1065.487061	1.52E+01	5.44E+06
4	12:45	0.042	18.5	21820.44888	3246.306	1343.541799	1.91E+01	9.13E+06
5	13:00	0.042	20	21820.44888	3509.52	1439.84738	2.05E+01	1.07E+07
6	13:15	0.042	21.8	21864.7509	3825.3768	1569.433644	2.23E+01	1.29E+07
7	13:30	0.042	22.8	21864.7509	4000.8528	1700.5765	2.42E+01	1.55E+07
8	13:45	0.042	24.4	21909.23318	4281.6144	1756.613804	2.50E+01	1.66E+07
9	14:00	0.042	22.6	21998.74293	3965.7576	1641.299711	2.33E+01	1.43E+07
10	14:15	0.042	21.1	21953.89682	3702.5436	1545.924632	2.19E+01	1.24E+07
11	14:30	0.042	20	22179.97465	3509.52	1427.434903	2.03E+01	1.04E+07
12	14:45	0.042	18.4	22225.75012	3228.7584	1336.27941	1.90E+01	8.98E+06

Table C.8: The results for case CTDG at 2.5 LPM on 05– 08 – 2018 (Nighttime)

NO.	Time	Flow Rate (Kg/s)	ΔT (C)	Re	Qu (w)	(h) (W/m^2*C)	Nu	Ra
1	19:00	0.042	6.6	21645.02165	1158.1416	467.0274194	6.66E+00	1.47E+05
2	19:40	0.042	9.7	21688.61348	1702.1172	674.8528371	9.63E+00	7.99E+05
3	20:20	0.042	12.4	21732.38125	2175.9024	892.7053756	1.27E+01	2.88E+06
4	21:00	0.042	15.4	21820.44888	2702.3304	1118.407767	1.60E+01	8.11E+06
5	21:40	0.042	18.2	21820.44888	3193.6632	1310.261116	1.87E+01	1.68E+07
6	22:20	0.042	16.1	21864.7509	2825.1636	1159.077141	1.65E+01	9.57E+06
7	23:00	0.042	14.3	21864.7509	2509.3068	1066.589647	1.52E+01	6.53E+06
8	23:40	0.042	12.7	21909.23318	2228.5452	914.3030862	1.31E+01	3.22E+06
9	0:20	0.042	11.8	21998.74293	2070.6168	856.9617959	1.22E+01	2.40E+06
10	1:00	0.042	11	21953.89682	1930.236	805.9322724	1.15E+01	1.81E+06
11	1:40	0.042	9.7	22179.97465	1702.1172	692.3059277	9.89E+00	9.02E+05
12	2:20	0.042	7.5	22225.75012	1316.07	544.6791075	7.78E+00	3.00E+05